Effect of additives on structural and physico-chemical properties of alkali borosilicate glass and alternative glass forming systems intended for immobilization of radioactive waste

By

Amrita Dhara Prakash
Enrolment No: CHEM01201404020
Bhabha Atomic Research Center, Mumbai

A thesis submitted to the

Board of Studies in Chemical Sciences

In partial fulfillment of requirements

for the Degree of

DOCTOR OF PHILOSOPHY

of

HOMI BHABHA NATIONAL INSTITUTE

March, 2021

HOMI BHABHA NATIONAL INSTITUTE

Recommendation of the Viva Voce Board

As the members of the Viva Voce Board, we certify that we have read the dissertation prepared by Amrita Dhara Prakash entitled "Effect of additives on structural and physico-chemical properties of alkali borosilicate glass and alternative glass forming systems intended for immobilization of radioactive waste" and recommend that it may be accepted as fulfilling the thesis requirement for the award of Degree of Doctor of Philosophy.

Chairman: Prof. B. S. Tomar		Date: 30/06/2021
Guide: Prof. C. P. Kaushik		Date: 30/06/2021
Co-guide: Prof. A. K. Tyagi		Date: 30/06/2021
Examiner: Dr. Ashis Kumar Mandal		Date: 30/06/2021
Member: Dr. N. L. Mishra		Date: 30/06/2021
Member: Dr. V. Sudarsan	Sudarsan.V	Date: 30/06/2021
Technical Advisor: Dr. T. P. Valsala		Date: 30/06/2021

Final approval and acceptance of this thesis is contingent upon the candidate's submission of the final copies of the thesis to HBNI.

I / we hereby certify that I / we have read this dissertation prepared under my direction and recommend that it may be accepted as fulfilling the dissertation requirements.

Date: 30/06/2021

Place: Mumbai

18/8/21

(Prof. A. K. Tyagi)
Signature of the co-Guide

(Prof. C. P. Kaushik)
Signature of the Guide

STATEMENT BY AUTHOR

This dissertation has been submitted in partial fulfillment of requirements for an advanced degree at Homi Bhabha National Institute (HBNI) and is deposited in the Library to be made available to borrowers under rules of the HBNI.

Brief quotations from this dissertation are allowable without special permission, provided that accurate acknowledgement of source is made. Requests for permission for extended quotation from or reproduction of this manuscript in whole or in part may be granted by the Competent Authority of HBNI when in his or her judgment the proposed use of the material is in the interests of scholarship. In all other instances, however, permission must be obtained from the author.

Amrita Dhara Prakash

DECLARATION

I, hereby declare that the investigation presented in the thesis has been carried out by me. The work is original and has not been submitted earlier as a whole or in part for a degree / diploma at this or any other Institution / University.

Amrita Dhara Prakash

List of Publications arising from the thesis

a. Journals (3)

1. A comparative study on the structural aspects of sodium borosilicate glasses and barium borosilicate glasses: Effect of Al_2O_3 addition, **Amrita Dhara**, R.K. Mishra, R. Shukla, T.P. Valsala, V. Sudarsan, A.K. Tyagi, C.P. Kaushik

   J. of Non-Crystalline Solids, **2016**, 447, 283–289.
2. Studies on Modified Borosilicate Glass for Enhancement of Solubility of Molybdenum, **Amrita Dhara Prakash**, Manjeet Singh, R.K. Mishra, T.P. Valsala, A.K. Tyagi, Arnab Sarkar, C.P. Kaushik

   J. of Non-Crystalline Solids **2019,** 510, 172-178.
3. Simultaneous quantification of low Z elements in phosphorous containing alkali borosilicate glass samples by in situ current normalized External (in air) PIGE method utilizing proton beam from FOTIA, **Amrita Dhara Prakash**, R.K. Mishra, T.P. Valsala, V. Sharma, R. Acharya, A.K. Tyagi, P.K. Pujari, C.P. Kaushik

   J. of Radioanal. Nucl. Chem. **2021,** 328, 519-526.

b. Symposium presentations (5)

1. Effect of Al_2O_3 on structural properties of sodium borosilicate glass and barium sodium borosilicate glass, **Amrita Dhara**, R.K. Mishra, T.P. Valsala, V. Sudarsan, A.K. Tyagi, C.P. Kaushik

   Symposium on Recent Advances in Nuclear Fuel Cycle Activities (NUFUC– 2015) organised by IANCAS, Tarapur Chapter in association with BRNS.
2. Effect of aluminium oxide and barium oxide on leaching behaviour of sodium borosilicate glasses, **Amrita Dhara**, R. K. Mishra, V. K. Mittal, T. P. Valsala, A. K. Tyagi, C. P. Kaushik

   International symposium on emerging trends in Analytical Chemistry (ETAC-2016), by AMD.

3. Effect of addition of MoO_3 on glass transition temperature of SiO_2-B_2O_3-P_2O_5 glass,

   Amrita Dhara Prakash, R. K. Mishra, V. K. Mittal, T. P. Valsala, A. K. Tyagi, C. P. Kaushik

   Symposium on Recent Advances in Nuclear Fuel Cycle Activities (NUFUC-2018), organised by IANCAS, Tarapur Chapter, pp-88-89.

4. Investigation of Solubility of Chromium in borosilicate glass using XRD,

   Amrita Dhara Prakash, R. K. Mishra, T. P. Valsala, A. K. Tyagi, C. P. Kaushik

   Symposium on Nuclear and Radiochemistry (NUCAR-2019), organised by BARC, pp-123.

5. Compositional characterization of phosphorous containing alkali borosilicate glass by quantifying low Z elements using in situ current normalized external (in air) PIGE method,

   Amrita Dhara Prakash, R. Acharya, V. Sharma, R. K. Mishra, T. P. Valsala, A. K. Tyagi, C P. Kaushik

   International Conference on Modern Trends in Activation Analysis (MTAA-15) in 2020, Organised by BARC, pp-169.

Amrita Dhara Prakash

ACKNOWLEDGEMENTS

I take a highly esteemed privilege to express my deep sense of gratitude to my research guide and mentor **Prof. C. P. Kaushik**, Associate Director, NRG, BARC, for his invaluable guidance during the thesis work. It is my pleasure to express my gratitude to **Prof. B. S. Tomar** for his encouragement and support and **Prof. A. K. Tyagi** Associate Director, CG, my co-guide for his constant guidance and enormous effort for timely submission of this dissertation. I express my deep gratitude to **Dr. N. L. Mishra, Dr. V. Sudarsan** ChD and **Dr. T. P. Valsala** Superintendent Laboratory FF for support and guidance for conducting various experiments. Their continuous efforts has sharpened this work. I sincerely acknowledge **Dr R. K. Mishra** WIP for his continuous guidance and valuable suggestions at each and every stages of the work.

I take this opportunity to thank **Dr. R. Acharya, Dr. Sangita Dhara Lenka, Dr. R. K. Lenka, Dr. Arnab Sarkar, Mr. Manjeet Singh and Mr. Vishal Sharma** in excecuting my work. I would also like to thank **Dr V. K. Mittal, Mrs. Vaishali De, Mr. D. A. Thakur** and other colleagues of Analytical Lab FF for extending support and help during the thesis work.

Last but not least, I would like to offer my whole-hearted indebtedness to my **family** and my husband for motivating me to complete the work. Special thanks to my parents, parents-in-law, sister and brother-in-law. I would also like to thank my newly born son **Tanush** who is the reason behind my positive attitude in spite of all the challenges.

I express my gratitude towards HBNI under whose auspices this dissertation work was carried out.

Amrita Dhara Prakash

TABLE OF CONTENTS

Chapter 1

Chapter 2

3.2. Experimental Details

3.3. Results and Discussion

3.3.2. MAS-NMR investigations

Chapter 4

4.2. Experimental Details

4.3. Results and Discussion

Chapter 7

SYNOPSIS

Development of society, rapid industrialization, population growth etc. lead to growing energy demand. Nuclear energy serves as a good option to meet this rising demand causing least impact on environment. However, growth of nuclear energy for various societal applications depends on proper management of radioactive waste. Unlike the waste generated from hospitals, industries, educational institutes, house hold activities etc., the waste from nuclear reactors/facilities are quite different and need to be processed based on well-established guidelines given by national and international agencies. As the number of nuclear facilities are increasing and technologies are rapidly advancing, nature of waste generated changes significantly and this demands newer and improved methods and technologies for their management.

Nuclear waste originates from the Nuclear Fuel Cycle (NFC) facilities, Non-Nuclear Fuel Cycle (Non-NFC) facilities and nuclear accidents [1]. The Nuclear Fuel Cycle (NFC) waste originate from a) the front-end, b) the reactor and c) the back end facilities. Isotope production, medical diagnoses, radiotherapy, research/ industrial applications and defense/military applications are associated with Non-Nuclear Fuel Cycle (Non-NFC) activities. Nuclear waste can be categorized as high level, intermediate level or low level depending up on its radioactivity concentration. Also depending on physical form, volume and extent of radioactivity, the methodology of handling waste differs. High Level Liquid Waste (HLW) originates from reprocessing of spent fuel [2]. The treatment of HLW involves immobilizing the radionuclides in a suitable matrix. Glass matrices are very popular as they exhibit solubility for a wide range of elements [3] and are extensively used for immobilization of a variety of radionuclide. Glass preparation is quite simple and can be carried out easily under remote handling conditions. Many glass matrices are chemically durable, corrosion resistant and exhibit long term integrity. These properties of glass matrices enable them for immobilization of HLW.

Although borosilicate glass matrix is an excellent host for immobilization of HLW, there are certain gap areas that need to be addressed. Borosilicate glass matrix shows good solubility for a wide range of elements. Solubility of transition metals, noble metals, lanthanide ions etc. in the matrix is quite limited. Hence, suitable additives are incorporated in the base-glass matrix to improve the solubility [4].

The present work focuses on management of HLW originating from 2nd and 3rd stage reactors. Depending on composition of HLW, base-glass composition needs to be suitably modified. To get an insight regarding the nature and extent of modification required in the glass, interaction of different components present in the waste with glass is investigated in detail. For example, in third stage of nuclear programme aluminum is likely to be used during the reprocessing of spent nuclear fuels. In view of this, in the present work the effect of Al_2O_3 addition on the structural aspects of borosilicate glasses has been investigated in detail. In a similar manner solubility of elements such as Mo and Cr in base borosilicate glass is studied extensively for effective management of nuclear waste. The introduction, experimental techniques and detailed studies carried out are described in seven chapters. The layout and content of these chapters are briefly given as follows.

CHAPTER 1

Introduction

This chapter gives an overview on nuclear energy, India's three stage nuclear programme, types of nuclear waste and challenges faced in this field. This chapter also discusses various processes adopted for management of nuclear waste, various matrices for immobilization of High Level Liquid Waste (HLW) etc. Presently HLW originating from reprocessing of PHWR spent fuel is immobilized in borosilicate glass matrix [5]. However, certain elements that show very poor solubility in borosilicate glass and are present in excess in HLW originating from 2nd and 3rd stage reactor requires a base-glass with modified composition and properties [6]. The nature of HLW and the problems associated with incorporation of elements of low solubility in borosilicate glass matrix are discussed in this chapter. Finally, the scope of the present work is discussed.

CHAPTER 2

Instrumental techniques and experimental methods

The technique adopted for synthesis of glass samples and basic principles of various instrumental techniques used for their characterization are presented in this chapter. All the glass forming chemicals were weighed accurately and the corresponding glass samples were prepared by melt quench method. Details of this method are discussed in this chapter.

Various instrumental techniques used for characterization of the samples are described briefly. X-ray Diffraction (XRD) was used to detect the presence of crystalline phase in glass samples. As the radioisotopes emit decay heat, glass transition temperature becomes an important parameter in determining thermal stability of glass. Differential Thermal Analysis (DTA) was used to evaluate glass transition temperature (Tg) of the samples. Particle morphologies over micrometer scales were investigated by Scanning Electron Microscopic (SEM) technique. Magic Angle Spinning Nuclear Magnetic Resonance (MAS-NMR) technique was used to study the changes in glass structure brought about by different additives.

Laser Induced Breakdown Spectroscopy (LIBS) was used for compositional characterization of the samples. Proton/Particle Induced Gamma Emission (PIGE) was also employed to quantify the samples for low atomic number elements. Leaching behavior of the glass samples were also studied for individual elements using Inductively Coupled Plasma – Atomic Emission Spectroscopy (ICP-AES). The complete procedure for making glass samples, evaluation of leaching behavior and details of all the experimental techniques employed are provided in this chapter.

CHAPTER 3

Effect of Al_2O_3 in borosilicate glass

This chapter deals with studies on the effect of Al_2O_3 addition in two different sets of borosilicate base glasses. Aluminum ions/species are expected to be present in HLW generated from the reprocessing of spent fuel of futuristic thoria-based reactors. Dissolution of thoria-based spent fuel requires hydrofluric acid. In order to precipitate the corrosive fluoride ions, $Al(NO_3)_3$ is added [7]. In this chapter, effect of Al_2O_3 addition on the structural aspects and thermal properties of sodium borosilicate and barium borosilicate glasses is presented

Sodium borosilicate and barium containing sodium borosilicate glasses having 0, 5, 10 and 15 mol% of Al_2O_3 were prepared by conventional melt-quench method. X-ray diffraction (XRD) patterns indicated that all the glass samples were completely amorphous without the presence of any crystalline phases. Structural studies using ^{29}Si, ^{27}Al, ^{11}B MAS-NMR techniques revealed that Al exists as AlO_4^- structural units with Si-O-Al type of linkages in all the glass samples. ^{11}B MAS-NMR studies revealed that in barium borosilicate glass there is an increased extent of BO_4^- structural units compared to sodium borosilicate glass. Using the Dell and Bray model different types of boron and silicon structural units present in the glass samples have been identified. The relative concentration of BO_3 and BO_4^- structural units evaluated from ^{11}B MAS-NMR patterns match well with that predicted by Dell and Bray model.

Differential Thermal Analysis (DTA) studies revealed that with addition of Al_2O_3, glass transition temperature (Tg) decreases. DTA studies also showed that glass transition temperature of barium borosilicate glass is higher compared to that of sodium borosilicate glass. All the results are discussed in detail in this chapter. Chemical durability of the glass samples was evaluated by semi-dynamic leaching experiments. The tests were performed for a period of 75 days at a temperature of 70°C using Demineralized Water (DM) as leachant. The elemental release in the leachant was quantified using ICP-AES technique. The leach rates of individual elements are discussed in this chapter.

CHAPTER 4

Study on enhancement of solubility of MoO_3 and CrO_3 in modified borosilicate glass

Certain elements present in HLW display limited solubility in borosilicate glass. Results on two such elements namely Mo and Cr are presented in this chapter. Molybdenum is a fission product with a high fission yield (7.6 atom%) in Fast Breeder Test Reactor (FBTR) [8]. Solubility of MoO_3 in sodium borosilicate glass is 1mol% and beyond this concentration Mo separates out from the glass structure in the form of alkali molybdate [9]. As Mo is most stable in +6 oxidation state MoO_4^{2-} species are formed within the glass. Further as Mo-O-Si bond is unstable owing to higher valency ion attached with oxygen atom, this bond breaks and hence alkali molybdate phase separates out from the glass [9]. Presence of Cr in HLW arises from stainless steel (SS) which is used for storing liquid waste, transfer pipelines and also as process vessels in various stages of reactor operation, reprocessing and waste management [10]. Exposure to high radiation, temperature, acid concentration over a long period of time accelerates corrosion rate of SS. Thus, Cr gets introduced in HLW as corrosion product. Cr in borosilicate glass can exist in +3 or +6 oxidation state [11]. Based on glass composition, thermal characteristics and oxidation state of Cr, various crystalline phases such as Na_2CrO_4, $NaCrSi_2O_6$, and Cr_2O_3 are formed in the borosilicate glass matrix beyond a concentration of 2mol% of CrO_3 [12]. Enhancement in solubility of MoO_3 and CrO_3 in modified sodium borosilicate glass is discussed in detail in this chapter.

Around 5 mol% P_2O_5 was added to sodium borosilicate glass to increase the solubility of MoO_3 and CrO_3. Generally, presence of phosphate-based glass matrix or phosphate structural units in borosilicate glass leads to an enhanced solubility for Mo and Cr. Two series of glass samples were prepared. One consisted of 1, 2, 3 and 4 mol% of MoO_3 and other series contained 1, 2, 3 and 4 mol% of CrO_3. XRD patterns confirmed that 4 mol% of MoO_3 and CrO_3 could be incorporated in the modified base glass without any phase separation. Phosphate containing base glass having as much as 4 mol% of MoO_3 and CrO_3 are completely amorphous in nature whereas, in the absence of P_2O_5, glass samples containing as low as 2mol % MoO_3 and 2.5mol% CrO_3 showed presence of various crystalline phases. SEM-EDS studies were performed to observe the microstructure of the sample. LIBS was used for quantification of Mo and Cr whereas PIGE was used for quantification of Si, B, P, Na in the glass samples. In LIBS experiments, due to absence of matrix matched standard, Si being the major element was chosen as internal standard. Variation of Mo/Si intensity was plotted against the Mo/Si mole fraction for all the samples. A linear increase in the intensity ratio with respect to concentration ratio (mole fraction) clearly reveals a proportional increase of Mo in the glass samples validating the composition. Alternatively, calibration curves were constructed from the emission lines of Mo and Cr after normalizing the same with respect to total light or whole spectrum area. Multivariate calibration model was applied for better results. Accuracy and precision for both Mo and Cr estimation was found to be 3-5%. PIGE data revealed that the concentrations of three major elements (Si, Na and B) in the glass are fairly in agreement with that of starting materials taken prior to glass preparation. In case of phosphorous, obtained results are found to be always 2-4% lower than the expected amount.

Glass samples containing both Mo and Cr in the same sample were also prepared. However, the samples were prepared in such way that the total concentration of Mo and Cr together was 4mol%. XRD studies were carried out to check for the formation of any crystalline phases in the samples due to the simultaneous presence of two elements. There were no sharp peaks in the XRD patterns corresponding to any of these samples confirming the absence of crystalline phase. LIBS studies were carried out for quantification of Mo and Cr in these samples.

CHAPTER 5

Study of thermal and chemical durability of MoO_3 and CrO_3 containing glasses

Additives generally modify the structure of glass as well as its physico-chemical properties such as glass transition temperature, thermal expansion coefficient, chemical durability etc. [13]. This chapter provides the glass transition temperature (Tg) data and the leach rate data of all the elements present in the glass samples. Glass transition temperature was measured for all the glass samples to understand the influence of MoO_3 and CrO_3 on thermal stability. It was observed that in borosilicate glass without P_2O_5, Tg increases on addition of Mo and Cr. It was also observed that addition of P_2O_5 reduces the Tg of borosilicate glass and addition of MoO_3 or CrO_3 decreases it further. However, the magnitude of this decrease of Tg in CrO_3 containing glass samples is higher compared to MoO_3 containing glass samples. All the experimental findings are explained in detail in this chapter. Leaching experiment was conducted for monitoring the chemical durability of the glass samples. The tests were performed for a period of 90 days.

The changes in leach rate of all the elements with respect to that of phosphorous, molybdenum and chromium are explained in detail in this chapter.

CHAPTER 6

Study of solubility of simulated HLW in modified borosilicate glass

In this chapter loading of HLW in phosphate modified borosilicate glass is compared to borosilicate base glass without phosphate. This HLW contains higher amount of MoO_3 and CrO_3, the details of the origin of this HLW is provided in this chapter. Total of six product glasses were prepared with different amount of base glass to HLW ratio. All the glass samples were analysed using XRD. Some glass samples showed visible phase separation. In borosilicate base-glass without phosphate, XRD patterns revealed presence of $BaCrO_4$ and Cr_2O_3 crystalline phases when waste oxide was increased to 27 wt%, whereas in phosphate modified base glass, crystalline phases such as Pyroxene, Powellite and Spinel crystalline phases were observed in glass sample containing 33 wt% waste oxide.

CHAPTER 7

Conclusions and future scope

Conclusion of studies mentioned in chapter 3 to 6 are described briefly in this chapter. Borosilicate glasses are attractive candidates for immobilization of HLW for a number of reasons. However, these glasses suffer from poor solubility of transition metal oxide and lanthanide ions. The present study is an attempt to understand and improve the waste immobilisation characteristics of borosilicate glasses. Keeping this in mind modified glass matrices were prepared and studied in detail. Various instrumental techniques helped to understand structural changes in the matrix which would be helpful for optimising the glass composition or formulation for optimum waste loading.

The effect of aluminum on structural, thermal and chemical properties of sodium borosilicate and barium borosilicate glasses were investigated in detail. In an attempt to increase the solubility of MoO_3 and CrO_3, a modified borosilicate glass with P_2O_5 was formulated. Homogeneity of these glass samples with respect to Mo and Cr was confirmed using LIBS technique. Incorporation of phosphate into borosilicate glass helps in immobilizing Mo and Cr into the glass matrix. However, thermal stability (glass transition temperature) degrades due to introduction of phosphate as well as MoO_3 and CrO_3 into the glass matrix.

The study on modified borosilicate glass is intended to enhance the solubility of different constituents. Data on thermal and chemical durability of these glasses will be beneficial for development of base glass for immobilization of HLW originating from futuristic reactors.

Future scope:

- Solubility of various other low soluble constituents in modified borosilicate glass needs to be investigated.
- Evaluation of compatibility of other HLW stream with the modified borosilicate glass needs to be studied.
- Radiation stability of the developed product glass is to be established.

LIST OF FIGURES

LIST OF TABLES

CHAPTER 1

Introduction

The world is expanding in terms of population, demands and innovations. With ever increasing demand comes the need of energy. The requirement of energy for everyday work has become indispensable. It is a means to improve the quality of life, economically and socially. All day-to-day activities like education, healthcare, cooking, running household appliances and industrial appliances, transportation etc. cannot be imagined without energy. However, the sources of energies are limited and are categorized under renewable and non-renewable sources. Renewable energy sources are available in plenty in nature, are continuously getting created and are inexhaustible like solar, wind, tidal etc. and non-renewable sources like coal, oil, natural gas, nuclear power, timber etc. have accumulated over a period of time and will eventually get exhausted [1]. Using renewable sources of energy for power production generates lower amount of greenhouse gases and cause less pollution but the limitation comes in their location specificity, storage capabilities etc. Whereas non-renewable sources of energy are easy to convert into power, store and use but comes with a price of pollution and emission of green-house gases [2]. Fig. 1.1. shows a graphical representation of CO_2 produced by various energy sectors. This report was released by university of Texas in the year 2020, it revealed that for production of 1kWh power, CO_2 produced by thermal power plants is 850g, solar power is 48g and nuclear power plants is 12g [3, 4]. Therefore, it is a challenge to create a sustainable future i.e. optimizing the demand of energy around the globe without substantially effecting the climate and thankfully nuclear energy serves as a boon in this regard. Therefore, transition from using fossil fuel to nuclear fuel is the need of the hour in achieving lower greenhouse gases emissions.

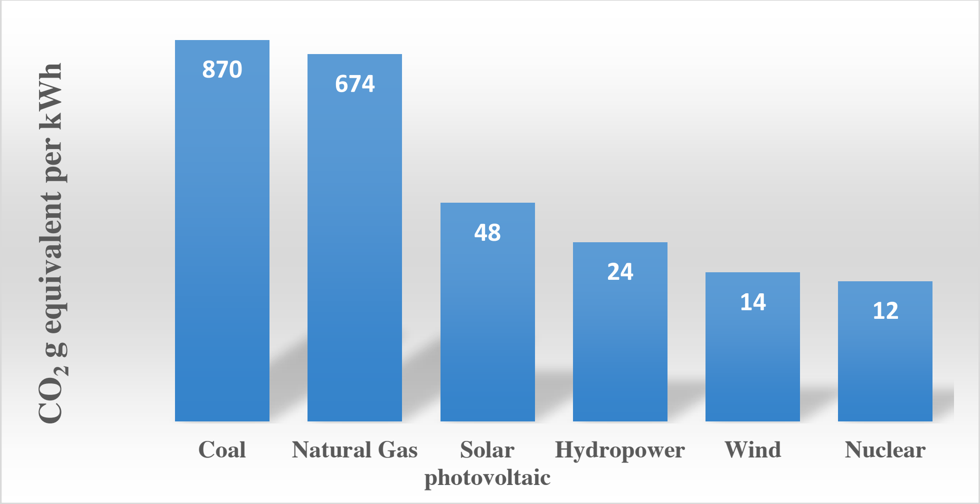

Figure 1.1. CO_2 production by various energy sectors [4]

1.1. Nuclear energy

Nuclear energy is a clean source of energy well known for its numerous societal applications. Power production, agriculture, medicine, food technology etc. are rapidly expanding their dimension with the use of nuclear energy [5]. With increasing population and rising demand, there is more and more dependency on nuclear energy.

India has made tremendous progress in the field of nuclear energy. In India nuclear power is the fifth-largest source of electricity. As of February 2021, India has 23 nuclear reactors under operation of which 2 are Boiling Water Reactors (BWR), 19 are Pressurized Heavy Water Reactor (PHWR) and 2 are Vodo-Vodyanoi Energetichesky Reaktor i.e. water-water power reactor (VVER), all together having a total installed capacity of 7,480 MW [6]. Apart from this, 8 more reactors are under construction with a combined generation capacity of 6,000 MW.

However, India’s dependency on nuclear energy for electricity production is lower compared to countries like France and Germany (Fig. 1.2) [7].

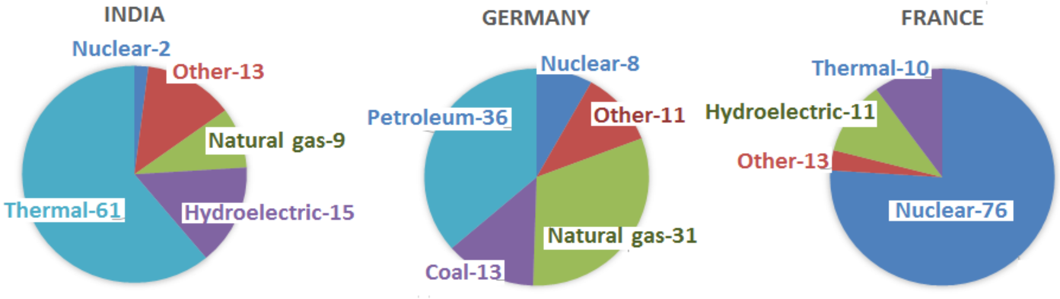

Figure 1.2. Dependency of electricity production on various energy sources [7]

According to a survey, the uranium reserves of India are not plenty. India has only around 1–2% of the global uranium reserves nonetheless, thorium reserves are vast consisting of 25% of the world's share [8]. With the idea to utilize thorium, India has opted for three-stage nuclear power program. The first stage consists of natural uranium fueled Pressurized Heavy Water Reactor (PHWR) using heavy water as moderator and coolant. The second stage comprising of Fast Breeder Reactor (FBR) that uses mixed oxide fuel of Pu-239 (reprocessed from stage 1) and natural uranium. FBR shall generate sufficient fissile material from thorium that will be utilized as fuel in the third stage of thermal breeder reactors- Advanced Heavy Water Reactor (AHWR) [9]. Thorium is a fertile material and therefore it has to be transmuted to uranium-233 in the second stage reactor [10]. The basic outline of this programme is shown in Fig. 1.3.

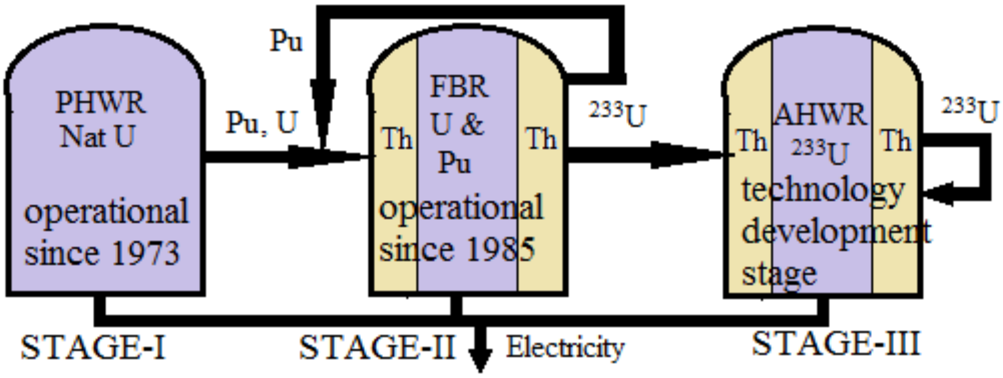

Figure 1.3. Indian three stage nuclear power programme

However, the use of nuclear power for societal applications has generated a debate about the safety and risks associated [11]. The acceptance of nuclear energy largely relies on safe handling of nuclear energy and proper management of nuclear waste so that not only the present but the future generations are secured as well.

1.2. Nuclear waste

Nuclear waste can be defined as any unwanted material that is containing radioactivity above permissible limit set by various atomic energy agencies [12]. Any facility that deals with radioisotopes generate nuclear waste. They are generated not only from nuclear reactors, front end and back end facilities of nuclear fuel cycle, but also from research centres, medical centres, hospitals, etc. [36]. In India, AERB (Atomic Energy Regulatory Board) regulates the disposal of radioactive wastes under Atomic Energy (Safe Disposal of Radioactive Wastes) Rules, 1987. AERB has issued guidelines for management of spent radioactive sources and radioactive waste that are arising from usage of radionuclides in medicine, industry, research centres and including decommissioning of such facilities. These guidelines are:

1. Protection of Human Health and Environment: Radioactive waste shall be managed in such a way as to provide an acceptable level of protection for human health and the environment.
2. Concern for Future Generations: Radioactive waste shall be managed in such a way that it will not impose undue burden on future generations and its predicted impact on the health of future generations will not be greater than relevant levels of impact that are acceptable today.
3. Establishing Legal Framework: Radioactive waste shall be managed within an appropriate legal framework including clear allocation of responsibilities and provision for independent regulatory functions.
4. Waste Minimisation, Management Interdependency and Safety of Facilities: Generation of radioactive waste shall be kept to the minimum practicable level. Interdependency among all steps in radioactive waste generation and management shall be taken into account. The safety of facilities for radioactive waste management shall be assured during their lifetime.

1.3. Categorization of waste and philosophies adopted to manage radioactive waste

Depending on nature of waste, the treatment methodology adopted also changes. Based on physical state of waste they are classified as solid, liquid and gases. Based on nature of waste i.e. radioactivity level, they are classified as low level, intermediate level and high level waste. Categorization of nuclear waste formulated by AERB is given in Table 1.1.

Table 1.1. Categorization of nuclear radioactive waste

Category	Solid (mGy/hr)	Liquid (Bq/m^3)	Gaseous (Bq/m^3)
I	<2	<3.7x10^4	<3.7
II	2-20	3.7x10^4-3.7x10^7	3.7-3.7x10^4
III	>20	3.7x10^7-3.7x10^9	>3.7x10^4
IV	Alpha Bearing	3.7x10^9-3.7x10^{14}	
V		>3.7x10^{14}	

The four principles adopted in management of liquid radioactive waste are as follows:

I. Delay and decay

II. Dilute and disperse

III. Concentrate and contain

IV. Recover and reuse.

In addition to radioactivity level or concentration, the volume of waste and presence of short or long-lived radioisotopes play a significant role in determining the methodology that should be adopted in their treatment. When the activity levels are around the discharge limit, liquid waste is diluted and dispersed. When the activity is due to short lived radioisotopes (^{106}Ru $t_{1/2}$- 1year, ^{95}Zr $t_{1/2}$- 65 days, ^{131}I $t_{1/2}$- 8 days), delay and decay methodology is adopted. Usually for treatment of liquid waste with low or intermediate activity level, chemical treatment, thermal evaporation, ion-exchange, membrane-based separations are adopted [12, 13]. Gaseous waste is passed through high efficiency filters like High Efficiency Particulate Air (HEPA) filter. Low level gaseous waste are subjected to scrubbing and solid waste are compacted or incinerated. Certain Intermediate Level Liquid

Waste (ILW) are immobilized in cement. In Tarapur India, ILW is passed through Resorsinol Formaldehyde Polycondensate Resin (RFPR) to separate Cs-137 which comprises of more than 90% of the activity of intermediate level waste [14]. Thus, segregating the waste into High Level Liquid Waste (HLW) comprising of Cs-137 and Low-level Liquid Waste (LLW) comprising of other radioisotopes having minimal activity. Useful radioisotopes like ^{137}Cs, ^{106}Ru, ^{241}Am are recovered from nuclear waste and they are used as blood irradiator, nuclear medicine, Radioisotope Thermoelectric Generator (RTG) etc. HLW is treated under concentrate and confine philosophy. HLW is immobilized in a suitable matrix and is stored in such a way that it is confined and isolated from people and environment [15]. The most commonly used matrix for immobilization of HLW is a glass matrix. A brief summary of treatment methodologies of nuclear waste is provided in Table 1.2.

Table 1.2. Various treatment methodologies of nuclear waste

	Low	**Intermediate**	**High**
Treatment Methodologies			
Solid	Compaction/ Incineration	Size Fragmentation/ Compaction/ Incineration	Repacking
Liquid	Chemical Treatment/ reverse osmosis/ Evaporation	Ion Exchange	solvent extraction/ vitrification
Gaseous	Absorption/ Adsorption/ Scrubbing	Prefilteration	High efficiency filteration like (HEPA)
Conditioning	Cementation /Polymerization		Vitrification

Most of the radioactivity of an entire nuclear fuel cycle is concentrated in HLW. Therefore, for long term management of HLW a three step strategy is adopted in India. The steps are as follows:

a) Immobilization: HLW is immobilized in a suitable matrix. In India, borosilicate glass matrix is used for immobilization. This is performed in an induction based metallic melter in Trombay and in a joule heated ceramic melter in Tarapur and Kalpakkam. Cold crucible ceramic melter is also an emerging technique under study for immobilization of HLW. This vitrified mass is transferred into a cask and further into an overpack (Fig.1. 4(a)).

b) An interim storage facility: These overpacks are stored in interim storage facility for a definite period. Here the processed waste is under continuous cooling and surveillance. This facility is operational in Tarapur (Fig. 1. 4(b))

c) Geological repository: Geological repository is a site where final disposal or storage of these highly radioactive processed waste will be done to ensure complete isolation from biosphere.

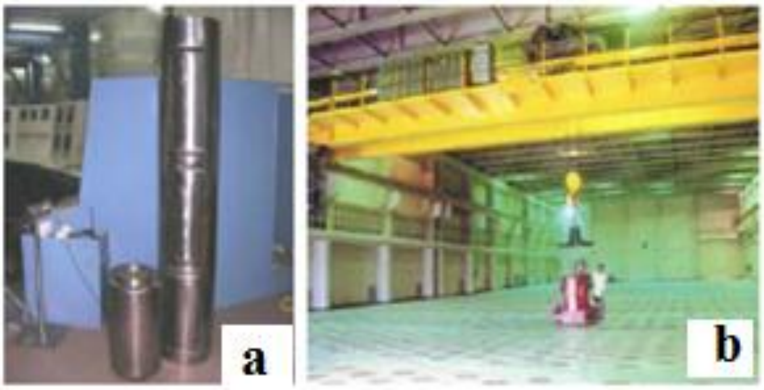

Figure 1.4 (a) canister and overpack (b) solid storage surveillance facility, Tarapur

1.4. High Level Liquid Waste-its generation and treatment

India has adopted for closed fuel cycle approach, where the reprocessing of spent fuel is carried out [16]. The spent nuclear fuel from PHWR are taken up for reprocessing to retrieve uranium and plutonium for using as fuel in second stage of reactors. PUREX (Plutonium Uranium Reduction Extraction) an aqueous separation technique, is a well adopted technology currently used in India, for reprocessing of spent fuel [17]. In brief, after dissolving the spent fuel in 8M HNO_3, 30% TBP in Dodecane is used as solvent for selectively extracting U and Pu. The remaining constituents present in the raffinate is termed as HLW. The main components of HLW are:

- Fission Products (^{137}Cs, ^{90}Sr, ^{106}Ru, ^{144}Ce etc.)
- Actinides (^{241}Am, ^{237}Np, ^{244}Cm etc.)
- Unrecovered U and Pu
- Corrosion Products (Fe, Ni, Cr, Mn etc.)
- Added Chemicals (e.g. HNO_3, traces of TBP and its degradation products, $NaNO_3$, SO_4^{2-} etc.)
- Soluble neutron poisons such as Gd, B and Cd etc.
- Gross α - β - γ activity (>1Ci/L)

The U and Pu extracted in first cycle is separated and again extracted using 30% TBP followed by further purification.

Treatment of HLW is challenging for various reasons. They are highly radioactive containing huge spectrum of elements. Many radioisotopes are long lived like ^{239}Pu ($t_{1/2}$- 24360 years), ^{99}Tc ($t_{1/2}$- 2x10^5 years) ^{129}I ($t_{1/2}$ -1.7x10^7 years) some have long biological half-life for example Sr-90 ($t_{1/2}$(biological) -49 years) biological half-life refers to time taken for the body to natural excrete the radioisotope, thus requiring remote handling in every step. Half-lives of long lived and medium lived radioisotopes present in HLW are presented in Table 1.3.

Table 1.3. Half-lives of fission products and transuranics

Fission products		**Transuranics**	
Isotopes	**Half-life (years)**	**Isotopes**	**Half-life (years)**
^{90}Sr	28	^{236}Np	1.2×10^{5}
^{137}Cs	30	^{237}Np	2.1×10^{7}
^{99}Tc	2.11×10^{5}	^{238}Np	2.11 days
^{126}Sn	2.3×10^{5}	^{239}Pu	2.4×10^{4}
^{79}Se	3.27×10^{5}	^{240}Pu	6.56×10^{3}
^{93}Zr	1.53×10^{6}	^{241}Pu	14.35
^{135}Cs	2.3×10^{6}	^{242}Pu	3.76×10^{5}
^{107}Pd	6.5×10^{6}	^{244}Pu	8.2×10^{7}
^{129}I	1.57×10^{7}	^{241}Am	432
^{87}Rb	4.89×10^{9}	^{243}Am	7.37×10^{3}
^{147}Sm	1.06×10^{11}	^{245}Cm	8.5×10^{3}
^{148}Sm	7.0×10^{15}	^{246}Cm	4.78×10^{3}
^{149}Sm	1.0×10^{16}	^{247}Cm	1.58×10^{7}
		^{248}Cm	3.4×10^{5}

Nuclear scientist around the globe have come up with numerous matrices to immobilize these troublesome wastes. The idea behind immobilizing HLW is to prevent escape of radioisotopes into the biosphere, reduce volume, easy handling and storage. The IAEA defines immobilisation as the conversion of a waste into a waste form by solidification, embedding or encapsulation [18]. Various matrices are envisaged as a potential host to immobilize HLW. Borosilicate glass, phosphate glass, glass ceramics, single crystalline and polycrystalline minerals, FUETAP (Formed Under Elevated Temperature and Pressure), vitromet etc. are among them. Immobilization of waste is achieved by two processes a) encapsulation, b) chemical incorporation [19].

A) Encapsulation: The matrix material entraps the radioisotopes within the voids or the grain boundary.

B) Chemical incorporation: The radioisotopes bond to the matrix elements. Chemical incorporation provides better durability to matrix structure.

1.5. Various matrices for HLW immobilization in brief

1.5.1. Crystalline materials

A material is said to be crystalline when it contains regular three-dimensional array of atoms. This regular arrangement is long range in order. They are thermodynamically stable offering a merit of being able to retain radioisotopes for millions of years. The crystalline materials can be single phasic or multi phasic. The single phasic ceramics like Zircon: $ZrSiO_4$, Zirconolite: $CaZrTi_2O_7$, etc. are beneficial when coming to immobilizing single radioisotopes. The multiphasic matrix can accommodate various radioisotopes in individual phases. The most famous polyphasic crystalline material for nuclear waste immobilization is Synroc (combination of various titanate minerals like Zirconolite, Perovskite: $CaTiO_3$ and Hollandite: $BaA1_2TiO_{16}$) [20]. Actinides occupy the Zirconolite phase in which trivalent actinides occupy Ca site, while tetravalent elements occupy Zr site, Hollandite retains fission products like Cs, Rb, Ba and perovskite retains Sr, Np and Pu. US Department of Energy opted for Synroc for treatment of approximately 4400m^3 of calcined reprocessed HLW, which was very heterogeneous in nature and consisted of components that were problematic to incorporate in glass.

UK Nuclear decommissioning authority has selected Synroc for plutonium containing waste. This waste was derived from early fuel developmental activities. However, the immobilization sites are very specific in nature and also the requirement of stringent conditions to prepare these crystals pose disadvantage.

1.5.2. Glass ceramic

In this form crystalline phases are encapsulated into a vitreous matrix or vitreous phase is embedded in crystalline matrix [21]. Since it contains both crystalline and amorphous phases within same material, they contain properties of both. They have higher thermal and mechanical stabilities, are more durable than glass but are difficult and costlier to prepare than glass. Whiteshell nuclear research establishment in Canada and Hahn Meitner institute in Berlin have developed a glass ceramic consisting of sphene ($CaTiSiO_5$) crystals, within a matrix of alumino-silicate glass. Actinides and Sr can be accomodated in the sphene crystals whereas the remaining larger radionuclides remain in the glass matrix.

1.5.3. Vitromet

Vitromet is another potential host that can immobilize HLW. Vitromet is composite material where the host matrix is lead and globules of nuclear waste embedded in glass is dispersed within the matrix. The slow corrosion of lead results in good retention properties for radionuclides [22]. For example in PAMELA (Process for Advanced Management of End of Life of Aircraft) process, in France, glass beads containing HLW were made and were fed into a container with molten lead alloy (Pb-Sn). The beads were of diameter 50mm and occupied 66% of total waste volume. In addition to lead, Al-based alloys (e.g. Al along with Si, Cu, Ti) and Cu are also used [23].

1.5.4. FUETAP

FUETAP (Formed Under Elevated Temperature and Pressure) is a concrete structure to contain HLW [21]. It was developed by Oak-Ridge National Laboratory and the Pennsylvania State University. It uses the inherent heat of the radionuclides and external heat sources to drive off up to 98% of the unbound water to form a hard, dense product of improved physical properties.

1.5.5. Glass

The most popularly used matrix for immobilization of HLW is glass. Glass is an amorphous material that lacks long range order as seen in crystalline solids. In general, glass is defined as a solid that is formed by rapid melt quenching. In this approach, HLW is mixed with suitable base glass, resulting in final product glass where radioisotopes get entrapped within the glass matrix.

1.6. Glass - a potential matrix - structure and properties

Vitrification of HLW is attractive for number of reasons. The open structure of glass allows accommodation of a wide range of elements, it is possible to design glass compositions which are tolerant to compositional variations in the waste stream. The most common glass matrix used for vitrification are two inorganic oxide glass, namely borosilicate glass containing $(SiO_4)^{4-}$, $(BO_4)^{5-}$, $(BO_3)^{3-}$ units and phosphate glass containing $(PO_4)^{3-}$ units. The final composition of product glass i.e. mixture of base glass and HLW is designed in such a way that it facilitates easy preparation, avoids phase separation or crystal formation without compromising on durability. The stability or strength of glass structure depends on how polymerized or interconnected the structure is. The glass forming material plays a vital role in determining the strength and processing temperature of glass. Certain inorganic oxides help in glass network formation whereas certain oxides result in depolymerization or breakage of glass network. Zachariasen in the year 1932 formulated set of rules for in an inorganic glass oxide (A_mO_n), the rules are as follows:

(1) Oxygen atom may be linked to no more than two A atoms.

(2) The number of oxygen atoms surrounding A atoms must be small.

(3) The oxygen polyhedra share only comers with each other, but not edges nor faces [24].

The rules state that corner sharing polyhedra provides a flexibility to A-O-A bond which ensures loss of crystallinity for example the bond angle Si–O–Si in glass can range from 120 to 180^0 while in a perfect crystal-like quartz it is a constant 109. 28’ [25]. These rules also state that ionic compounds show long range order and hence they are face and edge sharing, therefore making them a bad candidate for glass formation on the other hand covalent compounds like SiO_4^{4-} shows corner sharing ability, hence lack long range order, being a good candidate for glass formation. These oxides that help in formation of glass are called glass network formers. The ionic oxides like Na_2O, BaO etc. are called network modifiers because their presence breaks the glass network bond resulting in a depolymerized structure. Presence of metals with high oxidation number like actinides and transition metals are also network modifiers. Fig. 1.5 shows the random network structure of glass. There are also a third kind of oxides network intermediates that work as both network former and modifier depending on its concentration and surrounding, for example Al_2O_3, TiO_2 etc. With increased degree of polymerization, the processing temperature also increases. Increased processing temperature would mean a much stronger and durable product glass but it comes with a drawback of complex processing route and releasing highly volatile radionuclides during glass processing. Therefore, during preparation of product glass an emphasis is laid on optimization of composition of network former and network modifier including waste oxide.

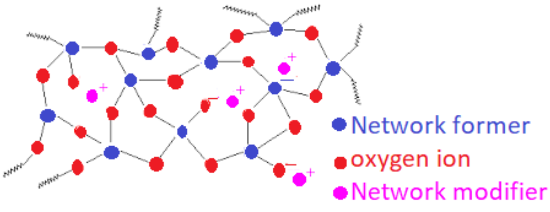

Figure 1.5. Random structure of glass network

Many studies have provided certain guiding principle for formulation of acceptable product glasses. Here are some of the important ratios that are considered during vitrification of borosilicate glass matrix [26].

Si/Al, B	>1.5	Chemical durability is better. However, the melting temperature of the glass increases as ratio increases
Oxygen/network formers	2.2-2.4	Glass formation is best and chemical durability
Network formers/network modifiers	2	This ratio should be 2 for good glass formation. As it decreases, the glass network is depolymerized and glass-forming ability decreases

The attractive properties of glasses that makes them the most chosen matrix worldwide are as follows:

- Incorporates wide range of radionuclides: the open random network of glass helps in incorporation of large spectrum of elements.
- Chemically durable: Chemical durability is a measure of how leachable the elements are. Their leach rate is low offering long term storage.
- Superior thermal and radiation stability
- Good thermal conductivity: Thermal conductivity is required so that the decay heat that is generated from the radioisotopes are dissipated.
- Provide high volume reduction
- Well established manufacturing technology
- Inexpensive raw materials

Although glass offers a number of desirable properties however there are many challenges related to incorporation of lower soluble radioisotopes into the glass matrix.

1.7. Plant scale vitrification- challenges associated with vitrification

HLW consists of a large number of elements and to add to its problem the composition of HLW does not remain constant always. Any change in reactor operation changes the fission product composition. With use of different types of fuel like ^{233}U, ^{235}U and ^{239}Pu the nature of fission products also varies. When compared to fission products produced in thermal reactors, in fast reactors the noble metals are of higher amount [27, 28]. The variation of fission yield curve (in atom%) against mass number for fuel type ^{233}U, ^{235}U and ^{239}Pu and reactor involving thermal and fast neutron is shown in Fig. 1.6. With increased burn-up of any reactor, the quantity of fission products also increases. Some other troublesome elements are the extra chemicals that get added in HLW during reprocessing. For example, in ThO_2 based fuel, Hydrofluoric acid (HF) is used for dissolution of the fuel and $Al(NO_3)_3$ is added to complex with the unreacted Fluorine (F) [29]. Thus, F and aluminum (Al) become the constituents of HLW. Due to radiation, heat and acidic environment throughout operation and reprocessing, corrosion products also get added up in HLW. Left over U and Pu after reprocessing and minor actinides also form a part of HLW.

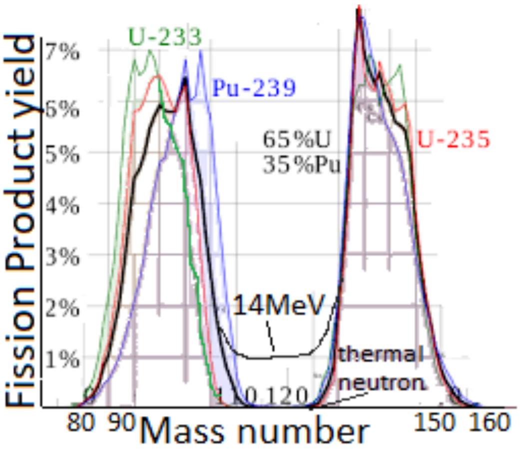

Figure 1.6. Fission yield curve with respect to mass number for ^{235}U, ^{233}U, ^{239}Pu, thermal and fast neutron

On one hand where some elements like boron, phosphorous, iron show excellent solubility (>15wt%) in borosilicate glass. On the other hand, noble metals, chromium, molybdenum, nickel shows very poor solubility (<3wt%) in borosilicate glass. At higher concentration these elements form a separate phase present either on the surface or within the glass matrix. These separate phases result in a number of undesirable properties. For example, many of these crystalline phases like Na_2MoO_4 are aqueous soluble, fission products like Cs exchange sites with Na and can easily get leached out of glass matrix [30]. Uneven thermal properties of crystalline phases and glass matrix result in cracks within the glass structure. All these properties compromise the chemical durability of glasses. The challenge lies in incorporating these elements in borosilicate glass matrix.

Numerous nuclear scientists are working world wide in formulating suitable base glass matrices to incorporate these troublesome elements present in HLW. To describe a few, sulphate ions exhibit very poor solubility in borosilicate glass, beyond a concentration of 1wt% a yellow phase separation is observed. A study was conducted to improve its solubility. The study revealed that addition of barium oxide to borosilicate glass increased its solubility [31]. Extension of same study revealed that addition of barium oxide to borosilicate glass enhanced that solubility of ThO_2 in borosilicate glass matrix. Similarly, Cs is very volatile and evaporates off easily during vitrification, a study showed that addition of TiO_2 to sodium borosilicate glass traps Cs into glass by forming Cs-titanate complexes [32]. Various works are reported on immobilizing another troublesome radionuclide i.e. ^{99}Tc in Iron-phosphate glass. ^{99}Tc rich waste stream are to be treated as HLW due to long half-life of ^{99}Tc ($2x10^5$years) and high mobility of $^{99}TcO_4^-$, but the high volatility of ^{99}Tc is cause for concern. Iron-phosphate glass having low melting temperature help in minimizing the evaporation losses.

1.8. Motivation for the present work

As discussed earlier, the constituents of HLW are not always constant and with changes in reactor and reprocessing operating parameter, the nature of HLW also changes. Present work is focused on enhancing the capability of borosilicate base glass in view of accommodation of certain troublesome elements. As discussed above, Al will serve as an additive when immobilizing HLW from Th based reactors. Therefore, a part of this work is about observing the effect of Al in two borosilicate glass systems, sodium borosilicate glass and barium containing sodium borosilicate glass. The structural information was obtained using Magic Angle Spinning Nuclear Magnetic Resonance (MAS-NMR) technique. The study also focused on improving the solubility of two troublesome HLW constituents i.e. Mo and Cr. The yield of Mo in Fast breeder reactor employing PuO_2 fuel is substantially higher, whereas its solubility in borosilicate glass is as low as 1wt% [33]. Cr also displays a very low solubility of 2wt% in borosilicate glass [34]. Cr in HLW is a result of corrosion of stainless steel (SS) material used in almost every part of reactor, reprocessing and storage [35]. In this work the borosilicate glass was formulated in such a way that it showed an increased solubility for Mo and Cr. Various analytical techniques like Laser Induced Breakdown Spectroscopy (LIBS), Particle Induced Gamma Emission (PIGE) and X-Ray Fluorescence (XRF) were employed for quantification of chemical composition of glass samples. Numerous glass samples were prepared in a furnace. X-Ray Diffraction (XRD) was employed for detection of crystalline phases in all the glass samples. This work also observed the thermal stability of glass with changes in composition. Differential Thermal Analysis (DTA) was carried out to determine the glass transition temperature. To study the chemical durability of glass samples numerous leaching experiments were conducted and Inductively Coupled Plasma- Atomic Emission Spectroscopy (ICP-AES) was used for characterization of the leachate samples. During the course of study, numerous glass samples were prepared and their properties were evaluated in detail using various experimental techniques. The experimental set up and working of various analytical techniques are provided in next chapter.

CHAPTER 2

Instrumental techniques and experimental methods

2.1. Introduction

An overview of the experimental techniques used for preparation of glass samples and their characterization is provided in this chapter. Depending on the nature of the glass samples and its applicability, various instrumental techniques were employed to characterize the glass samples. The working principle and related theories of the instruments are discussed in this chapter.

2.2. Glass preparation

The glass samples were prepared by melt-quench technique. In this technique, the necessary raw materials (starting chemicals to make oxide glass) were taken and mixed together, heated up to a temperature where they were in molten state and finally the melt was quenched to obtain glass For preparation of glass samples analytical grade chemicals procured from M/s MERCK, India, M/s MERCK, Germany, M/s S. D.Fine Chem Ltd., India and M/s Loba Chemie, India were used. Depending on the composition of the glass samples, the raw chemicals were accordingly chosen and weighed appropriately on Afcoset Electronic weighing machine. The mixture was finely grounded on a mortar- pestle for homogeneity. The resulting mixture was taken in a crucible. The mixture was charged in a furnace. These mixtures were at first maintained at a temperature of 700^{o}C for 2 hours for calcination and then at 900^{o}C for fusion for 4 hours. As different glass samples have different pouring temperature, hence the furnace was held at pouring temperature of the sample for 1 hour to ensure complete homogenisation, followed by pouring the melt on a stainless-steel plate. All the glass samples were of 100g batch size and were prepared at atmospheric condition.

During charging of glass in furnace the samples undergo the following transformations: a) Evaporation, b) Calcination, c) Fusion and d) Soaking/Homogenisation [37]. The very first step involves evaporation of water. The starting materials used for preparation of oxide glass samples were in the form of oxides, phosphates, nitrates. During calcination the salts decompose to form the respective oxides with liberation of various gases like O_2, NO_2, NH_3. During fusion, the oxides bond with one another forming a continuous and random oxide network. Soaking for a period of 4 hours is provided for homogenisation of glass melt. Finally the glass melt is poured on a stainless steel plate where it rapidly undergoes quenching. The sudden decrease in temperature results in formation of amorphous glass rather than more ordered crystalline material.

The furnace used was Indfurr superheat furnace with silicon carbide heating elements. Temperature sensor was Platinum/Rhodium R type resistive temperature detector with a temperature controller to maintain the temperature within ±5°C. The crucibles used were high Cr based crucibles for molybdenum and chromium containing glass samples and sillimanite crucibles for remaining glass samples.

2.3. Structural characterization

Various methodologies were employed to study the structural changes in the glass samples. Presence of crystalline phases within the amorphous structures and bonding within the glass network etc. were studied using the following instruments.

2.3.1. X-Ray Diffraction (XRD)

XRD is the most common method employed for material characterization. It is widely used for characterization of crystalline materials, determination of unit cell dimensions, measurement of sample purity etc. In present study XRD was employed to identify the presence of crystalline phases with in the glass samples. When X-ray falls on a crystalline substance, the lattice plane in the substances act as diffraction gratings. XRD determinations are based on interpreting the constructive interferences formed by the diffracted monochromatic X-ray. Crystal lattice consists of parallel array of atoms and incident x-ray beams are diffracted from these atoms. The interaction of the incident rays with the sample produces constructive interference when the Bragg's Law is satisfied

$$n\lambda = 2d \sin \theta$$

n- order of diffraction

λ- wavelength of X-rays (Å)

d- inter-planar separation (Å) and

θ- glancing angle (called as Bragg's angle) (degree)

since X-ray from a definite source (Cu) is used, wavelength remains constant, angle of incidence is changed and intensity of the diffracted peak is recorded with varying 2θ. The peaks are characteristic to d value at which constructive interferences are observed. This d value provides useful information regarding identification of the mineral as each of them would contain a unique set of d-spacing.

X-ray diffractometers consist of an X-ray tube, a sample holder and an X-ray detector (Fig. 2.1). X-rays are generated in a cathode ray tube. The most common target material used for generation of X-ray is Copper (Cu Kα radiation = 1.5418Å). Usually, filtering is required to produce monochromatic X-rays needed for diffraction, which is obtained by using foils of Z-1 element or crystal monochromator. The X-rays are collimated and directed onto the sample. The position of the sample and detector are rotated and a detector records the intensity of the diffracted X-ray with respect to angle of rotation [38, 39].

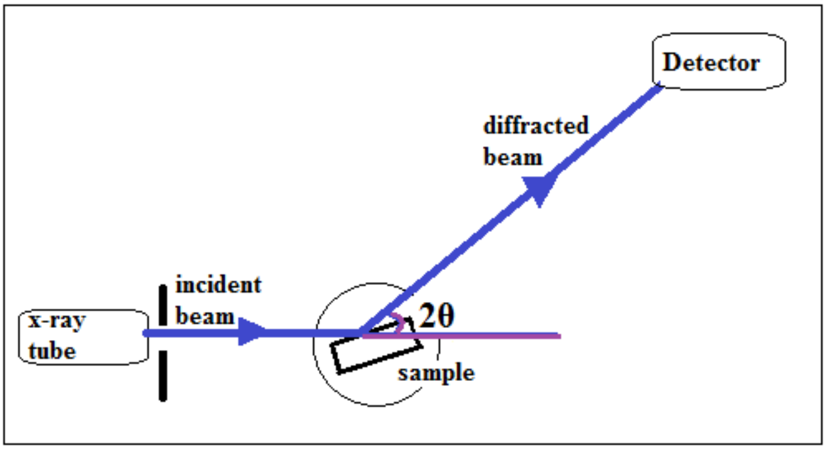

Figure 2.1. Schematic of XRD instrument

In this study the powder X-ray diffraction patterns of the compounds were measured using a Rigaku Miniflex-600 powder X-ray Diffractometer and Philips X'PertPro Diffractometer in θ–2θ Geometry. The Diffractometer uses Cu Kα radiation (1.5406 Å) obtained from a Cu target tube operated at 40 kV and 15mA. A NaI (Tl) scintillation detector was used for the detection of diffracted X-rays from the sample. For XRD measurements, the sample was ground finely in a pestle mortar and mixed with collodion. The powder XRD patterns were recorded from 10-80^0. For XRD measurements a 2θ scan at a scanning rate of 4 degree per minute was used and counts were collected at every 2 seconds. The observed diffraction patterns were compared with JCPDS (Joint Committee on Powder Diffraction Standards) files.

2.3.2. Nuclear Magnetic Resonance (NMR) spectroscopy

NMR spectroscopy is a well-known technique for the determination of molecular structure. Depending on the kind of studies or results intended, various NMR techniques are available. NMR spectroscopy can be used for studying physical properties at the molecular level like phase changes, conformational exchange, diffusion, solubility, to determine molecular conformation in solution etc. In this study ^{29}Si, ^{11}B, ^{27}Al MAS-NMR technique was used to study the structural changes occurring within glass matrix upon changing the composition of sample.

Principle of NMR

Within an atom the subatomic particles (electrons, protons and neutrons) spin on their own axes. In many atoms (such as ^{12}C, ^{16}O etc.) these spins are paired against one another (where number of neutrons and the number of protons are both even), resulting in no overall spin. However, in some atoms (such as ^{1}H, ^{13}C, ^{19}F and ^{31}P) the nucleus possess an overall spin. Here, if the number of neutrons plus the number of protons is odd, then the nucleus has a half-integer spin (i.e. 1/2, 3/2, 5/2) and if the number of neutrons and the number of protons are both odd, then the nucleus has an integer spin (i.e. 1, 2, 3).

The principle behind NMR spectroscopy is based on spin of the nucleus and its interaction with external magnetic field. A nucleus with spin I would contain degenerate energy level in the absence of magnetic field. There is nuclear magnetic moment (μ) for such nucleus associated with nuclear spin (I)

$$\mu=\gamma I$$

where γ is the gyromagnetic ratio of nucleus

In the presence of an external magnetic field (B_0), the degenerate energy level splits into 2I+1 spin states. Each level is given a magnetic quantum number (m). The magnetic moment of the lower energy state is aligned with the external field, but that of the higher energy spin state is aligned against the external field. It is possible to excite these nuclei from lower level into the higher level with external energy (E). During the return to ground state the energy that is emitted gives the NMR spectrum of the particular nucleus.

The emitted radio frequency (υ) is proportional to external magnetic field (B_0),

$$\upsilon = \frac{\gamma B0}{2\Pi}$$

The nucleus is spinning about an axis having rotational frequency called precessional frequency and is given by

$$\omega = \gamma\, B_0$$

when the frequency of rotating magnetic field equals that of precessing nucleus they are called to be in resonance [40, 41]. However, each nucleus would exhibit a shift in its frequency based upon its chemical surrounding, known as the chemical shift. High electron density around the nucleus shields the nucleus from external magnetic field and lower electron density deshields the nucleus from external magnetic field. During shielding the signals are up-fielded and during deshielding the signals are relatively down-fielded in an NMR Spectrum (Fig. 2.2). This shift is recorded in parts per million (δ, ppm) with respect to a reference.

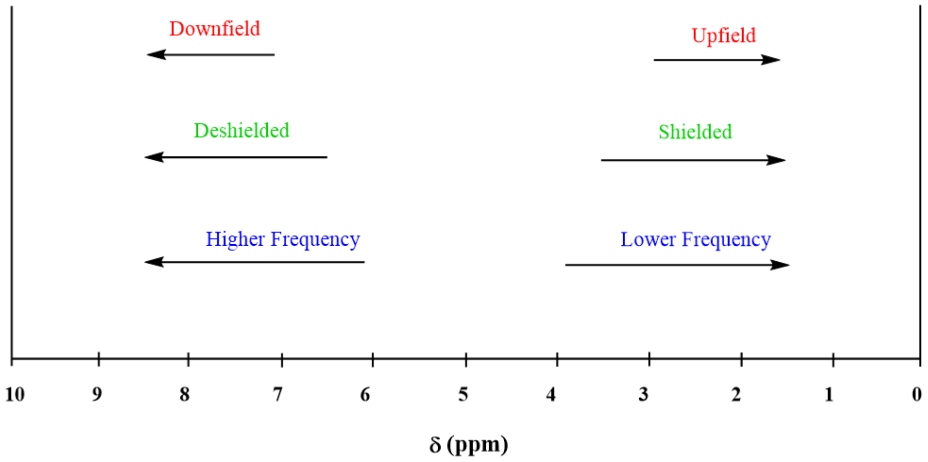

Figure 2.2. Typical NMR Spectrum

Magic Angle Spinning NMR (MAS-NMR)

In contrast to solution NMR where sharp lines are observed, very broad line shapes are obtained in solid state NMR spectroscopy. This broadening of the NMR lines in solid samples occurs mainly due to (i) anisotropic effect, (ii) dipolar interaction and (iii) quadrupolar effect, for the nuclei with spin >1/2. In solution state this anisotropy is averaged out due to random movement of the molecules. The anisotropic and orientation dependent interaction can be overcome by magic angle spinning NMR technique.

MAS-NMR technique involves rotating the powdered samples at very high speeds, at an angle of 54.7° (magic angle) with respect to the applied magnetic field (B) direction. When $\theta = 54.7°$, the term $3\cos^2\theta$ becomes 1. This term arises as a quadrupolar term in the series expansion of the magnetic dipole moment experienced as result of other nearby dipoles. Since Hamiltonian for different anisotropic interactions have $3\cos^2\theta - 1$ term, these anisotropic interactions become zero at $\theta = 54.7°$ thereby zeroing down the anisotropic effect and giving rise to sharp NMR peaks. Thus, MAS-NMR technique simplifies the solid-state NMR patterns and individual chemical environments can be correlated with corresponding chemical shift values obtained from these samples. Figure 2.10 shows schematic of typical NMR instruments [42].

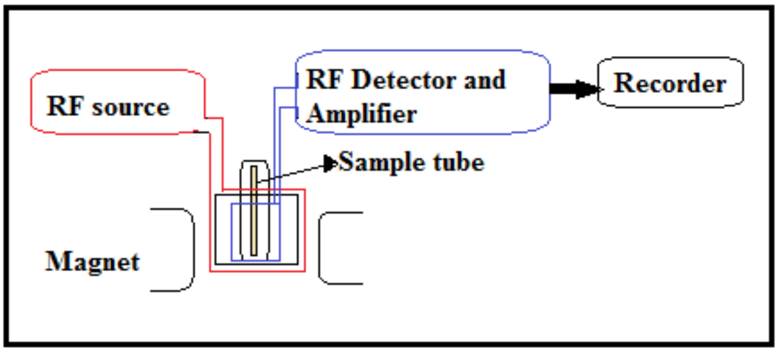

Figure 2.3. A schematic of typical NMR instruments

NMR instruments consists of:

Sample holder – It is a glass tube which is 8.5 cm long and 0.3 cm in diameter.

Magnetic coils – Magnetic coil generates magnetic field whenever current flows through it.

Permanent magnet – It helps in providing a homogenous magnetic field at 60 – 100MHz.

Sweep generator – Modifies the strength of the magnetic field which is already applied.

Radiofrequency transmitter – It produces a powerful but short pulse of the radio waves.

RF detector – It helps in determining unabsorbed radio frequencies.

Recorder – It records the NMR signals which are received by the RF detector.

The sample in a uniform 5 mm glass tube is oriented between the poles of a powerful magnet and is spun to average any magnetic field variations, as well as tube imperfections. Radio frequency radiation of appropriate energy is broadcast into the sample and emission of RF signal is monitored by dedicated electronic devices and a computer. An NMR spectrum is acquired by varying or sweeping the magnetic field over a small range while observing the RF signal from the sample or the frequency of the RF radiation is varied while holding the external field constant. To maintain the current, the solenoid that produces the field is immersed in liquid helium to maintain the superconducting state. Surrounding the magnet volume is a set of vacuum jackets and a liquid nitrogen–filled volume to isolate the low-temperature regions from room temperature. The magnet has a bore to house the sample probe and a Room-Temperature Shim (RTS) coil assembly to reduce inhomogeneity of the magnetic field across the active sample volume.

In the present study, ^{29}Si, ^{27}Al and ^{11}B MAS-NMR patterns of the glass samples were recorded using a Bruker Avance 400 machine. Powdered samples were packed inside 4 mm zirconia rotors and subjected to a spinning speed of 10 kHz. Typical 90° pulse durations for ^{29}Si, ^{27}Al and ^{11}B nuclei were 3.2, 4.5 and 2.09 μs, respectively with corresponding delay times of 4, 6 and 2 seconds respectively. The chemical shift values for ^{29}Si, ^{27}Al and ^{11}B NMR spectra were reported with respect to tetramethylsilane, 0.1M $Al(NO_3)_3$ in water and 0.1M aqueous solution of H_3BO_3 respectively. To improve the signal to noise ratio of ^{29}Si MAS-NMR patterns, around 4000 transients were recorded for each sample. Relaxation delay used was maintained at 6 seconds for all the ^{29}Si MAS-NMR patterns. Experiments carried out with variable relaxation delay times up to 60s showed identical line shapes with negligible difference in the relative concentration of Q^n structural units (where Q^n represents silica structural units having “n” number of bridging oxygen atoms). The base glass without Al_2O_3 is characterized by a broad asymmetric peak centered around -97 ppm. De-convolution based on a Gaussian fit was carried out that resulted in two peaks with chemical shift values around -100 and -91 ppm. ^{29}Si MAS-NMR patterns were subjected to Gaussian line profile fitting using the commercially available Origin Software. Line width and peak positions were varied simultaneously and sequentially to get a reasonably good quality fit of the experimental data. Fitting was performed only for line shapes which showed asymmetry. Errors involved in the area calculations are less than 2%. Those fits with error more than 5% were not deconvoluted. Errors in peak positions are negligibly small and less than 0.5%.

2.3.3. Scanning Electron Microscopy (SEM) and Energy Dispersive X-Ray Spectroscopy (EDS)

Scanning Electron Microscopy (SEM) is surface technique employed for studying the surface morphology and microstructure of the samples. Energy Dispersive X-ray Spectroscopy (EDS) is a chemical microanalysis technique used in conjunction with scanning electron microscopy. The EDS technique detects x-rays emitted from the sample during bombardment by an electron beam to characterize the elemental composition of the analyzed volume. Features or phases as small as 1 μm or less can be analyzed.

When the sample is bombarded by electron beam, electrons are ejected from the atoms comprising the sample's surface. The resulting electron vacancies are filled by electrons from a higher state, and an x-ray is emitted to balance the energy difference between the two electrons' states. The x-ray energy is characteristic of the element from which it was emitted [43].

Fig. 2.7 shows the schematic of a typical SEM instrument. In this instrument, interaction of mono-energetic (20-25 keV) electron beam with the sample gives rise to a number of signals which can be used to understand the texture, topography etc. of sample. A beam of electrons is produced by heating a metallic filament. The electron beam is focused on the sample through electromagnetic lenses. On hitting the sample, backscattered or secondary electrons are ejected from the sample. Detectors collect the secondary or backscattered electrons, and convert them to a signal, producing an image. Backscattered electrons intensity is, to a first approximation, a function of the chemical composition, the brighter an area is, the greater the mean atomic number of that area is relative to adjacent areas. Images obtained in the secondary electron mode show extremely high edge definition and emphasize the small details on the surface of the samples [44, 45].

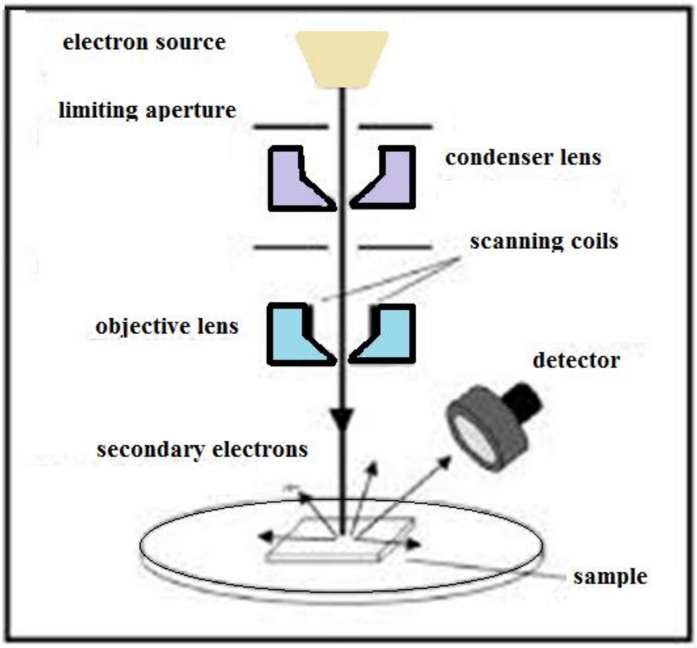

Figure 2.4. A schematic of typical SEM instruments

The EDS x-ray detector measures the relative abundance of emitted x-rays versus their energy. The detector is typically a lithium-drifted silicon, solid-state device. When an incident x-ray strikes the detector, it creates a charge pulse that is proportional to the energy of the x-ray. The charge pulse is converted to a voltage pulse (which remains proportional to the x-ray energy) by a charge-sensitive preamplifier. The signal is then sent to a multichannel analyzer where the pulses are sorted by voltage. The energy, as determined from the voltage measurement, for each incident x-ray is sent to a computer for display and further data evaluation. The spectrum of x-ray energy versus counts is evaluated to determine the elemental composition of the sampled volume

In our study, surface micrographs of the glass samples were taken using a SEM (ZEISS, Evo18, Oxford Instruments) at different magnifications. Composition at different locations have been evaluated after analyzing the EDS spectra. Cobalt is used as internal calibration standard for EDS analysis. The samples were polished and Gold is used for coating the sample surface.

2.4. Chemical characterization

Preparation of glass samples involve subjecting the melt to a very high temperature (>1000°C). To determine evaporation losses, elemental characterization of glass samples is very important. Three instruments were used for chemical characterization and are discussed in the following sections.

2.4.1. Particle/proton Induced Gamma Emission (PIGE)

When a charged particle/proton approaches a target nucleus and the energy of the particle /proton is high enough to overcome the repulsive coulomb force due to the nucleus, the particle /proton penetrates into the nucleus, resulting in interaction with the nucleus. Depending on the energy of the particle/proton and the target nucleus various nuclear reaction occur, like production of gamma rays. Basically, after absorption of energy a compound nucleus is formed that disintegrates or de-excites by emission of gamma rays. The energy and intensity of the gamma rays yield information about the elemental composition of the sample.

PIGE is based on detection of prompt gamma. Detectors that are usually used to detect the gamma rays are Ge based detector like HPGe or lithium drifted Germanium Ge(Li) detectors, cooled at liquid nitrogen temperature (77°K). Detection limits vary from element to element but it is typically between 10 and 100 ppm [46].

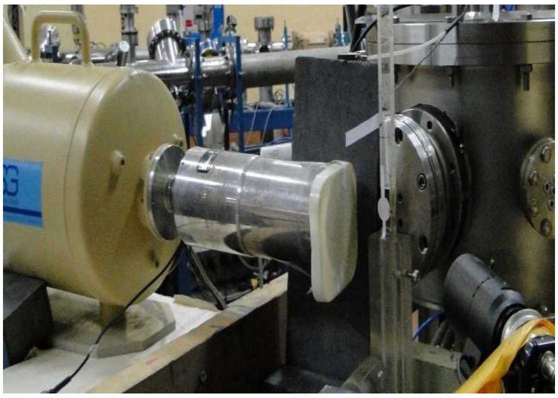

Figure 2.5 (a) External PIGE facility, FOTIA BARC along with pellet sample mounted on the Perspex sample holder

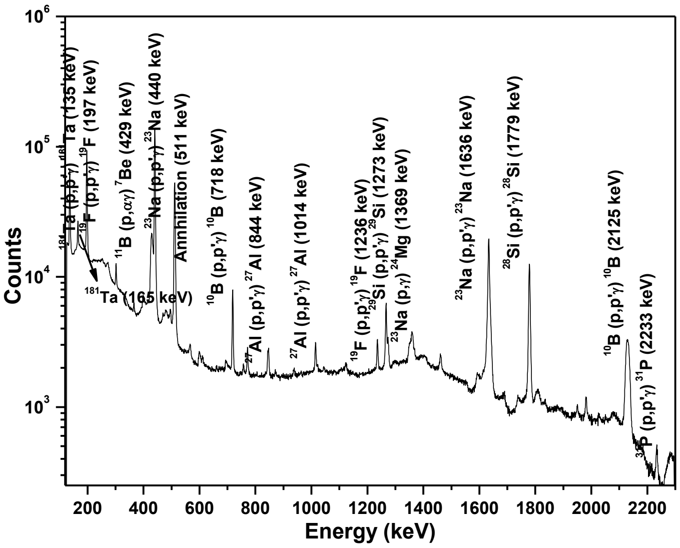

Figure 2.5 (b) Gamma ray spectrum of alkali borosilicate glass having phosphorous in external PIGE method

Samples and certified reference material (glass CRM, Rock phosphate CRM and synthetic standard) pellets were irradiated by the proton beam (E=3.5MeV, I~10-15nA) extracted into the atmosphere through the thin Ta window utilizing tandem accelerator facility of FOTIA, BARC. External PIGE facility, FOTIA BARC along with pellet sample mounted on the Perspex sample holder is shown in Fig. 2.5(a) [47]. Online measurement of prompt gamma produced during the irradiation was carried out using High purity Germanium (HPGe) detector based high resolution gamma spectrometry. Beam current fluctuation during the irradiation was monitored with the help of fluorine as CaF_2, added as in situ in the pellets. Major elements (Si, Na, B, and P) were quantified by using (p,p'γ) inelastic scattering and (p,αγ) reactions namely ^{28}Si (p,p'γ) ^{28}Si; ^{23}Na (p,p'γ) ^{23}Na; ^{10}B(p,αγ)^{7}Be; ^{10}B(p, p'γ)^{10}B; ^{11}B(p, p'γ)^{11}B and ^{31}P (p,p'γ) ^{31}P and corresponding gamma-rays used for calculation are 1779, 440, 429, 718, 2125 and 2233keV respectively [47]. External PIGE gamma-ray spectrums of alkali borosilicate glass is shown in Fig. 2.5(b)

Sample preparation for PIGE

Sample stoke was prepared by grounding the glass samples into fine powder with the help of agate mortar pestle. A representative sample mass (200 mg) for each sample was taken for the analysis. The representative sample was then diluted with the cellulose and a constant amount of fluorine (effective 5mg in pellet) in the form of CaF_2 was admixed. Finally homogeneous mixture was pelletize (12mm diameter) with the help of pelletizer by applying pressure of 2 ton. Similarly, pellets of standard reference materials and synthetic sample were prepared.

In situ current normalized relative PIGE method

In this study, the quantification of analytes of interest were carried out by relative in situ current normalized PIGE method by comparing the current normalized count rate of analyte present in reference material and sample. Since, we were using dilute sample we assumed the stopping power in the standard and sample to be same. In this relative method, the concentration (mg kg^{-1}) of element of interest in sample is given by equation.

$$C_{x,sam}(mgkg^{-1}) = \frac{(CPS_x)_{sam} \times (S_{CN})_{std}}{(CPS_x)_{std} \times (S_{CN})_{sam}} \times C_{x,std}$$

$$\text{where, } S_{CN} = \frac{CPS_{CN}}{C(mgkg^{-1})_{CN}}$$

where CPS_x and CPS_{CN} *are* count rate of analyte S_{CN} is the sensitivity of current normalizer in sample and standard, C_{CN} and $C_{Std,x}$ are the concentration (mg kg^{-1}) of in situ added in pellets and amount of analyte present in standard.

2.4.2. Laser Induced Breakdown spectroscopy (LIBS)

Laser Induced Breakdown Spectroscopy (LIBS) is a type of atomic emission spectroscopy where the source is highly energetic laser pulse. This laser pulse is focused on a small area on the sample to form a plasma, the temperature of the plasma can reach 100000K which atomizes and ionises the atoms in the sample. All these species absorb energy and get excited to higher energy levels. The emission lines during return to ground level are recorded. These emission lines are characteristic of the atoms present [48].

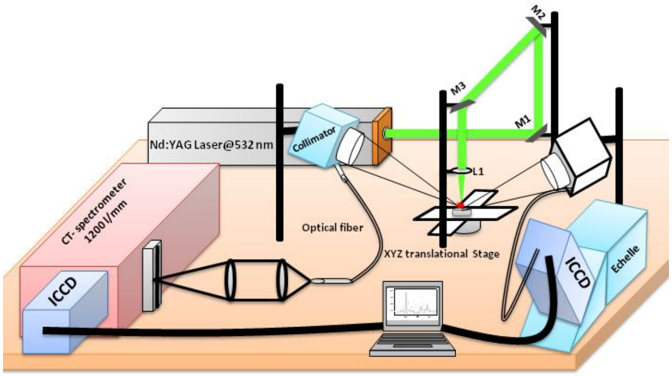

Figure 2.6. Experimental setup of LIBS used for the present study

A common configured LIBS system developed in FCD, BARC was used in this study (Fig. 2.6). A 2^nd^harmonic Nd:YAG laser (M/s Quantel Laser, France) with a 5 ns pulse-width was focused through an appropriate optical configuration (f = 10 cm) to produce a micro-plasma on the surface of the samples. The plasma emission was collected at ~45° angle with respect to the laser beam direction, simultaneously through two collimators equipped with off axis parabolic mirror, placed at opposite side of the plasma. Both the collimators image the plasma on to a 200µm dia optical fiber. The collected light from one of the collimators was fed to an Echelle spectrometer (EH) (Mechelle, ME5000, Andor, UK) equipped with 50-µm entrance slit width. The EH covers 200–950nm wavelength regions simultaneously with a spectral resolution of ~ 4750 CSR (λ/Δλ). The light collected through other collimator is imaged via two bi-convex lens placed in series in front of the entrance slit (10µm width) of a 75cm focal length Czerny-Turner spectrometer (CT) (Shamrock SR750, Andor, UK) equipped with a 1200 lines/mm grating which results in spectral resolution of 55pm and simultaneous spectral range of 14nm. Both the spectrographs are equipped with an ICCD (iStar, Andor, UK,1024 × 1024 pixels), which is synchronized with the Q-switch of laser pulse to control acquisition time delay (t_d) and detector gate width (t_g). NIST certified

Deuterium–Quartz–Tungsten–Halogen [DH2000, Ocean Optics, USA] and Hg–Ar lamps [HG-1, Ocean Optics, USA] were used for wavelength and intensity calibration, respectively. The digital spectra recording and controlling the delay generation were carried out with data acquisition software (Solis 4.28). The recorded spectra were analysed with an in-house made Labview based Lorentzian peak fitting program. An in-house written program in LabVIEW (LabVIEW2012, National Instruments) was used for PLSR analysis.

Due to the irregularity in shape of the glass samples, digging mode LIBS analysis was chosen for this study [49]. 10 repetitive LIBS spectra were recorded at different location on sample surface for each glass samples. Each spectrum consists of 60 single-shot LIBS spectrum accumulation at a particular location on the glass surface. LIBS analyses of all the samples were carried out in air atmosphere with 60mJ of laser energy. To avoid any loss of data in the image mode recording of EH, 2 Hz repetition mode was selected. The t_d of 1.2 μs and t_g of 50 μs was used for spectrum accumulation. EH can record 200-950 nm simultaneously. But CT has a spectral range of 14 nm using 1200 lines/mm grating. For selecting appropriate wavelength region, 300 - 500 nm spectrum region was recorded in 14 nm segment for glass samples. Based on spectrum comparison studies and availability of spectrally pure Mo and Cr emission lines, 276-290 nm region was selected for CT study. Fig. 2.7 shows spectra obtained in the 276-290 nm region for some Mo and Cr containing glass samples using CT. LIBS was employed for determination of Mo and Cr in glass samples.

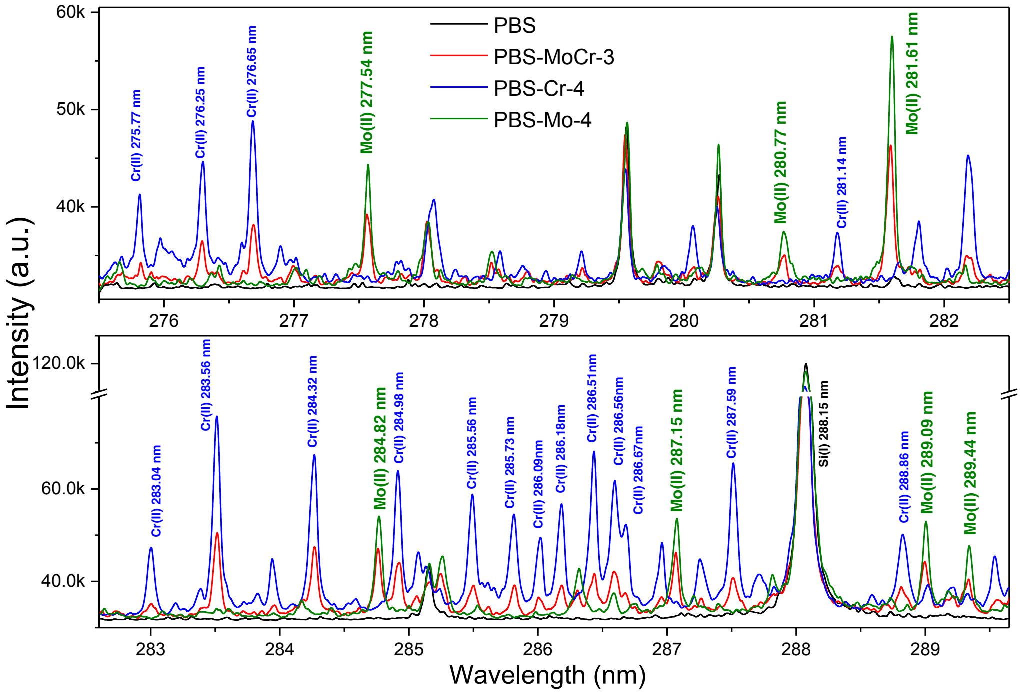

Figure 2.7. Emission spectrum of glass samples obtained under identical experimental condition in 276-290 nm region using Czerny-Turner spectrograph.

PLSR algorithm

Multi-variate analytical methods like Partial Least Squares Regression (PLSR) is known to be better suited for complex and unresolved spectra [47]. In this work two different models of PLSR, standard-PLSR and Analytical Spectral Dependent-Partial Least Squares Regression (ASD-PLSR) were used. Calibration of the LIBS spectra was carried out with PLSR, which is purely an empirical approach based on dimension reduction method. When one has the complete spectral data available, the use of all the relevant signals from the spectra will lead to a better analytical result. PLSR use the complete spectral data for analysis. In short, a matrix of all required spectral intensities were initially complied. Then a PLSR coefficient matrix was calculated using matrix calculations, which correlates individual element's concentration to the relevant reference spectra. For the unknown sample, a mathematical inversion of the pre-computed PLSR coefficient matrix was applied to its spectrum pixel data matrix to calculate the concentration of the unknown sample. For concentration of each element, a separate calibration model was developed. The dimension reduction capability makes the PLSR useful even when spectra were only partially resolved, like in the present case, where the presence of multiple high Z elements makes availability of spectrally pure emission peak a difficult job.

Due to the limited availability of samples, cross validation based analytical parameters, viz., relative standard deviation of cross-validation (%RSDcv) and relative cross-validation accuracy(%RAcv) were used as figure of merit, which are defined as,

$$\%\mathrm{RA}_{cv} = \frac{100}{i_{\max}} \sum^{i=i_{\max}} \left(C_s^i - \frac{1}{j_{\max}} \sum^{j_{\max}} C_j^i \right) \Big/ C_s^i$$

$$\%RSD_{cv} = \frac{100}{i_{\max}} \sum^{i_{\max}} \frac{1}{C_s^i} \sqrt{\frac{1}{j_{\max}-1} \sum^{j_{\max}} (C_j^i - \frac{1}{j_{\max}} \sum^{j_{\max}} C_j^i)^2}$$

Here, 'i' represents the total number of samples used for the particular calibration model, 'j' is the number of replicate analyses, which is 10 in the present case. Cij is the predicted concentration of jth replicate of ith sample by calibration model. Cis is the working standard concentrations of ith sample. For comparison of multivariative models for analysis, predictive residual sum of squares (PRESS) and standard error of cross validation (SEcv) were used. The minimum PRESS or SEcv value represents good analytical model.

2.4.3. X-Ray Fluorescence (XRF)

On absorption of light energy by a target atom, an electron can get ejected from its atomic orbital. However, the energy with which the electron is bound to the nucleus of the atom has to lower than the energy of the photon. The vacancy created by ejection of electron is filled by another electron of higher energy level. During this transition a photon (X-ray) may be emitted from the target atom. As this X-ray depends on the energy difference between the two orbitals, by recording the energy or wavelength of the characteristic X-ray it is possible to determine the identity of the elements and the intensity of the photons depends on amount of that element in the sample. Schematics of the instrument is given in Fig. 2.8.

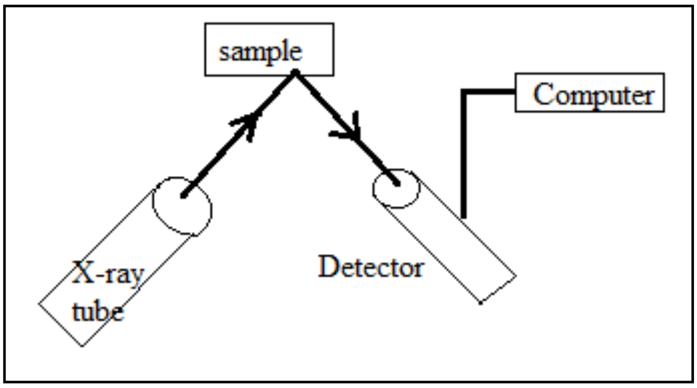

Figure 2.8. Schematic of XRF instrument

In EDXRF (Energy Dispersive X-Ray Fluorescence) the detector is capable of measuring the different energies coming directly from the sample. This detector is called energy dispersive detector. Micro X-ray Fluorescence (µXRF) technique allows examination of very small sample area achieved by restricting x-ray beam using a pinhole sized aperture. This technique is particularly useful when the sample is inhomogeneous or irregular in shape.

The Pellets that were prepared for PIGE technique were utilized for micro-XRF analysis. Each sample was irradiated with the X-ray photon (I= 1mA) emitted from the low power X-ray tube with Rh anode (with operating voltage

50keV and an air-cooled X-ray tube with Be window having a thickness of 100μm) for 800s using a ATI-EDXRF spectrometer from Atomistitut, Vienna. Characteristic X-rays were measured using a peltier cooled KETEK silicon drift detector having an active area of 30 mm^2 and sample to detector distance is 16 mm. Typical X-ray spectrum of one glass sample by micro-XRF method is shown in Fig. 2.9. XRF was used for quantification of phosphorous in glass samples.

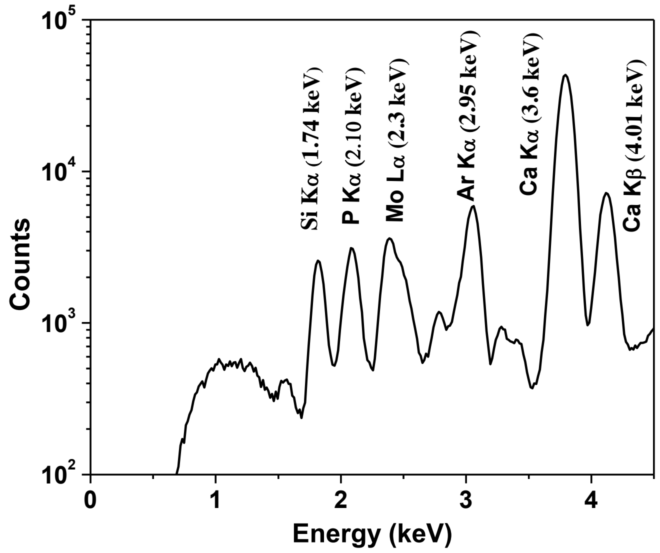

Fig 2.9. X-ray spectrum of glass sample by micro-XRF method

2.5. Thermal characterization using Differential Thermal Analysis (DTA)

Differential Thermal Analysis (DTA) is performed on a sample in order to observe the transitions in a sample with respect to temperature. This technique is useful in identification of melting, crystallization, glass transitions temperature, enthalpy change and decomposition reactions. In DTA, the sample and reference temperatures are increased/decreased simultaneously under identical conditions and the difference between the temperature of sample and reference material is monitored. Any chemical, physical and structural changes in the sample lead to the absorption (endothermic event) or evolution (exothermic event) of heat relative to reference (which is thermally inactive).

Radioactive decay of various radioisotopes overtime within the glass leads to the production of decay heat. If this heat is enough to cause melting of sample, then the atoms can re organise to form crystalline phases inside glass matrix. This process will devitrify the glass. In order to understand the thermal stability of glass samples with respect to additives, DTA investigations were carried out on the glass samples. DTA analysis of all the glass samples shows an endothermic hump. This hump is known as Glass transition temperature (Tg), which appears due to glass transition process (i.e., onset of structural relaxation process) and can be clearly seen in all the samples. Nucleation rate for formation of crystalline phases is higher near Tg. Therefore, Tg is one of the crucial parameters which is taken into consideration while incorporating radioactive waste into glass matrix. Here in this study, Tg was recorded for all the samples. Lower Tg attributes to lower thermal stability of glass samples, which means the glass can devitrify at lower temperature. The Tg values are mentioned in the respective DTA plots. [50-52].

A DTA consists of a sample holder, thermocouples, sample containers, a ceramic or metallic block, a furnace, a temperature programmer and a recording system as given in Figure 2.8(a). A known weight of sample and same amount of reference such as Al_2O_3 are placed in the furnace in a platinum crucible. The furnace is controlled under a temperature program and the temperature of the sample and the reference are changed/increased. During this process, a differential thermocouple is set up to detect the temperature difference (ΔT) between the sample (T_S) and the reference (T_R). The DTA plot shows changes in temperature difference with respect to temperature. Fig 2.1(b) shows a typical DTA plot change in temperature difference (ΔT) against temperature detected with the differential thermocouple.

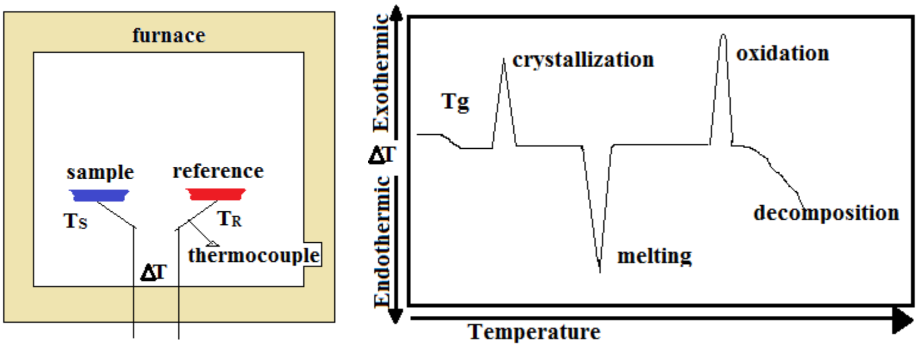

Figure 2.10 (a) Schematic of a DTA cell and (b) a typical DTA curve.

For the present study, DTA patterns of the glass samples were recorded on Shimadzu Differential Thermal Analyzer System DTA-30. The instrument was calibrated using zinc and aluminum as standards and alumina as reference. The melting point of zinc is 419.5°C and that of aluminum is 660.3°C. Sample and reference of weight around 40 mg was taken in a platinum crucible and heated up to 900°C in atmospheric condition. Rate of increase in temperature was maintained at 10°C/min for all the samples. Platinum-platinum-rhodium (10%) thermocouple was used for temperature detection. An endothermic hump characteristic of glass transition temperature was recorded for all the samples. For determination of Tg, the onset temperature of endothermic peak was noted down. The instrument provides the change in slope of the extrapolated baseline within an uncertainty of ±1°C. 3 number of measurements were taken for each sample.

2.6. Chemical durability

Once HLW is immobilized in the glass matrix, the vitrified product has to be stable for millions of years. Therefore, the chemical durability of the glass structure is an important parameter. To evaluate the chemical durability of a glass sample, leaching experiment is performed. Leaching is defined as a process by which water soluble substances are washed out from any matrix like soil, glass etc. This study is carried out to analyze how strongly the radioisotopes are bonded into the glass matrix. The experimental part and the analysis of leachate using ICP-AES is given in the following section [53, 54].

2.6.1 Experimental

There are standard tests to determine the chemical durability of vitrified product developed by Materials Characterization Centre (MCC) of Pacific northwest national laboratory, USA. These tests are accepted worldwide. In our study we have chosen MCC-3 (ASTM C1285) test. It is a standard test method for determining chemical durability of nuclear, hazardous, and mixed waste glasses and multiphase glass ceramics: The Product Consistency Test (PCT) [55].

In this test the glass was crushed and passed through sieve of dimension ASTM 16 and ASTM 40. The resulting glass particles have diameter of ~0.5mm. A known weight of sample i.e. 1.0g is accurately weighed and packed in a stainless steel mesh packet. This packet was taken in a Teflon bottle along with 10mL water. This set up was kept in oven at a temperature of 90^{o}C for an extended period of time but the leachate is replaced by fresh water in definite interval. The surface area of glass sample to leachant volume ratio was maintained constant throughout the experiment for all the samples. The glass samples were subjected to semi dynamic leaching study as the leachate was replaced after different intervals of static leaching. The leachate was collected every time and ICP-AES analysis of this leachate gives an idea on the amount of individual elements getting leached.

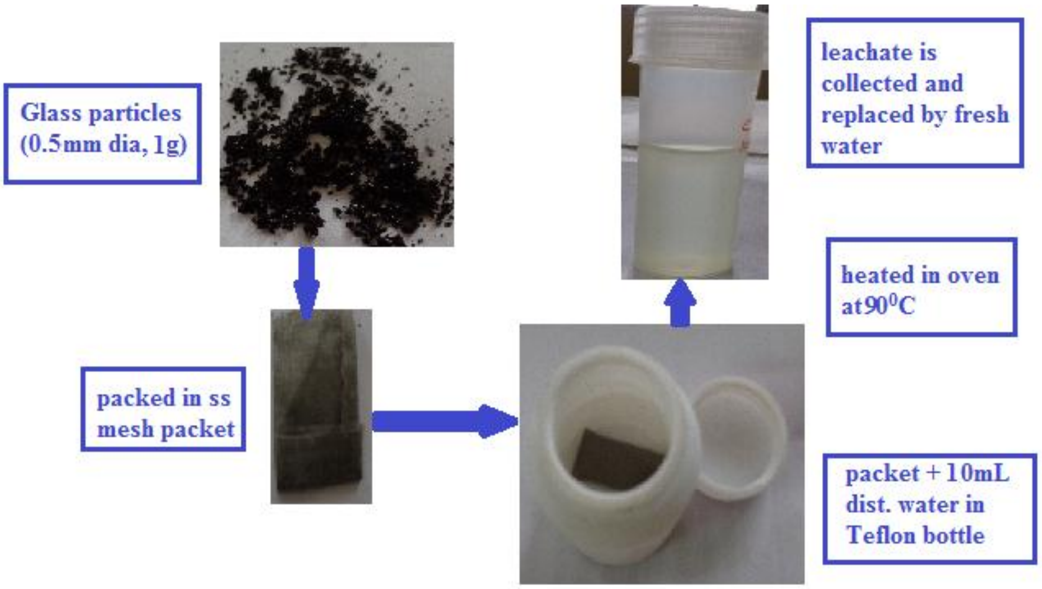

Figure 2.11. A brief summary of sample preparation

2.6.2. Inductively Coupled Plasma- Atomic Emission Spectroscopy (ICP-AES)

Ones the leachate were collected ICP-AES of the leachate was carried out to determine concentration of all the elements. ICP-AES is one of the most popular emission spectroscopies for simultaneous determination of multi elements. It uses inductively coupled plasma as source of energy to excite atoms and ions to higher energy level. The temperature of the plasma ranges from 6000 to10,000 K. Certain elements like silicon, aluminum etc. that are poorly excited by flame can be done with the application of plasma based excitation system. Elements that are carried into the plasma get excited. When these excited atoms return to ground state, they emit electromagnetic rays corresponding to a particular element. Hence, the position of the lines represents the element [56].

The instrument consists of a source i.e. plasma, monochromator and a detector to measure each specific wavelength and its intensity. A Nebulizer that creates very small droplets that are carried by the argon carrier gas into the plasma.

Schematics is given in Fig. 2.10. The plasma torch is normally made of quartz and it consists of three tubes. There is an outer tube and the sample injector. Where Argon gas passes through the outer tube and swirls around in a spiral flow. A middle tube of stream of Ar, at a much slower flow rate, also called auxiliary gas, changes the position of the plasma relative to the injector. An inner tube carries the sample along with Ar with the aid of a nebulizer through the injector and into the plasma (Fig. 2.10.).

A coil connected to a Radio Frequency (RF) generator surrounds the top of the ICP torch. When power is applied (usually about 1100 W), an alternating current creates a magnetic field in the area inside the coil at the top of the torch. With argon flowing through, a high-voltage spark ionizes some of the argon. This causes a chain reaction within the magnetic field, breaking down the argon gas to contain argon gas, argon ions, and electrons. This rapidly moving steam of Ar ions, electrons and atoms and the inelastic collisions between them creates the plasma. This plasma can reach a temperature of about (10,000K) and this energy is used by the sample for excitation. During their return to ground state the characteristic wavelength light emitted by all the atoms or ions present in the sample are collectively focussed on a diffraction grating where it is separated into its component wavelengths in the optical spectrometer. Within the optical chamber(s), after the light is separated into its different wavelengths (colours), the light intensity is measured with a photomultiplier tube or charge coupled devices (CCDs) (Fig. 2.11).

The position of the lines are characteristic of the elements and the intensity is proportional to the quantity. The intensity of each line is then compared against a set of standards.

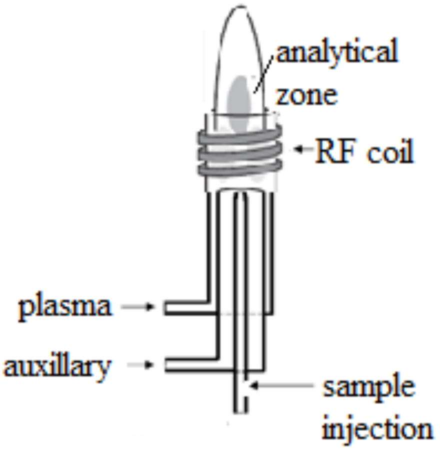

Figure 2.12. Plasma

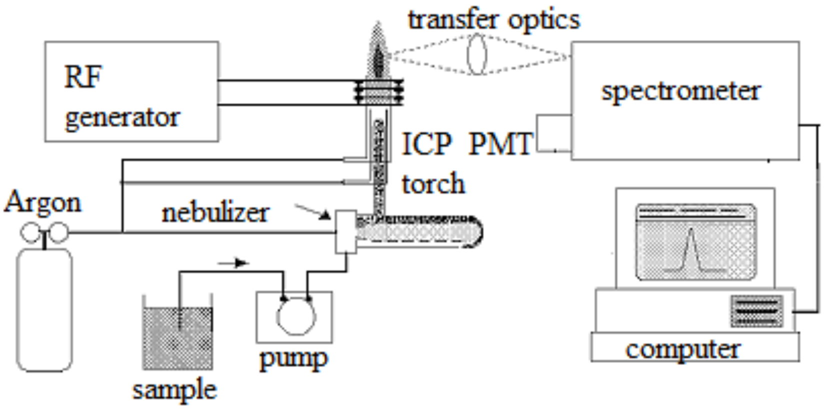

Figure 2.13. Schematic of ICP-AES

The elemental analysis of the leachate was done by HORIBA Scientific ICP-AES.

Calculation of Leach rate

- Leach rate (LR) of radioactive nuclides is calculated using the expression:
- $LR = \frac{\frac{Nf}{Ni}.w}{SA.t}$ (g/cm^2/day)

Nf- Ions in leachate

Ni- Ions initially present

w- Weight of sample

SA- Surface area of sample (cm^2)

t- Time (day)

SA of the sample is calculated using the formula

- $SA = \frac{3w}{\rho r}$ (cm^2)

w- Weight of sample (g)

ρ- Density of glass sample (g/cm^3)

r- Radius of the sample particles (cm)

All these analytical techniques served as an essential tool for characterization of glass samples.

CHAPTER 3

Effect of Al_2O_3 in borosilicate glass

3.1. Introduction

India has a vast reserve of thorium, nearly 25% of world's reserve. With the view of utilizing thorium (Th), India has adopted for a three-stage nuclear power programme. However, Th is a fertile element i.e., it cannot undergo fission to produce energy but can be transmuted to uranium-233 (^{233}U), which is a fissile element and can be utilized in a nuclear reactor to produce energy. In the first stage, natural uranium fueled pressurized heavy water reactors (PHWR) produce electricity and also generate plutonium-239 (^{239}Pu). In the second stage breeder reactors mixed U-Pu oxide fuel will be used to produce energy/electricity. Also, in second stage reactors, Th is used as a blanket material which on irradiation with neutron produces ^{233}U as a result of nuclear reactions. The nuclear reaction is given below:

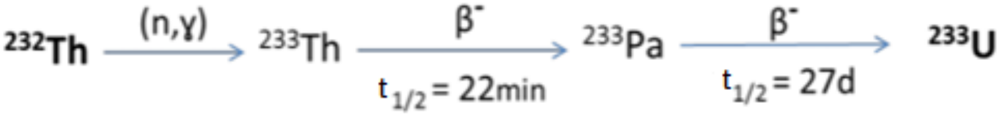

The third stage reactor or Advanced Heavy Water Reactor (AHWR) would involve ^{232}Th-^{233}U MOX fuelled reactors. Table 3.1 provides an insight on ongoing work on Th based plants in India [57].

Table 3.1. Thorium Utilization in various power and research reactor in India.

Name	Type	Power	Fuel
KAMINI	Test reactor	30 kWt	Al-^{233}U
PURNIMA-II,III	Test reactor	1W	^{233}U (PURNIMA-I) Al-^{233}U (PURNIMA-III)
CIRUS	Test reactor	40 MWt	Natural U (ThO_2-Reflector region)
DHRUVA	Test reactor	100 MWt	Natural U (ThO_2- reactivity load)
FBTR	Test reactor	40 MWt	U-Pu cabide (ThO_2 blanket)
KAPS 1&2	PHWR	220MW(e)	Natural U (ThO_2 - For neutron flux flattening of initial core after start-up)
KGS 1&2	PHWR	220MW(e)	
RAPS 2,3&4	PHWR	220MW(e)	

As mentioned in chapter-1, any change in reactor operation can change the chemistry of HLW, thus the reprocessing methodology used to deal with Th based spent fuel introduces extra additives in HLW. An aqueous reprocessing methodology adopted to separate ^{232}Th and ^{233}U/^{233}Pa from fission products and other impurities present in the spent fuel is THOREX (Thorium Uranium Extraction) process [58]. Similar to PUREX (Plutonium Uranium Reduction Extraction), 5% TBP (Tributyl Phosphate) in n-dodecane is used as solvent to selectively extract U, followed by extraction of Th using 40% TBP. The problem lies with dissolution of thoria. The reason for difficulty in dissolution is the non-variable oxidation state of thorium, i.e., Th(IV) being very stable oxidation state makes oxidative-reductive dissolution difficult to occur unlike for U and Pu oxides [59].

Dissolution of thoria in pure nitric acid is very slow and incomplete, therefore, addition of highly reactive fluoride ions become necessary to accomplish the dissolution of thoria by fluoride complexation [60]. For dissolving thoria based fuel, a mixture of nitric acid, sodium fluoride and aluminum nitrate is used after chemical decladding of stainless-steel (SS) clad using aqueous NaOH. Since presence of fluoride ions initiates corrosion of SS there is a need to arrest the presence of free fluoride ions [61]. Therefore, aluminum nitrate is added which forms complex with free fluoride ions present in the solution and thereby reducing the corrosion of SS. This step is an essential part of THOREX process which results in addition of aluminum in HLW. HLW from third stage reactor is likely to contain more than twice the amount of Al as compared to PHWR based reactor [62].

Presence of any additive above certain concentration generally modifies the structure of glass as well as its properties like glass transition temperature, thermal expansion coefficient, chemical durability, extent of evaporation of different constituents etc. [63]. Therefore, it is essential to study the structure of glass matrix with respect to concentration of any additive. This chapters intends to study the effect of Al_2O_3 on sodium borosilicate glass.

Literature survey revealed that addition of aluminum ions in the glass causes significant changes in the physico-chemical properties of glass samples. For example, Quintas et al. studied the effect of various alkali metals and alkaline earth metals on nature of Al coordination in borosilicate glass [64]. They studied the crystallization tendency of glass when the cooling rate was as low as 1K/min and observed formation of apatite crystalline phase within glass network. Structural changes around Al environment in borosilicate glasses is also reported by Criscenti et al. [65]. They observed that octahedrally coordinated Al ion facilitates preferential leaching of Al over Si, which results in formation of a silica rich gel layer at the alumino-silicate glass-water interface. McCloy et al. observed crystalline phase formation tendency in sodium borosilicate glass with alumina. They reported that at high concentration of boron, nepheline like crystals are formed and Na, Si, Al rich phase separates from borate rich region [66]. Lee et al. studied the effect of pressure in causing structural changes in the silicate and alumino-silicate glasses [67].

The present chapter deals with the effect of Al_2O_3 addition on the structural aspects, thermal properties and leaching behavior of sodium borosilicate and barium borosilicate glasses. The choice of two separate base glass matrix was due to the fact that these two glass systems are widely used for immobilization of HLW. Sodium borosilicate glass (NBS) is used for immobilization of conventional radioactive reprocessing waste whereas barium borosilicate glass (BBS) for immobilization of sulphate bearing waste as reported by Mishra et al. [68]. Al_2O_3 content was increased gradually i.e. 5, 10, 15 mol% of Al_2O_3 was added to sodium and barium borosilicate glass systems. Effect of Al_2O_3 in glass samples have been investigated in the present work, which is discussed in the subsequent sections.

3.2. Experimental details

3.2.1. Synthesis of glass samples

Two batches of glass samples were prepared by melt quench method in sillimanite crucible (Table 3.2). One batch comprised of sodium borosilicate base glass with Al_2O_3 composition being 0, 5 10, 15 mol%. Similarly, the other batch contained barium containing sodium borosilicate glass with Al_2O_3 composition varying from 0, 5 10, 15 mol%. Beyond 15mol%, the pouring temperature of the glass samples exceeded 1100°C and hence was avoided. Glass samples were prepared using appropriate amounts of different chemicals like silica, boric acid, barium nitrate, aluminum nitrate and sodium nitrate of high purity grade for 100 g batch size scale. The details of the preparation are given in chapter 2.

Table 3.2. Composition of Sodium borosilicate and barium borosilicate glasses containing different amounts of Al_2O_3

Sample name	Composition in mol%				
	SiO_2	B_2O_3	Na_2O	BaO	Al_2O_3
NBSAl-0	50	30	20	-	-
NBSAl-5	47.5	28.5	19	-	5
NBSAl-10	45	27	18	-	10
NBSAl-15	42.5	25.5	17	-	15
BBSAl-0	45	27	18	10	-
BBSAl-5	42.75	25.65	17.1	9.5	5
BBSAl-10	40.5	24.3	16.2	9	10
BBSAl-15	38.25	22.95	15.3	8.5	15

3.2.2. Structural characterization

Information regarding the structural aspect of glass samples are important in order to understand the variations in the glass samples with respect to alumina addition. For structural elucidation X-Ray Diffraction (XRD) analysis of the samples were carried out. The nature of bonding with respect to Al_2O_3 addition was studied using Magic Angle Spinning Nuclear Magnetic Resonance (MAS-NMR technique). ^{29}Si, ^{11}B and ^{27}Al MAS-NMR technique was employed to study how glass network is affected at different concentrations of Al_2O_3. Immobilization of HLW in glass results in generation of decay heat and this in turn initiates temperature-based devitrification process in the glass matrix. Hence, it is important to understand the thermal stability of glass with change in composition. Therefore, glass transition temperature has been evaluated with respect to Al_2O_3 content for all the glass samples. Leaching experiments were carried out for all the samples. This experiment was conducted for 75 days. The experimental part is provided in chapter 2. The leachate obtained during the experiment was analysed using ICP-AES for concentration of different elements. The results obtained are discussed below.

3.3. Results and Discussion

3.3.1. XRD investigations

XRD measurements of glass samples were carried out as described in Chapter 2. McCloy et al. reported presence of crystalline aluminosilicate phase (nepheline phase) in borosilicate glasses containing high concentration of Al_2O_3 [66]. Therefore, it is necessary to study the XRD pattern of these glass samples. Fig. 3.1 (a) and (b) show XRD patterns of Al_2O_3 containing sodium borosilicate glass and barium containing sodium borosilicate glasses. The patterns reveal broad hump over a 2θ range of 15-35°. This broad hump is characteristic of amorphous nature of the samples. The peaks indicate presence of short range order (and in some cases medium range order) in glasses. Sharp peaks characteristic of crystalline phases were absent in the XRD patterns confirming that no crystalline phase separation has taken place in these samples. To understand the bonding and role of Al within the glass network, detailed structural studies were carried out using ^{29}Si, ^{27}Al and ^{11}B MAS-NMR techniques. MAS-NMR techniques provided structural elucidation of the glass samples and the results are described as follows.

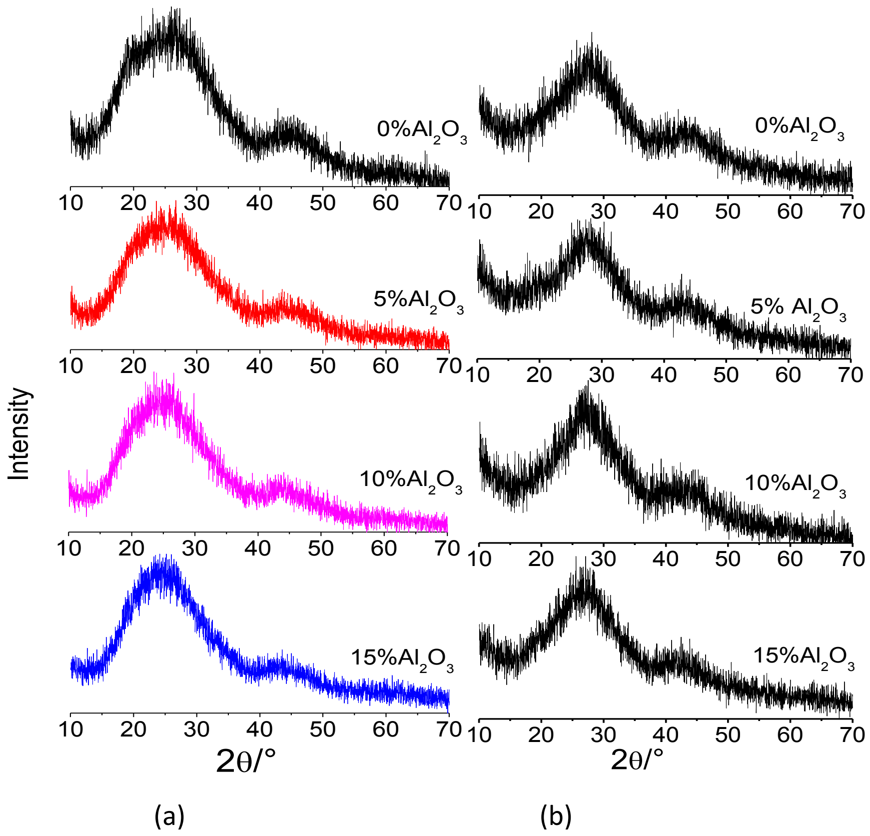

Figure 3.1. XRD patterns of (a) Sodium borosilicate and (b) Barium borosilicate glasses having different amounts of Al_2O_3

3.3.2. MAS-NMR investigations

3.3.2.1. ^{29}Si MAS-NMR

^{29}Si MAS-NMR spectra of sodium borosilicate glasses containing different amounts of aluminum oxide are shown in Fig. 3.2(a). Literature studies of ^{29}Si MAS-NMR on borosilicate glasses reveal that, the peaks around -100 and -91 ppm correspond to the Q^3 and Q^2 structural units of silicon respectively [69-71]. In the base glass, the relative concentration of Q^3 and Q^2 structural units are found to be in the ratio 35 and 65. Keeping the ratios of SiO_2/Na_2O and SiO_2/B_2O_3 constant and with incorporation of Al_2O_3 in the glass, peak maximum of ^{29}Si MAS-NMR pattern shifted systematically to the left as can be seen from Fig. 3.2 (a). The increase in chemical shift value can be attributed to the fact that, with increase in Al_2O_3 content in the glass, Si-O-Si/B linkages are replaced by Si-O-Al type of linkages. Because of the change in the near neighbor environment, the silicon nucleus is de-shielded thereby leading to increase in chemical shift values. The inference is further supported by earlier ^{29}Si MAS-NMR studies on alumino-silicate glasses [72]. However, the patterns could not be de-convoluted into individual Gaussian peaks due to the significant overlapping of constituent peaks and lack of asymmetry in the patterns. Based on these results, it can be inferred that these glass samples mainly consist of linear chains of Q^2 structural units of silicon along with lower amounts of Q^3 structural units. ^{29}Si MAS-NMR spectra for barium borosilicate glass incorporated with different amounts of Al_2O_3 are shown in Fig. 3.2.(b). For BBS glass without any Al_2O_3, de-convolution of the spectrum based on Gaussian fit resulted in two peaks with chemical shift values around -96 and -86 ppm with relative intensities of 28 and 72 respectively and these peaks are due to Q^3 and Q^2 structural units of silicon respectively. The increase in chemical shift values compared to sodium borosilicate glass, is attributed to presence of Ba which is more electropositive than Na in the glass. Like in sodium borosilicate glasses, in barium borosilicate glasses also the chemical shift value of the composite peak slightly shifted towards higher chemical shift values with increase in Al_2O_3 content, suggesting formation of Si-O-Al linkages. These results also indicate that in these glass samples Al^{3+} ion is acting as network former at these concentrations and must be existing in tetrahedral (AlO_4^-) configurations. Formation of AlO_4^- structural unit will also have implications in the nature of boron structural units. To confirm this ^{27}Al and ^{11}B MAS-NMR experiments were carried out on the samples and the results are described in the following section.

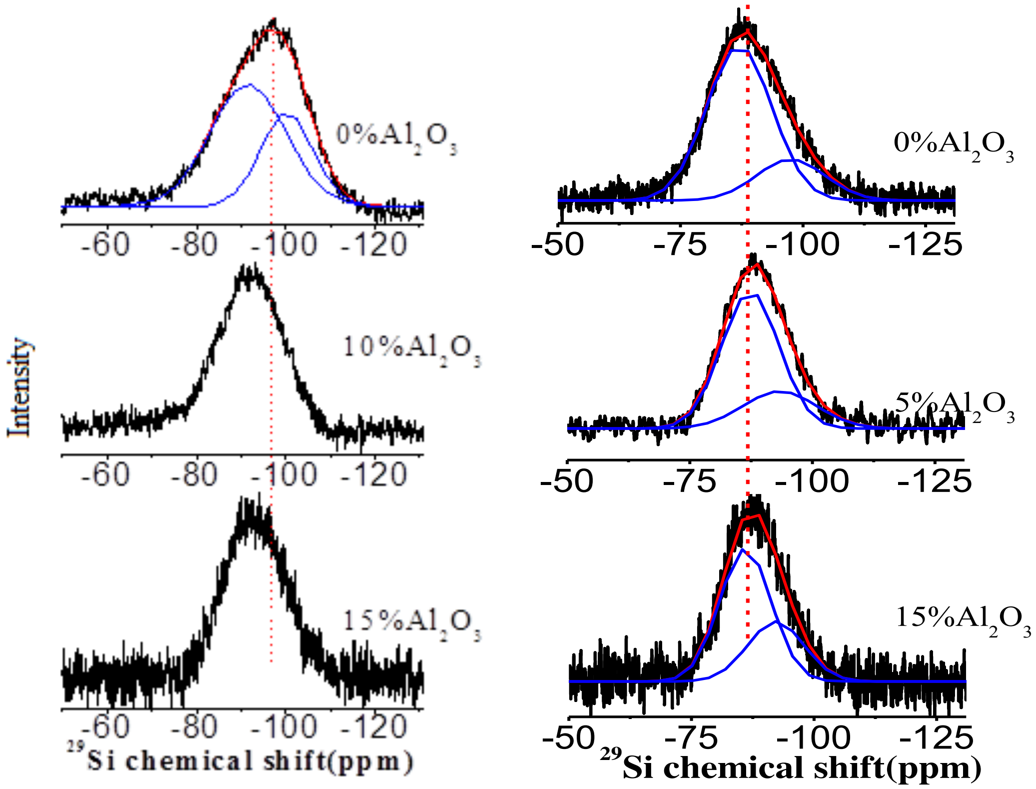

(a) (b)

Figure 3.2. ^{29}Si MAS-NMR patterns of (a) Sodium borosilicate and (b) Barium borosilicate glasses having different amounts of Al_2O_3

3.3.2.2. ^{27}Al MAS-NMR

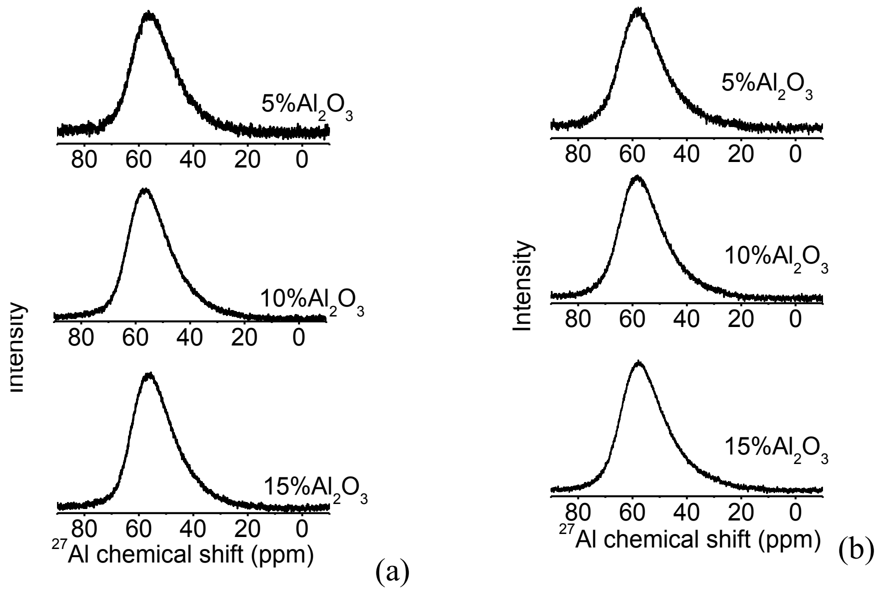

Figure 3.3. ^{27}Al MAS-NMR patterns of (a) Sodium borosilicate and (b) Barium borosilicate glasses having different amounts of Al_2O_3

^{27}Al MAS-NMR spectra of sodium borosilicate and barium borosilicate glasses are shown in Fig. 3.3 (a) and (b) respectively. All the patterns are characterized by a broad peak centered around 56 ppm characteristic of tetrahedrally coordinated Al species. Octahedrally coordinated Al show a peak around 0 ppm, absence of this characteristic peak [16] could be observed in the NMR patterns of both series of glass samples. Based on these results it is confirmed that, all Al^{3+} species enters in the borosilicate network as network former and stay as AlO_4^- structural units. Negative charge present in the structural unit is neutralized by alkali and alkaline earth metals. However, BO_4^- structural units also require cation for charge neutralization and hence redistribution of Na^+ /Ba^{2+} ions occur in these glasses. Such a redistribution of Na^+ ions will result in change in the relative concentration of BO_3 and BO_4^- structural units and this is reflected in the ^{11}B MAS-NMR patterns which is presented in the following section.

3.3.2.3. ^{11}B MAS-NMR

^{11}B MAS-NMR spectra of sodium borosilicate and barium borosilicate glasses having varying amounts of aluminum oxide are shown in Fig. 3.4(a) and (b). All the patterns are characterized by a sharp peak centered around 0.5 ppm and broad peak around 12 ppm. As boron is a quadrupolar nucleus with spin $I = 3/2$, cubic symmetry around B will lead to sharp peak and as BO_4^- structural unit in glass is having nearly cubic symmetry, it appears as a sharp peak at 0.5 ppm, whereas non-cubic symmetry will lead to broad peak and hence BO_3 structural unit due to its non-cubic symmetry appears as a broad peak at 12 ppm. From the area under the broad and sharp peaks, the relative concentration of BO_3 and BO_4 structural units have been evaluated and are presented in Table 3.3. It is seen from Table 3.3 (also from Fig. 3.5) that, the relative concentration of BO_3 structural units is more for sodium borosilicate glass compared to barium borosilicate glass. This is understandable, as the ratio of relative concentration of B_2O_3 to network modifier is lower in BBS glasses compared to NBS glasses. The presence of (Na_2O + BaO) are helping in stabilizing the negatively charged BO_4^- unit. Similar results are also reported by Quintasa et al. [73] in borosilicate glasses containing both alkali and alkaline earth metal oxides. Also, with increase in Al_2O_3 there is requirement of Na^+/Ba^{2+} ions for stabilization of AlO_4^- structural units causing relative decrease in availability of Na^+/Ba^{2+} ions for stabilization of BO_4^- structural units. This is reflected in increase of BO_3 structural units. All the above structural changes are reflected in T_g values of the glass samples. The DTA patterns are provided in section 3.3.3 for better understanding of effect of Al_2O_3 on thermal characteristics of glass samples.

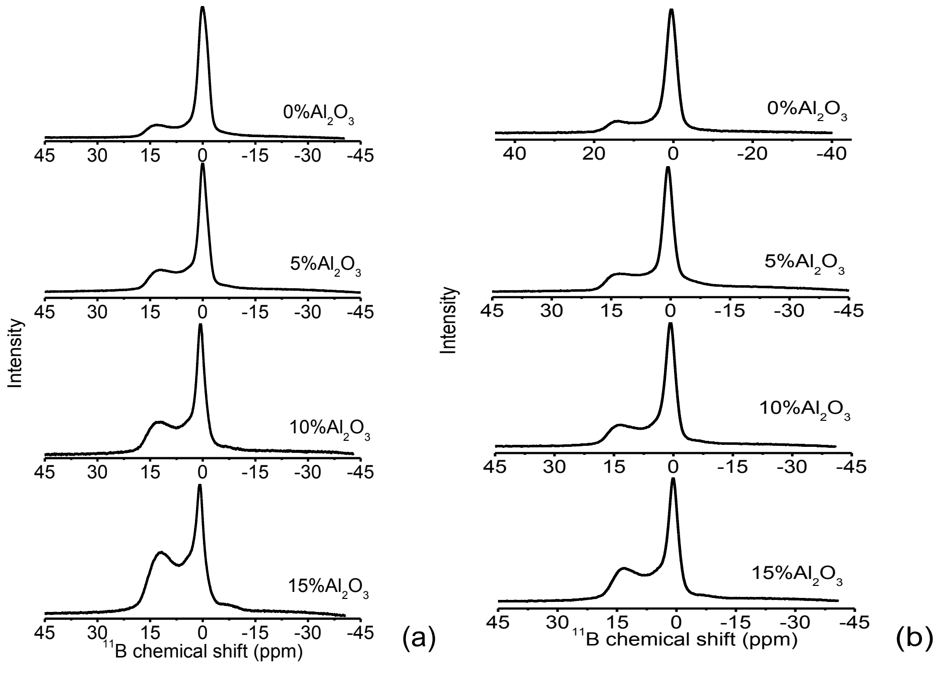

Figure 3.4. ^{11}B MAS-NMR patterns of (a) Sodium borosilicate and (b) Barium borosilicate glasses having different amounts of Al_2O_3.

Thus, the NMR studies have given information regarding the different types of structural units present in both the series of glasses and its influence on glass transition temperature. However, it will be interesting to know how these structural units combine with each other to form the glass network. In this regard, the structural model suggested by Dell et al. [74] can be used for visualizing the way in which the polyhedra are connected in glasses. This aspects is described in the following section

3.3.3. Dell-Bray model

The model is based on the ^{11}B NMR results on ternary Na_2O-SiO_2-B_2O_3 glasses. The two important parameters in the model are “K” and “R” which are defined as, K = [SiO_2]/[B_2O_3] and R = [Na_2O]/[B_2O_3]. ^{27}Al MAS NMR studies discussed in the earlier section have confirmed that all Al^{3+} ions incorporated in the glass, exists as AlO_4^- structural units with Na^+ or Ba^{2+} neutralizing the negative charge. As one mole of Na_2O or BaO is required for 1 mole of Al_2O_3 conversion to AlO_4^- structural units, the actual amount of alkali oxide available for borosilicate network formation can be calculated by subtracting Al_2O_3 content from the total alkali/alkaline earth metal oxide content. The values of R obtained from the effective concentration of alkali/alkaline earth metal oxide (after subtracting the amount required for Al_2O_3 conversion to AlO_4^-structural units) is shown in Table 3.3.

According to this model, relative concentrations of different boron structural units change with variation in "K" and "R" values. For values of "R" less than or equal to 0.5, (low concentrations of Na_2O), BO_3 structural units are formed at the expense of BO_4^- structural units (for NBSAl-5, NBSAl-10, NBSAl-15 and BBSAl-15). When the value of R is in between 0.5 and 0.5+0.0625K (i.e. 0.604), reedmergnerite structural units having the formula ½(Na_2O-B_2O_3-SiO_2) are formed. Above this value of R (i.e. 0.604), and below R = 0.5+0.25K (i.e. 0.915), added Na_2O leads to the de-polymerisation of the glass network and creates non-bridging oxygen atoms attached with silicon (for BBSAl-5 and BBSAl-10). Alkali ions are proportionally distributed among silicon and boron structural units. When the value of "R" is in between 0.5+0.25K (0.915) and 2+K (i.e., 3.66), part of BO_4^- structural units start getting converted to BO_3 structural units (with non-bridging oxygen atoms) (for BBSAl-0).

For sodium borosilicate glass without any Al_2O_3 content (NBSAl-0), the value of R is 0.666 with K value 1.66. According to the model, the value of "R" for this glass composition is in between 0.5+0.0625K and 0.5+0.25K. Under this range, the relative concentration of BO_4^- structural units (N_4) will be 0.5+0.0625K=0.604. The value determined from corresponding NMR spectrum is slightly lower as can be seen from Table 3.3. This might be due to the error involved in the area estimation. With increase in incorporation of Al_2O_3 content in the glass, R value decreases systematically and is 0.49, 0.29 and 0.078 for 5%, 10% and 15% Al_2O_3 containing sodium borosilicate glasses. As the value of R is less than 0.5, as mentioned earlier, concentration of BO_4^- structural units for these glasses should be same as R value itself. This is in accordance with the value of N_4 calculated based on ^{11}B MAS-NMR spectra (Table 3.3.).

From the earlier studies by Dell et al. [74] as well from the ^{11}B MAS-NMR patterns of present study, it is confirmed that in sodium borosilicate glass without any Al_2O_3, diborate and reedmergnerite structural units with non-bridging oxygen atoms attached with silicon (as shown in the schematic diagram in Fig. 3.5.(a)) must be the main structural configurations present. For higher Al_2O_3 containing glasses, mainly diborate and trigonal BO_3 structural units with bridging oxygen atoms are the main configurations present in the glass as shown in Fig. 3.5.(b). For barium borosilicate glasses without any Al_2O_3, the 'R" value is 1.037 which is in the range of 0.5+0.25K to 2+K. In this range both diborate and reedmergnerite structural units will get converted to pyroborate structural units with non-bridging oxygen atoms depending upon the value of R and K. The relative concentration of BO_3 and BO_4^- structural units can be determined from the expression derived from the model [75] and the value is found to be 54% for BO_4^- structural units and 46% for BO_3 structural units. The values are in agreement with the experimentally determined relative concentrations of BO_4^- and BO_3 structural units by ^{11}B MAS-

NMR technique as can be seen from Table 3.3. The representative structural units constituting the glass are shown in Fig. 3.5 (c). For barium borosilicate glasses, containing 5, 10 and 15 mol% Al_2O_3, the “R” values are 0.842, 0.625 and 0.383 respectively (calculated based on the logic used for sodium borosilicate glasses). For glass with R value 0.842 and 0.625, the relative concentration of BO_4^- structural units must be around 60% for both the glass samples, according to the model. However, the value is slightly lower than that calculated from the ^{11}B MAS-NMR patterns (possibly due to the loss of intensities in side band area calculation). For the 15mol% Al_2O_3 containing glass, the “R” value is 0.38 and this value is in agreement with the relative concentration of BO_4^- structural units determined from ^{11}B MAS-NMR studies (Table 3.3). The structural units present in this glass composition (shown in Fig. 3.5 (e)) are similar to that existing in the case of 10 mol% Al_2O_3 containing sodium borosilicate glass. Thus, from the NMR studies it is confirmed that barium borosilicate glass has a wide variety of boron structural units with different numbers and types of non-bridging oxygen atoms. These different polyhedra give an openness to the glass structure which is beneficial for immobilization of nuclear waste. These polyhedra of various shapes help accommodate a wide range of radionuclides present in HLW.

Table 3.3. Relative concentration of BO_4^- and BO_3 configurations determined from ^{11}B MAS-NMR patterns. The values predicted by Dell model is given in brackets. Errors is less than 3%

Sample name	**fraction of BO_4**	**fraction of BO_3**	**R=(R_2O+RO-Al_2O_3)/B_2O_3**	**K = SiO_2/B_2O_3**
NBSAl-0	0.56 (0.60)	0.44 (0.40)	0.66	1.66
NBSAl-5	0.52 (0.49)	0.48 (0.51)	0.49	1.66
NBSAl-10	0.30 (0.29)	0.70 (0.71)	0.29	1.66
NBSAl-15	0.10 (0.08)	0.90 (0.92)	0.079	1.66
BBSAl-0	0.57 (0.54)	0.43 (0.46)	1.04	1.66
BBSAl-5	0.56 (0.60)	0.44 (0.40)	0.842	1.66
BBSAl-10	0.55 (0.60)	0.45 (0.40)	0.625	1.66
BBSAl-15	0.41 (0.38)	0.59 (0.62)	0.383	1.66

NBS glass with

0%Al_2O_3

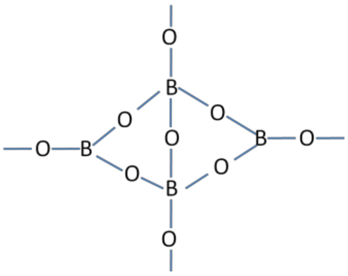

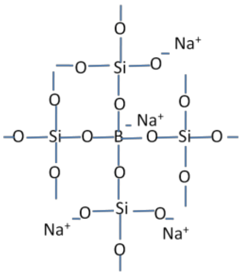

(Diborate) Reedmergnerite(a)

NBS glass with 5,

10 and 15%Al_2O_3

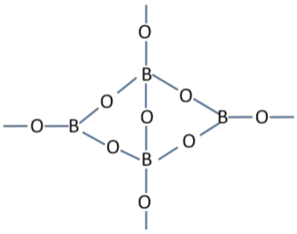

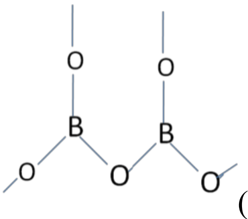

(b)

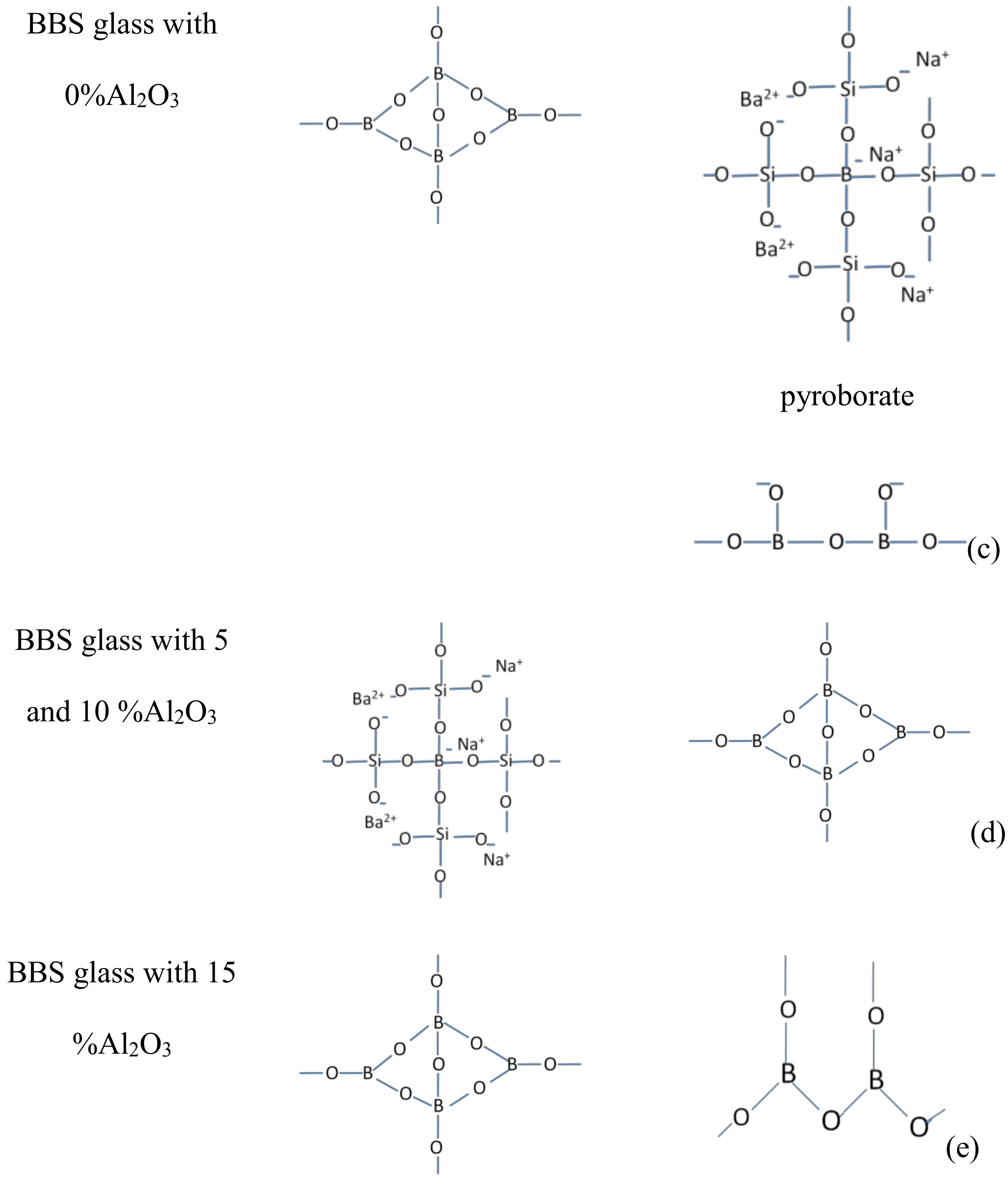

Figure 3.5. Schematic representation of different types of boron structural units present in (a and b) Sodium borosilicate (NBS) and (c, d and e) Barium borosilicate (BBS) glasses

4.3.4. DTA investigations

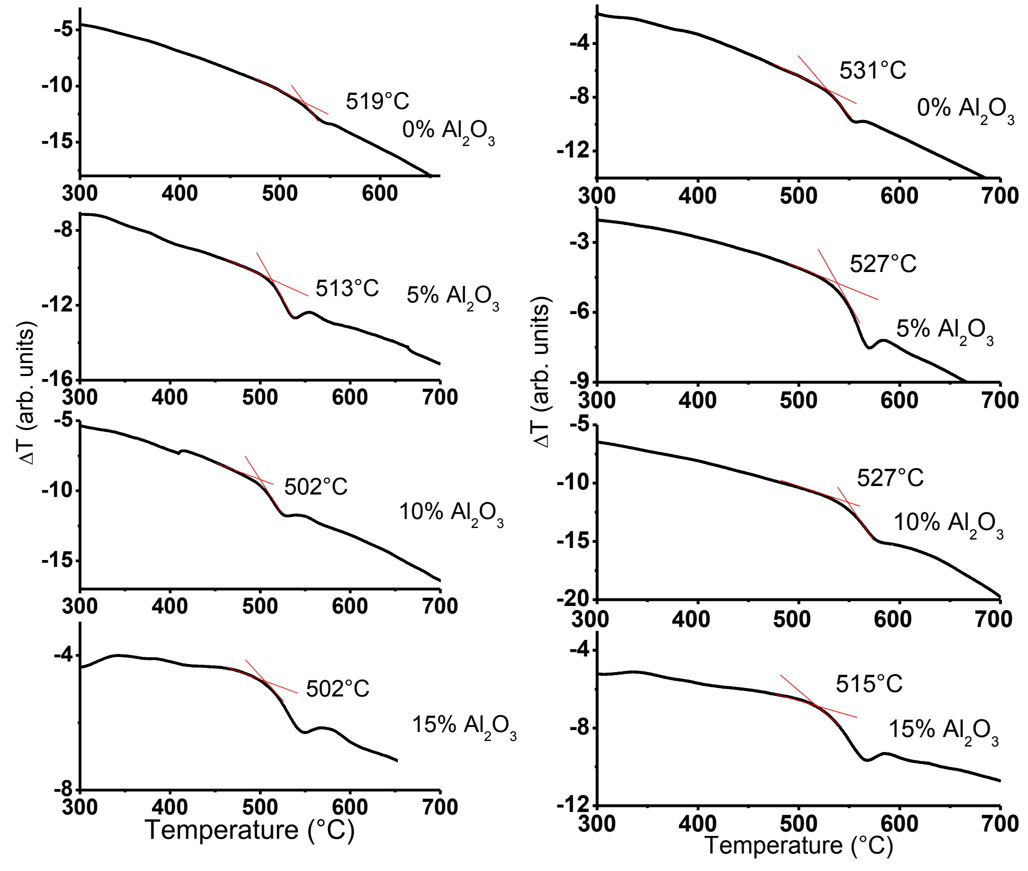

(a)

(b)

Figure 3.6. DTA patterns of (a) sodium borosilicate and (b) barium borosilicate glasses having different amounts of Al_2O_3.

Tg has been evaluated from different DTA scans and are indicated in the Fig. 3.6. For base glass i.e. samples without Al_2O_3, Tg value was found to be lower for sodium borosilicate glass (519°C) compared to BaO containing sodium borosilicate glass (531°C). From this results it is inferred that, even though network modifier concentration is more in BBS glasses compared to NBS glasses, BBS glasses network is thermally more stable compared to NBS glasses. One reason for this could be the increased extent of relatively more polymerized tetrahedral BO_4^- structural units formed at the expense of less polymerized BO_3 structural units in barium borosilicate glass, brought about by the increased network modifying oxide i.e BaO content [76]. This data is further confirmed in ^{11}B MAS-NMR analysis. Further for both the glass systems, the DTA patterns reveal that increased concentration of Al_2O_3 incorporation lead to decrease in Tg values. This can be attributed to the replacement of relatively stronger Si-O-B linkages with weaker Si-O-Al linkages. The bond energies of Si-O, B-O and Al-O are 798kJ/mol, 806kJ/mol and 512kJ/mol, respectively. Therefore, relatively less energy is required to break Al-O bond. ^{29}Si MAS-NMR spectra revealed formation of Si-O-Al linkages. However, Al_2O_3 is added to sodium borosilicate glasses holding $R = Na_2O/B_2O_3$ and $K = SiO_2/B_2O_3$ constant. The recruitment of alkali/alkaline earth ions for charge compensation of AlO_4^- leads to an increase in BO_3 structural unit at the expense of BO_4^- structural unit as evident in the MAS-NMR spectra in Figure 3.4. Concurrently, there is a small increase in Si polymerization as evident in Figure 3.2. The formation of Al – O – Si bonds vs. B – O – Si or Si – O – Si leads to a weaker network with a reduction in T_g. Additionally, formation of BO_3 structural unit with Al_2O_3 incorporation will also lead to a reduction in T_g. Overall, these two effects largely counteract the increasing Si polymerization leading to T_g remaining largely unaffected by Al_2O_3 addition. Therefore, with increasing concentration of Al_2O_3 from 0 to 15mol% decrease in Tg values are decreasing but not linearly because of competing effects with respect to formation of more polymerized Q^3 silica units with introduction of Al_2O_3.

3.3.5. Leaching studies

Leaching of elements from glass matrix is a natural phenomenon. Understanding leaching behavior of every element present in glass matrix is an important parameter to ascertain the chemical integrity of glass. A study was undertaken to examine the leaching behavior of all the constituent elements present in sodium borosilicate glass (NBS) and barium borosilicate glass (BBS) containing variable amount of Al_2O_3.

3.3.5.1. Effect of aluminum oxide on leaching characteristics

Fig. 3.7 shows the leach rate of individual elements in different glass samples. For all the elements the leach rate decreases exponentially. The rapid rate of decrease in leach rate initially is due to leaching of elements from the glass surface. Ones the elements on the surface have leached or reached an equilibrium, the elements from the bulk glass starts to get released in the leachate. This diffusion from bulk is slow and hence the decrease in leach rate is gradual.

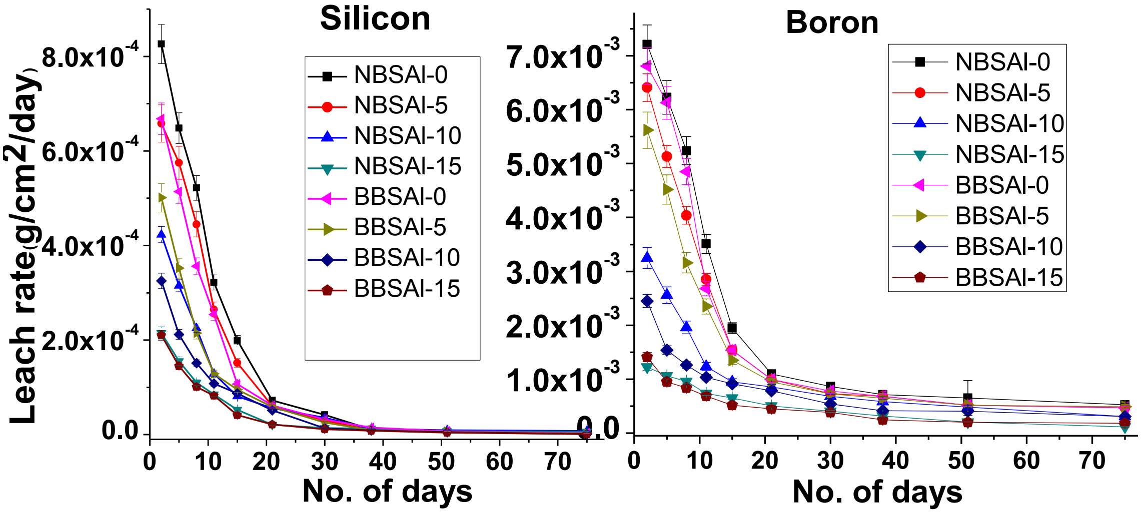

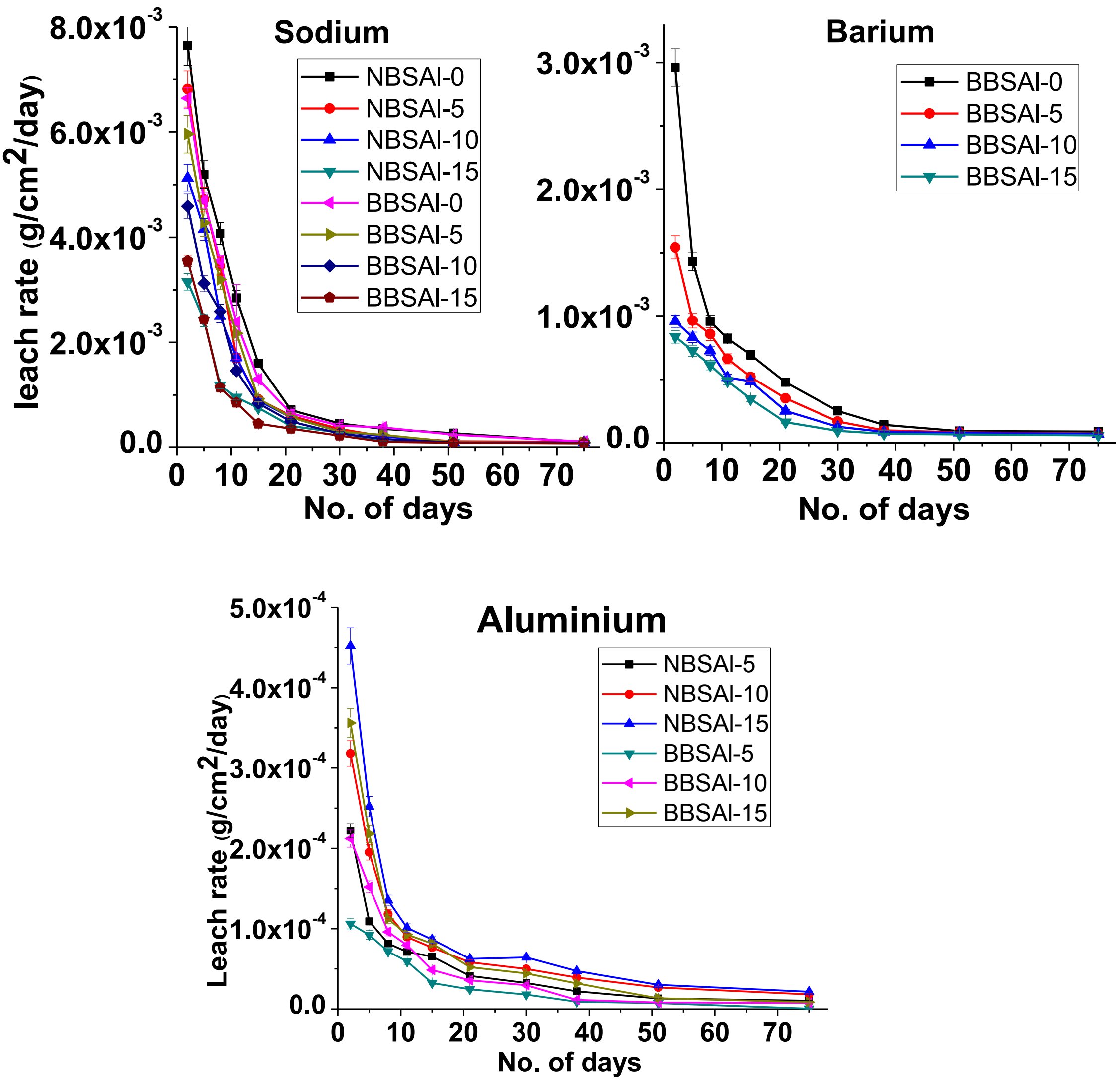

Figure 3.7. Leach rate of all elements for various glass samples

Table 3.4. pH of leachate

sample	7 day	15 day	26 day	41 day
NBSAl-0	9.66	9.62	8.98	8.58
NBSAl-5	9.11	9.07	9.12	9.28
NBSAl-10	8.41	8.58	8.55	8.35
NBSAl-15	8.36	8.58	8.61	8.34
BBSAl-0	9.25	9.48	9.42	8.54
BBSAl-5	8.88	9.55	9.48	8.89
BBSAl-10	8.36	8.42	7.99	8.08
BBSAl-15	8.48	7.73	7.26	7.67

The pH values of the leachate is also noted and given in Table 3.4. They were found to be above pH=7.This observation is due to release of Na^+ ion in exchange to H^+ present in leachate. The reactions taking place in the glass-water interface are given below [77].

$-Si-O^-Na^+ + H_2O \rightarrow -Si-O^-H^+ + Na^+ + OH^-$

These hydroxyl ions further attacks the siloxane bond resulting in depolymerization of glass network and dissolution of silicon.

$-Si-O-Si- + OH^- \rightarrow -Si-O^- H^+ + -Si-O^-$

This reaction does not stop over here. $-Si-O^-$ can further react with water molecule to regenerate hydroxyl ion.

$-Si-O^- + H_2O \rightarrow -Si-O^- H^+ + OH^-$

Therefore, on the glass surface, release of sodium ions occur that raises the pH of the leachate and since it was subjected to static leaching for some days this rise in pH lead to dissolution of Si into the leachate. Ingress of water molecule into the voids, can further dissolve Na and Si in the glass-water interface. However, it is seen that with rise in Al_2O_3 content from 0 mol% to 15 mol% leached fraction of Si, B and Na reduced whereas leach fraction of Al increased. Therefore, dissolution of aluminum is inhibiting the dissolution of Si into the leachate.

Xiao and Lasaga reported that activation energy for hydrolysis of the Si–O–Al linkage was 8 kcal/mol lower than that for hydrolysis of the Si–O–Si linkage because Si–O–Al bond is more basic than Si–O–Si, hence it is readily attacked by proton [78]. Therefore, dissolution of Al in water is more feasible and can take place through a number of species formation. Criscenti et al. found one such species and reported that when alumino-silicates are subjected to hydrolysis, Al–OH–Si can form. They characterised this hydroxyl group by IR spectroscopy. Bouyer et al. also studied the formation of aluminol Al–OH and Al–OH_2 groups as a result of hydrolysis of alumino-silicates [79]. Due to formation of all these species, Al that take part in the network formation, depolymerizes from the silicate network and gets dissolved in the leachate. However, Barry R. Bickmore et al. observed that $Al(OH)_4^-$ ion dissolved in leachate inhibits dissolution of silicon by forming aluminosilicate layer on surface of glass [80] which acts as a barrier against silicon dissolution.

Fig. 3.7. shows a decrease in leach rate of Na on increasing Al_2O_3 content. This can be attributed to lower substitution energy of BO_4^- than AlO_4^- unit which results in high strength by which Na^+/Ba^{2+} ions is attracted to AlO_4^- unit compared to BO_4^- unit. Therefore, with increasing Al_2O_3 leach rate of Na^+/Ba^{2+} ions decreases.

Another observation from Fig. 3.8 was that, leach rate of B was higher than Si and Al. This is due to higher basicity of B4–O–B4 (B4- tetrahedrally coordinated) bond, which makes it more prone to hydrolysis. Ce´line Cailleteau et al. reported the high solubility of boron as $B(OH)_3$ and $B(OH)_4^-$ groups [82]. Irrespective of Boron occupying trigonal or tetrahedral structural unit, both are prone to hydrolysis. The mechanisms are discussed by Gre´gory Geneste [81].

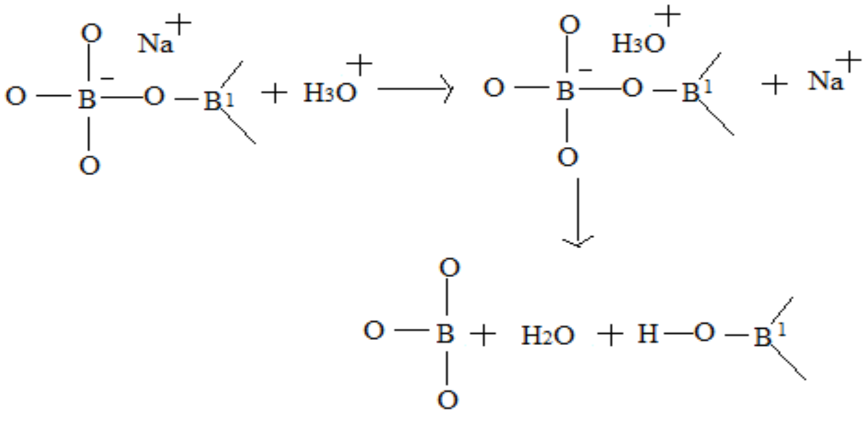

B^1 can be trigonal/tetrahedral B or Si. Here although Na^+ ion is acting as a charge compensator it gets replaced by a hydronium ion, also the hydronium ion does not stabilize the BO_4^- unit resulting in depolymerization of network. Followed by creation of $B(OH)_3$ unit and subsequent dissolution in leachant. In 10 and 15% Al_2O_3, the aluminosilicate phase on glass surface can be a reason to decrease the dissolution.

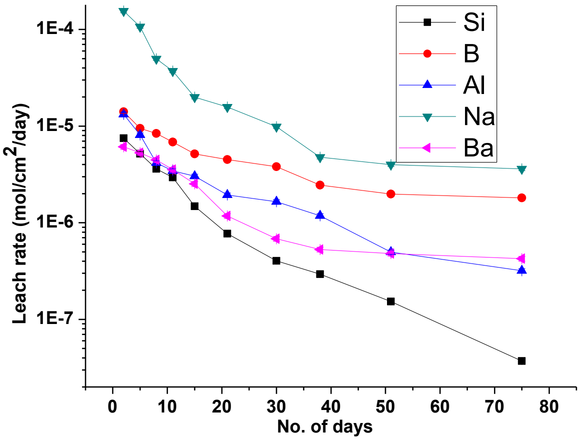

Figure 3.8. Leach rate of Si, B, Al, Na, Ba of BBSAl-15 glass sample

3.3.5.2. Effect of barium oxide on leaching characteristics

The effect of barium on sodium borosilicate glass is discussed here. During preparation of glass samples, in BBSAl-10, 10 mol% BaO was added to NBSAl-0 glass and concentration of all other elements were reduced without changing the ratio. With introduction of barium the leach rate of all the elements reduced, as shown in Fig. 3.9. On comparing NBSAl-10 and BBSAl-10 glass, in NBSAl-10 glass, Na_2O content is 18 mol% whereas in BBSAl-10, (Na_2O + BaO) content is 25.2 mol% but due to addition of barium the leach rate of Si and B decreased by a factor of 1.2 to 1.5 times and the leach rate of Na decreased by a factor of 1.5 to 2 times. The decrease in leach rate of Na is attributed to the fact that during dissolution of an ion from bulk to glass surface, the migration of the ion to neighboring sites require an activation energy and this activation energy for diffusion/migration of alkali and alkaline earth metal would depend on the radius ratio of both the ions. The more dissimilar the ions are the greater would be retardation in diffusion. Mishra et al. reported retardation in mobility of Na due to presence of Ba [83]. In glasses with one modifier ion i.e Na^+ in the case of NBSAl glass systems, Na^+ occupies the voids present in the glass sample and ones the Na^+ from the surface diffuses into the leachate, concentration gradient initiates jump of another Na^+ ion from bulk glass towards the surface. In glass with two modifiers as in the case of BBSAl glass system, where the concentration of Ba^{2+} is higher than Na^+, Ba^{2+} can jump to another nearby site as a result of concentration gradient but cannot occupy the sites created by Na^+ due to its bulky nature. Konstantinos Konstantinou reported that when two modifiers of dissimilar radius are present, the diffusion activation energy of smaller ion is less effected when compared to larger one [84]. This explains the lower leach rate of Ba when compared to Na, as shown in Fig. 3.9. Sumit kumar et al. reported that in glass systems where the difference in modifier ion field strength is large, show a greater binding [85]. This also explains the reduced leaching of all the constituent elements in Barium containing glass systems.

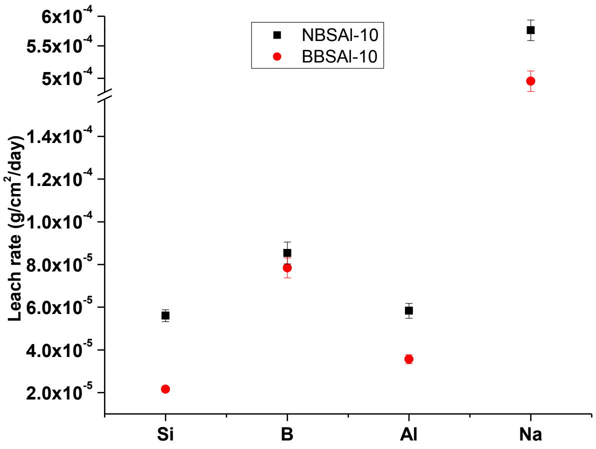

Figure 3.9. Leach rate of Si, B, Al, Na of NBSAl-10 and BBSAl-10 glass samples (14th day)

3.4. Conclusions

The effect of Al_2O_3 in two glass systems i.e. sodium borosilicate and barium borosilicate glasses were studied thoroughly. XRD patterns confirmed that addition of 15mol% of Al_2O_3 did not result in crystalline phase formation in these two glass systems. However, the behavior of Al in multi-elemental system is yet to be studied. DTA studies show that even though alkali and alkaline earth metal oxide content is more in barium borosilicate glass compared to sodium borosilicate glass, Tg of barium borosilicate glass is higher. This has been explained based on the increased extent of more connected BO_4^- structural units in barium borosilicate glass due to presence of more charge compensating alkali and alkaline metal elements. Addition of 15 mol% of Al_2O_3 resulted in gradual decrease of Tg value. MAS-NMR reveals that in both the glass systems Al exists as AlO_4^- structural units and interacts with silica structural units forming Si-O-Al linkages. The relative concentrations of BO_3 and BO_4^- structural units were calculated experimentally which is in good agreement with Dell-Bray model. Leaching experiments reveal that presence of Al_2O_3 helped in formation of aluminosilicate layer that hinder further leaching of all other elements. The work presented in this chapter is published in Journal of Non-Crystalline Solids (447 (2016) 283–289). These observations will be helpful during immobilization of any HLW with increased Aluminum content. However, Al_2O_3 being a network intermediate has shown a wide solubility range in borosilicate glass matrix but there are certain radionuclides that show very poor solubility in borosilicate glass matrix. As, HLW comprises of wide range of elements therefore immobilization of these troublesome radionuclides should also be studied in detail. With this view the next chapter focusses on enhancement of solubility of two troublesome elements namely molybdenum and chromium in borosilicate glass.

CHAPTER 4

Study on enhancement of solubility of MoO_3 and CrO_3 in modified borosilicate glass

4.1. Introduction

Glass has emerged out as one of the most popular candidates for immobilization of High Level Liquid Waste (HLW). Borosilicate glass has been chosen as the base glass matrix by a number of countries like France, USA, UK, Japan, Germany, Belgium, etc. The fascinating properties of glass matrix includes its wide solubility range, cheap raw materials easy fabrication, good chemical durability etc. The disordered and relatively loose arrangement of atoms in the glass structure helps achieve this wide tolerance limit for many elements. However, the present composition borosilicate base glass matrix that is used for immobilization of HLW generated from reprocessing of Pressurized Heavy Water Reactor (PHWR) spent fuel may not be the best option for immobilization of HLW originating from the fast neutron reactors. The second stage of Indian nuclear program would employ mixed oxide fuel (MOX) i.e., Pu and U oxide in a fast neutron reactor [86]. The fission products obtained from second stage nuclear reactors would contain elevated amount of fission products due to high burn-up of fuel; therefore, HLW originating from these spent fuels would also contain larger amount of fission products [87]. As ^{239}Pu is a constituent of MOX fuel, the composition spectrum of the (fission products) FPs are also going to vary when compared to ^{235}U based PHWR reactor. One such FP whose concentration will be relatively higher in HLW originating from second stage programme is molybdenum (Mo). Mo is a fission product with a high yield of nearly 6.03 at% in PHWR based reactor.

Table 4.1. Concentration of molybdenum in atom% originating as fission product from various radioisotopes bombarded by (0.025eV) thermal neutron [88].

	^{233}U	^{235}U	^{239}Pu
$_{42}Mo^{99}$	4.91	6.53	6.21
$_{42}Mo^{100}$	2.7	6.29	6.91
$_{42}Mo^{101}$	3.42	5.28	6.14
$_{42}Mo^{103}$	2.88	3.05	7.12

Table 4.1 shows that ^{239}Pu based fuel yields higher amount of Mo compared to U based fuel. This table shows fission yield values of only 4 Mo isotopes whereas as many as 19 Mo isotopes are generated as fission product. Therefore, it is clear that second stage reactors that would use Pu-239 as fuel will contain larger amount of Mo in HLW compared to PHWR generated HLW. The challenge that arises in immobilization of Mo containing HLW is that MoO_3 show very poor solubility of (1 mol%) in borosilicate glass [89]. Apart from molybdenum there are many other elements present in HLW that show low solubility in borosilicate glass. For example, chlorides, fluorides tend to form crystals of alkali halides. Noble metals Rh, Pt and Pd exhibit solubility of less than 1 wt% [90]. Another such element is Cr, the solubility of CrO_3 in borosilicate glass is very low i.e., 2mol% [91]. Chromium is a corrosion product and the origin of Cr in HLW is from the usage of stainless steel (SS). SS vessels are used as process vessel during various stages in reactor operation, reprocessing and waste management, for storage of

liquid waste and transfer systems. SS contains mainly Fe, 16-18% Cr, 10-14% Ni and traces of other elements [92]. Cr has a property of adding strength and corrosion resistance to SS alloy. Cr forms a layer of chromium oxide on the surface of the alloy and this retards further corrosion. Even though this mechanism helps in prevention of corrosion but still a number of ways are reported that favours corrosion of SS and thereby releasing Cr in HLW. One of the most common ways of corrosion of SS is Pitting corrosion. In this form of corrosion, a localized site becomes anodic and the nearby area becomes cathodic or a localized site becomes cathodic and the nearby area becomes anodic, followed by selective removal of ions from the alloy. Chloride is a well-known agent for initiating pitting corrosion. Presence of oxidizing agents or reducing agents in SS process vessels also elevates corrosion. In another study, it is observed that corrosion accelerates in SS in stagnant solution or areas where precipitates are formed on SS surfaces or at the edges where oxygen concentration can reduce over time. Marsh et al. reported that radiation field does not directly initiate or accelerate corrosion process [94]., but formation of peroxide in solution due to radiolysis, not only alters the potential of the solution but also produces reactive free radicals. Consequently, this plays a key role in accelerating corrosion process [93-96]. All these corrosion processes increase the chances of Cr releases in HLW. The present chapter deals with MoO_3 and CrO_3 solubility enhancement in borosilicate glass.

Both Cr and Mo being transition metals and displaying a high oxidation states behaves very similarly in borosilicate glass. Mo being present mainly in the form of Mo^{6+} tend to crystallize in the form of alkali and alkaline earth metal molybdates and separate out from the silicate matrix [96]. This crystalline phase is highly undesirable as alkali molybdates has a tendency to trap Cs, Sr and due to water soluble nature of these molybdates, these glasses exhibit higher leaching characteristics resulting in accidental radioactivity exposure. There are many literatures on behavior of MoO_3 in borosilicate glasses. Rose et al. reported formation of $Na_3Li(MoO_4)_2·6H_2O$ and $(Na,Sr,Nd,La)MoO_4$ powellite crystal structure in simulated product glass. $(Na,Sr,Nd,La)MoO_4$ are potential host for Am and Cm [97]. Not only this, these molybdates also lead to accelerated corrosion of Inconel melter and accelerates volatilization of some component species. Similarly, Cr also shows a limited solubility of 2 mol% in borosilicate glass. Sambasiva Rao et al. observed several complexes of Cr^{3+} and Cr^{6+} ions in $Na_2O–PbO–Bi_2O_3–SiO_2$ glass ceramic. In these glasses Cr_2O_3 acted as a nucleating agent and formed several crystalline phases like $NaCrO_4$, $Na_2Cr_2O_7$ and $PbCrO_4$ [99]. In another work, Jesse Alton et al. studied the kinetics of a $(Fe,Ni,Mn)(Fe,Cr)_2O_4$ spinel crystal formation during HLW vitrification [100]. These crystals being denser than glass settle at the bottom of the melter causing significant problems in melter operation [98].

Many works have been reported with a view of increasing the solubility of Mo and Cr in borosilicate glass. Szumera et al. showed that in a silica-phosphate glass containing 40 mol% P_2O_5, 4.4 mol% of MoO_3 can be included, but weakening of the structure was observed [101]. Borophosphate glass also shows enhanced solubility of MoO_3 [102]. However, phosphate glass is undesirable in nuclear industry especially owing to its poor thermal and chemical characteristics [103].

This work was focussed on formulation of a base glass composition that can exhibit an increased solubility of Mo and Cr. To improve their solubility, three different base glass matrices were studied and compared. These three base glass matrices were sodium borosilicate glass (NaBS), barium containing sodium borosilicate glass (BaBS) and phosphate containing sodium borosilicate glass

(NaPBS). The experimental details and their findings are provided in the forthcoming sections.

4.2. Experimental

4.2.1. Synthesis of glass samples

Three batches of glass samples were prepared by melt quench method as given in chapter 2. First batch was a sodium borosilicate base glass, second batch was barium containing sodium borosilicate base glass and the third batch was phosphate containing borosilicate base glass. In these three base glasses different amounts of MoO_3 and CrO_3 was added individually and both together in the same sample. All the compositions are given in Table 4.2, Table 4.3 and Table 4.4. The poring temperature was maintained at 1100^{o}C. The glass sample preparation and furnace details are provided in chapter 2.

Table 4.2. Composition of three base glasses containing different amounts of MoO_3

Sample name	Composition in mole fraction					
	SiO_2	B_2O_3	Na_2O	BaO	P_2O_5	MoO_3
NaBS	0.5	0.3	0.2			
NaBS-Mo-1	0.495	0.297	0.198	-	-	0.01
NaBS-Mo-2	0.49	0.294	0.196	-	-	0.02
BaBS	0.449	0.269	0.182	0.1	-	
BaBS-Mo-1	0.445	0.267	0.178	0.099	-	0.01
NaPBS	0.420	0.330	0.200	-	0.050	
NaPBS-Mo-1	0.415	0.327	0.198	-	0.0495	0.01
NaPBS-Mo-2	0.412	0.323	0.196	-	0.0490	0.02
NaPBS-Mo-3	0.408	0.320	0.194	-	0.0485	0.03
NaPBS-Mo-4	0.404	0.316	0.192	-	0.0480	0.04

Table 4.3. Composition of three base glasses containing different amounts of CrO_3

Sample name	Composition in mole fraction					
	SiO_2	B_2O_3	Na_2O	BaO	P_2O_5	CrO_3
NaBS-Cr-2.5	0.487	0.293	0.195	-	-	0.025
BaBS-Cr-2	0.49	0.294	0.178	0.098	-	0.02
NaPBS-Cr-1	0.415	0.327	0.198	-	0.0495	0.01
NaPBS-Cr -2	0.412	0.323	0.196	-	0.0490	0.02
NaPBS-Cr -3	0.408	0.320	0.194	-	0.0485	0.03
NaPBS-Cr -4	0.404	0.316	0.192	-	0.0480	0.04

Table 4.4. Composition of phosphate containing borosilicate glasses containing different amounts of MoO_3 and CrO_3

Sample Name	Composition in mole fraction					
	SiO_2	B_2O_3	Na_2O	P_2O_5	MoO_3	CrO_3
PBS-MoCr-1	0.404	0.316	0.192	0.048	0.035	0.005
PBS-MoCr-2	0.404	0.316	0.192	0.048	0.025	0.015
PBS-MoCr-3	0.404	0.316	0.192	0.048	0.02	0.02
PBS-MoCr-4	0.404	0.316	0.192	0.048	0.015	0.025
PBS-MoCr-5	0.404	0.316	0.192	0.048	0.005	0.035

4.2.2. Structural and elemental characterization

X-ray diffraction patterns (XRD) were recorded for determining the presence of crystalline phase, if any, in glass. X-ray amorphous could still contain up to around 4% crystals. Therefore, for further confirmation of non-crystallinity of glasses Scanning Electron Microscopy - Energy Dispersive X-Ray Spectroscopy (SEM-EDS) was done for the glass composition containing highest amount of MoO_3 and CrO_3, to confirm the absence of phase separation. Particle Induced Gamma-ray Emission (PIGE) method was employed for quantification of low Z elements like Si, B, Na and P. X-Ray Fluorescence (XRF) was used for confirmation of phosphorous value. Laser Induced Breakdown Spectroscopy (LIBS) was carried out for quantification and to confirm the homogeneous inclusion of Mo and Cr in glass.

4.3. Results and Discussion

4.3.1. XRD investigations

XRD patterns of MoO_3 containing glasses are shown in Fig. 4.1. XRD pattern of NaBS-Mo-1 and NaBS-Mo-2 glass samples are shown in Fig. 4.1(a). NaBS-Mo-1 glass containing 1 mol% of MoO_3, shows broad hump confirming the existence of a complete amorphous system. Whereas, NaBS-Mo-2 glass containing 2 mol% of MoO_3, shows sharp peak seen over the broad amorphous hump revealing presence of Na_2MoO_4 crystalline phase (ICSD-151970). These crystalline phase formations in borosilicate glasses were reported previously. Farges et al. reported the formation of alkali molybdate due to high oxidation state of Mo^{6+} cation and its high field strength (1.89-1.935A^{-2}) exerting a strong ordering effect on its neighbouring atoms [104]. Also, the bond Si-O-Mo induces a higher bond valence on O, resulting in breaking of this bond and separation of sodium molybdate from silicate network. This causes separation of Mo from silicate network along with Na. Similarly in BaBS base glass addition of only 1 mol% of MoO_3 leads to the formation of crystalline phases of $BaMoO_4$ (JCPDS-08-0455) in the glass (Fig. 4.1(b)). Here XRD analysis could not detect any crystalline Na_2MoO_4 peaks. The formation of $BaMoO_4$ over Na_2MoO_4 may be attributed to the difference in their free energy of formation. The free energies of formation of $BaMoO_4$ (-1439.6 kJ/mol) is lower than Na_2MoO_4 (-1354.34 kJ/mol), resulting in formation of $BaMoO_4$.

Fig. 4.1(c) shows the XRD patterns of third batch of glass samples i.e, the four glass samples of NaPBS-Mo series. The characteristic broad peak over the 2θ range of 15–35° confirms the amorphous nature of the glass. There are no sharp peaks confirming that no crystalline phase separation has occurred.

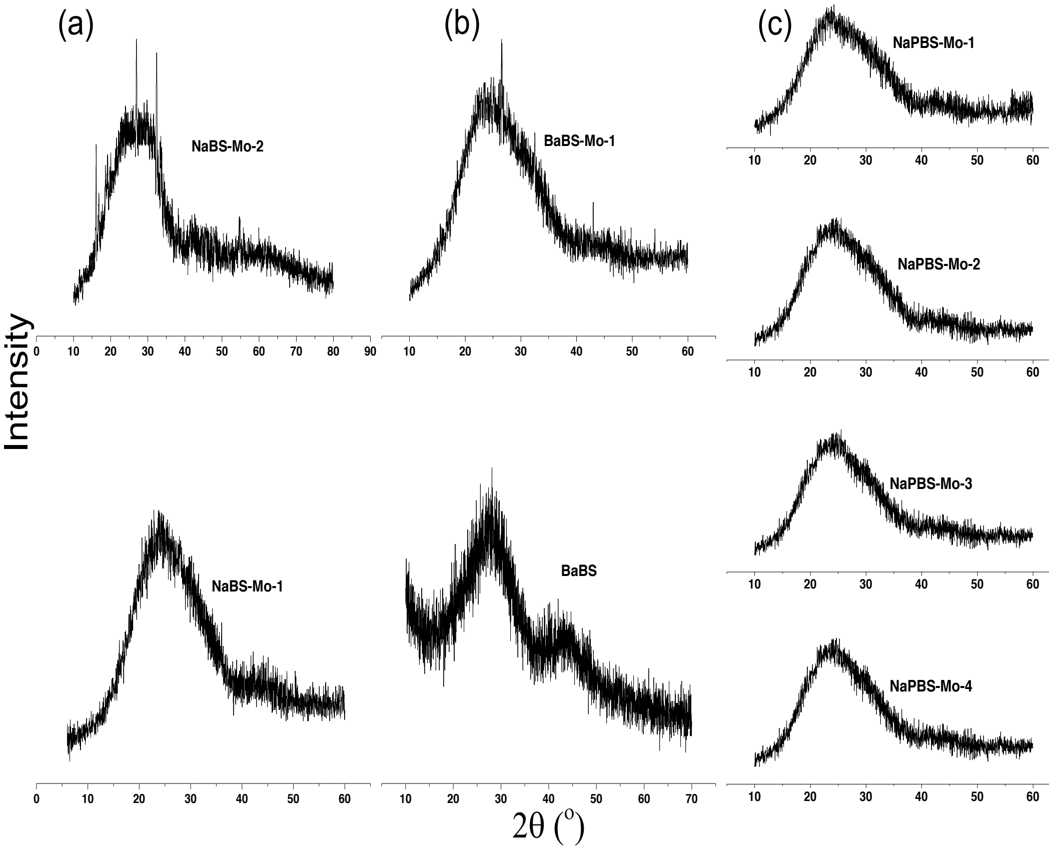

Figure 4.1. XRD patterns of (a) NaBS-Mo-1 and NaBS-Mo-2 (b) BaBS without Mo and BaBS-Mo-1(c) XRD patterns of NaPBS-Mo-x (x= 1 to 4 mol%) glasses

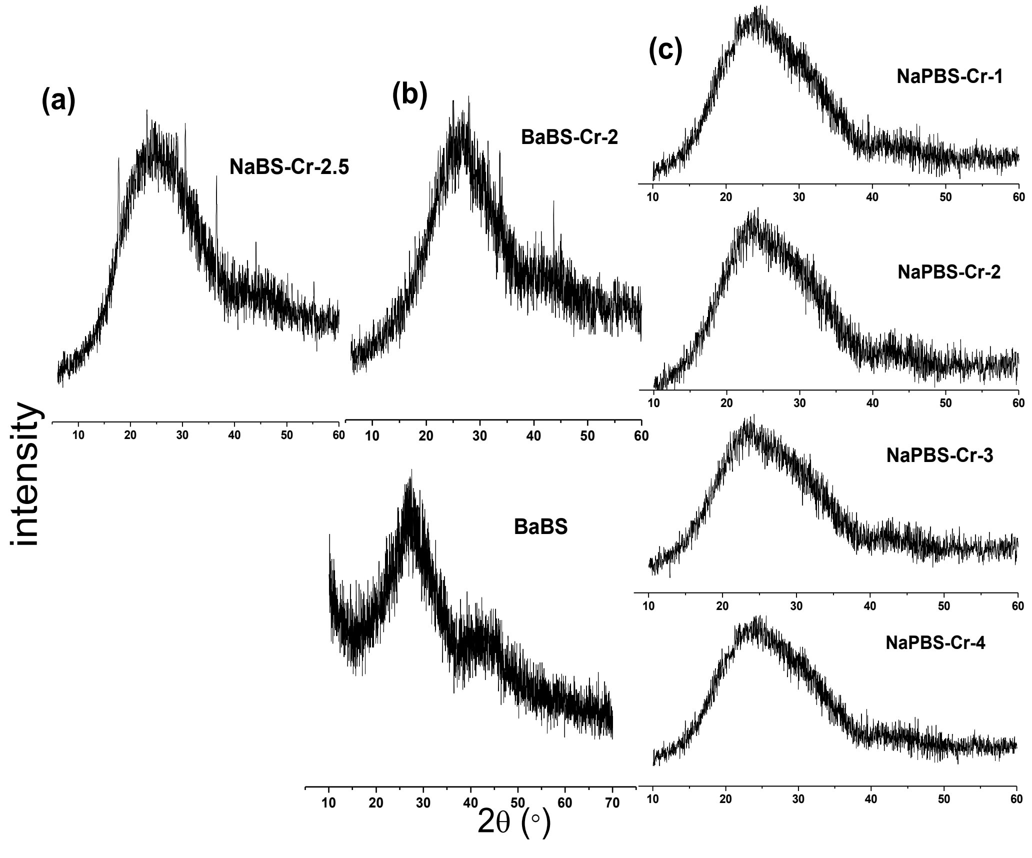

Figure 4.2. XRD patterns of (a) NaBS-Cr -2.5 (b) BaBS without Cr and BaBS-Cr-2 (c) XRD patterns of NaPBS-Cr-x (x= 1 to 4 mol%) glasses

XRD patterns of CrO_3 containing glasses are shown in Fig. 4.2. Similar to MoO_3, CrO_3 showed presence of Cr_2O_3 crystalline phases over the broad amorphous hump as seen in Fig. 4.2(a). Pavel Hrma et al. observed the behaviour of Cr in multielement borosilicate glass. They observed formation of eskolite crystals (Cr_2O_3) in melts with more than 2wt% Cr_2O_3 [91, 100]. Fig. 4.2(b) revealed formation of $BaCrO_4$ crystalline phases within BaBS glass structure [105]. Therefore, in base glasses NaBS and BaBS as low as 2.5 mol% and 2mol% of CrO_3 caused phase separation. The XRD patterns of glass samples PBS-Cr-x (x=1-4) are shown in Fig. 4.2(c). All the four glass samples showed a broad hump which is a characteristic pattern of amorphous solids. There are no sharp peaks in the XRD patterns indicative of absence of crystalline phases. Very similar to the glass samples with MoO_3, the reason for high solubility of Cr_2O_3 in phosphate glass is due to the formation of Cr-O-P bond. Cr-O-P bond not only inhibits Cr phase separation but also improves the chemical durability of phosphate groups [21, 22].

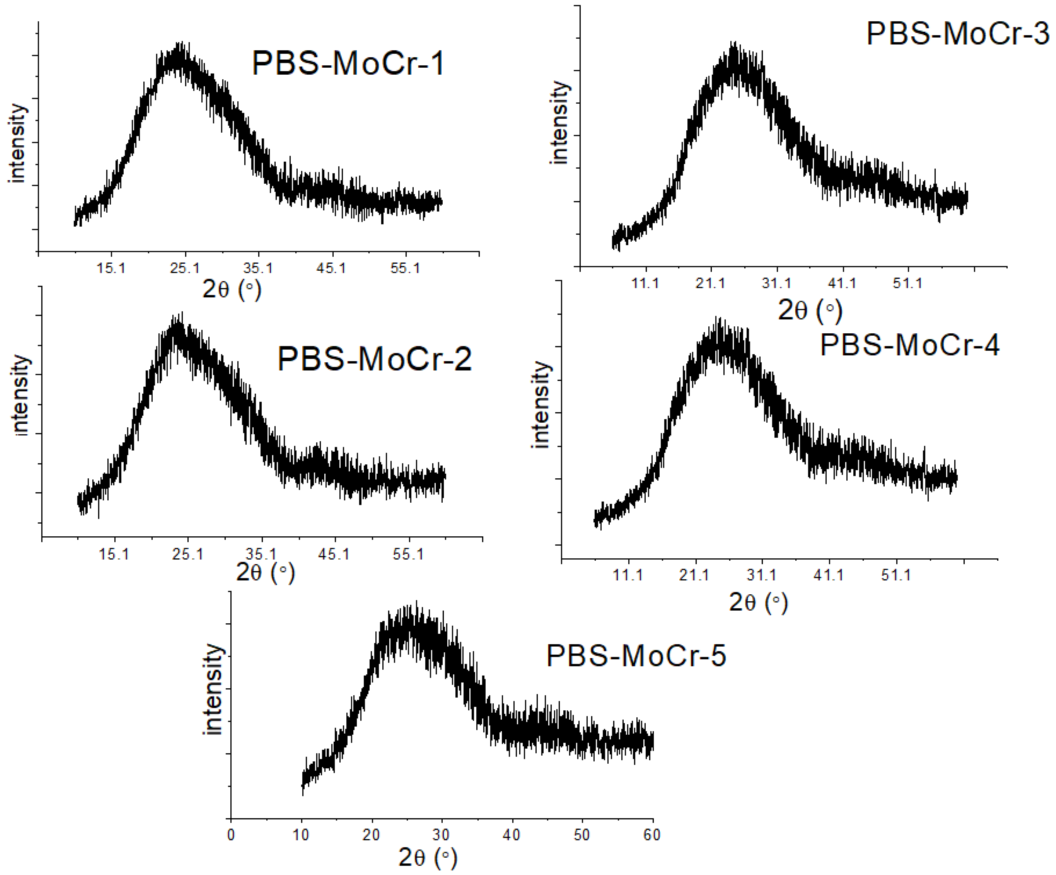

Figure 4.3. XRD patterns of PBS-MoCr-x (x=1-5)

Multi component glass is the final product during vitrification of HLW. Formation of crystalline phases in glass largely depend on presence of other elements. For example, formation of spinel (Cr_2O_3) crystal in high level waste glass increases in the presence of noble metals [105]. John S. McCloy and Ashutosh Goel stated that in presence of alkali metals, alkali molybdates form and in presence of alkaline earth metals more durable alkaline earth metal molybdates form, whereas when composition of glass changes, the availability of alkali and alkaline earth metals vary and thus effecting crystallization during vitrification of HLW [108]. Brandon J. Greer and Scott Kroeker characterized molybdate and chromate phase assemblages in borosilicate waste glasses. They also observed that several crystalline phases like Na_2MoO_4, $Na_2MoO_4 \cdot 2H_2O$, Cs_2CrO_4, $Cs_3Na(MoO_4)_2$ etc. precipitated out from the glass matrix and a random substitution of Cr into Mo sites of $Cs_3Na(MoO_4)_2$ occur [109]. Therefore, although the glass samples PBS-Mo-x (x=1-4) and PBS-Cr-x (x=1-4) were all completely amorphous in nature and did not contain any crystalline phase, the samples PBS-MoCr-x (x=1-5) were also recorded for XRD pattern to check if presence of MoO_3 and Cr_2O_3 together in the same sample effects the formation of crystals. However, the XRD patterns are presented in Figure 4.3 and a broad peak in the 2θ range of 15–40° and absence of sharp peak confirmed the absence of crystalline phases.

4.3.2. SEM/EDS investigations

SEM/EDS analysis of two glass samples (NaPBS-Mo-4 and NaPBS-Cr-4) were carried out and are shown in Fig 4.4(a) and Fig 4.5(a). Since samples that are XRD amorphous still have the possibility of showing presence of crystalline phase in microscopic level, SEM/EDS analysis were carried out. The micrograph of both the glass samples displays homogeneous nature of the glass sample with no evidence of presence of crystalline phase separation. EDS analysis on two spots were also carried out. The spots are marked in Fig. 4.4(a) and Fig. 4.5(a) and the elemental patterns are shown in Fig. 4.4(b) and Fig. 4.5(b). The results show homogeneousness of the glass samples at those two spots. As the glass sample that contained highest amount of MoO_3 and CrO_3 did not display any phase separation. Therefore, other samples with lesser MoO_3 were not analysed by SEM-EDS with an idea that as they contain lesser amount of Mo and Cr, these glass samples would also not contain any crystalline phase.

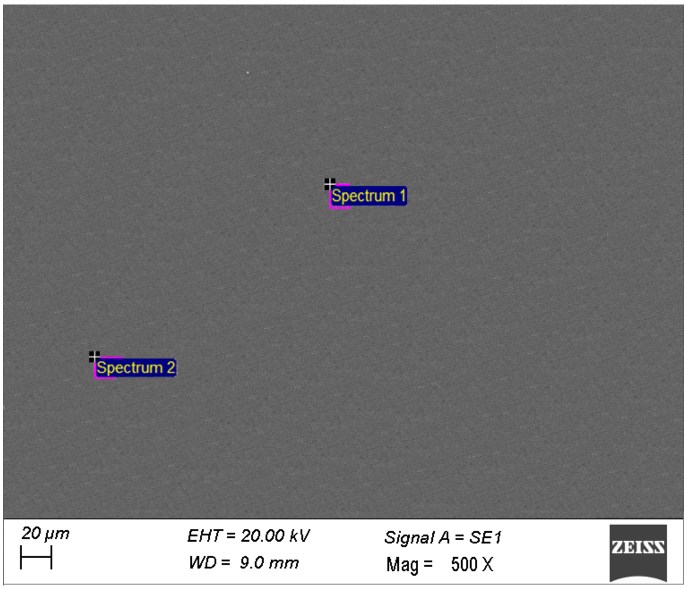

Figure 4.4 (a) SEM micrograph of NaPBS-Mo-4

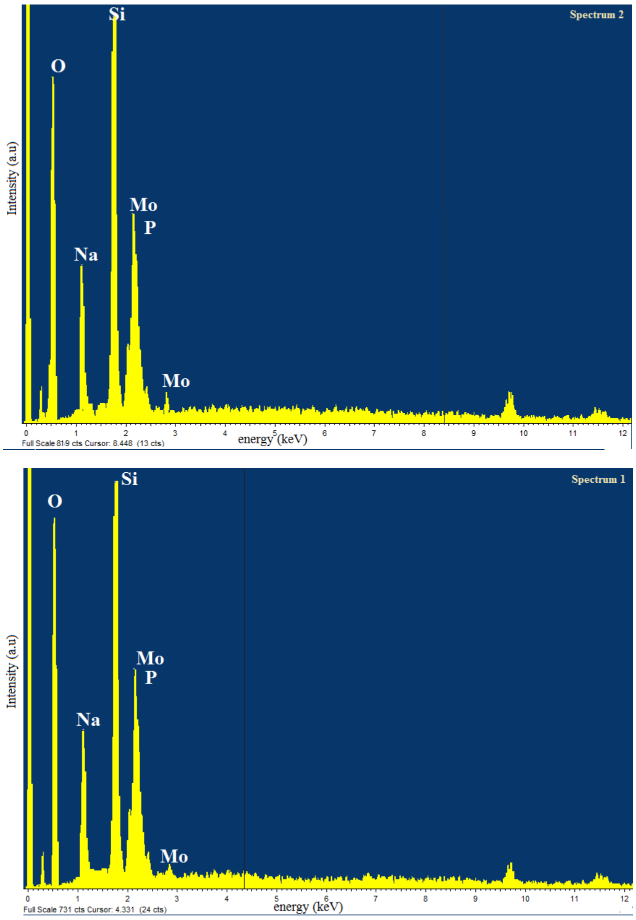

Figure 4.4 (b) EDS pattern of NaPBS-Mo-4

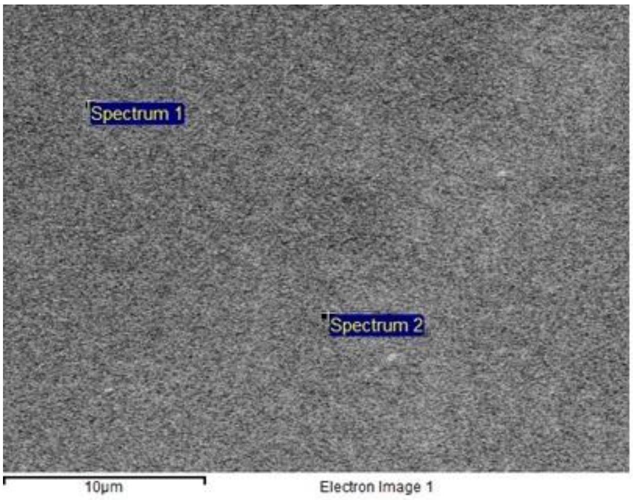

Figure 4.5 (a) SEM micrograph of NaPBS-Cr-4

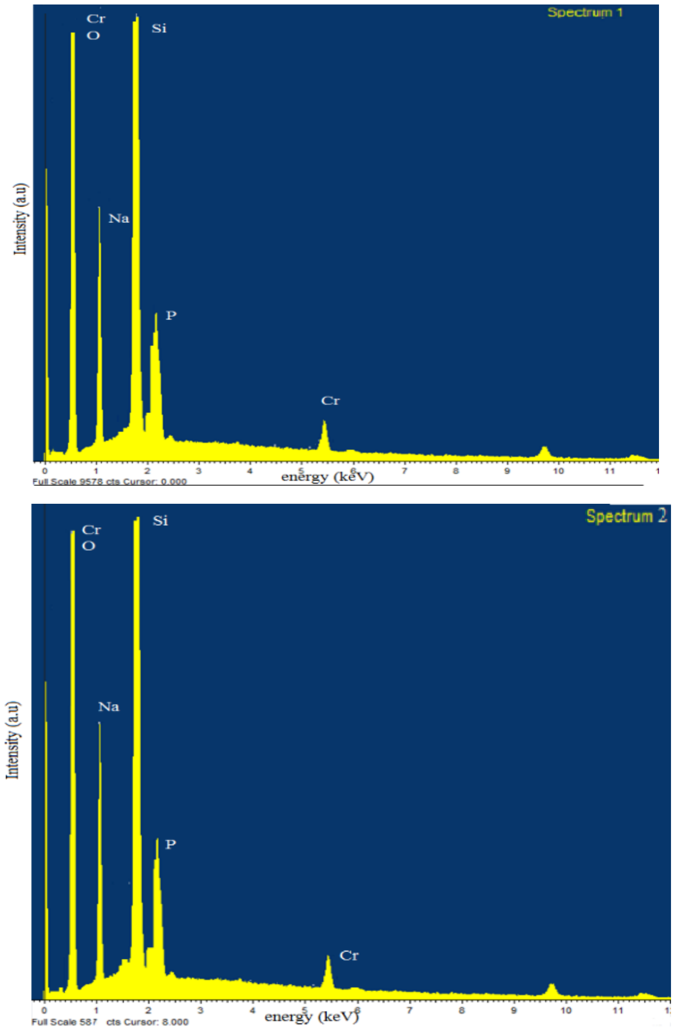

Figure 4.5 (b) EDS pattern of NaPBS-Cr-4

4.3.3. PIGE investigations

All the glass samples were subjected to a temperature of 1100ºC. Boron and phosphorous are known to exhibit high volatility at such a high temperature. Shaodong et al. reported loss of boron during preparation of glass at a melting temperature of 1200ºC [110]. Similarly, Pawel Stoch et al. reported adding 20% excess ammonium phosphate during preparation of glass to compensate for the loss of phosphorus. However, the temperature associated was greater than 1300ºC [111]. Therefore, it was important to determine the elemental composition so that the base glass composition could be rightly determined that is necessary to accommodate 4mol% of Cr and Mo.

External in situ current normalized PIGE (Ext-PIGE) method has been validated using three different control samples namely synthetic elemental standard, glass CRM, Rock phosphate (BCR-032) CRM. Determined concentration (wt%) of four low Z elements (Si, Na, B and P) in synthetic elemental standard, borosilicate glass certified reference material (CRM) and phosphate rock (BCR-032) by external in situ current normalized PIGE (Ext-PIGE) method using fluorine as current normalizer along with % deviation and zeta-score are given in Tables 4.5 and 4.6, respectively. The absolute concentration results are found to be in good concurrence with the expected and certified values with the % deviation within ±3% and zeta score below 1 at 95.5 % confidence level for all four elements in three different standards. The uncertainties given along with the results are the expanded uncertainties (EU) (at k=2) at 95.5 % confidence level. The expanded uncertainties associated with the results are found to be in the range of 2-5% which are due to propagation of counting statistics error from sample, standard and in situ current normalizer, their corresponding uncertainties on masses and uncertainty on standard concentration. It is observed that among Si, Na, and B, there is higher uncertainty associated with the result of P. The total EU for P was found to be nearly 5% which may be due to counting statistics. Particle Induced Gamma-ray (PIGE) method deals with the prompt gamma-ray of $^{31}P(p,p')^{31}P$ scattering reaction at 2233 keV, which has lower thick target gamma-ray yield for proton induced inelastic reactions at proton energy 3.5 MeV, as a result we are getting lower count rate of the P present in the sample. Lower count rate leads to higher uncertainty due to counting statistics.

Table 4.5. Determined concentration (wt%) in a synthetic mixed elemental standard of four low Z elements by in situ current normalized PIGE method using fluorine as in situ current normalizer

Element	**Elemental Standard**		
	Present work (Mean ± EU))	**Expected**	**% deviation**
Si (%)	13.2 ±0.3	13.4	-1.8
Na (%)	4.53 ±0.08	4.4	2.9
B (%)	3.98 ±0.12	4.1	-2.9
P (%)	8.76 ±0.40	8.9	-1.6

Table 4.6. Determined concentration (wt%) in borosilicate glass CRM (Title No. M4FT-12SR0307084) and BCR-032 (phosphate rock CRM) by in situ current normalized PIGE method using fluorine as an in situ current normalizer along with % deviation and zeta-score (at 95.5 % confidence level)

Oxide	Elemental Standard			
	Present work (Mean (EU))	Certified	% deviation	Zeta-score
SiO_2	55.9±1.1	56.2 ±1.5	-0.5	0.16
Na_2O	12.6 ±0.2	12.2 ± 0.7	3.3	0.05
B_2O_3	17.1±0.8	17.3 ± 0.9	-1.2	0.02
BCR-032 (IRMM-CRM)				
P_2O_5	32.1 ±1.5	32.98 ±0.17	-2.7	0.57

Table 4.7. Determined concentrations (wt%) in seven different alkali borosilicate glass samples by *in situ* current normalized PIGE method using fluorine as *in situ* current normalizer and their comparison with raw material taken for fabrication (wt%)

Element	NPBS-Mo1			
	Obtained result (wt%)	Expanded Uncertainty (EU)	Amount added (wt%)	%deviation
Si	17.2	0.2	16.99	1.2
Na	13.4	0.1	13.31	0.7
B	9.27	0.12	9.55	-2.9
P	4.36	0.30	4.48	-2.7
	NPBS-Mo2			
Si	17.1	0.2	16.67	2.6

Na	13.3	0.1	13.03	2.1
B	9.06	0.14	9.34	-3.0
P	4.28	0.30	4.39	-2.5
	NPBS-Mo3			
Si	16.6	0.2	16.32	1.7
Na	12.4	0.1	12.75	-2.7
B	8.97	0.14	9.14	-1.9
P	4.16	0.30	4.29	-3.0
	NPBS-Mo4			
Si	16.42	0.2	15.99	2.7
Na	12.18	0.1	12.49	-2.5
B	8.95	0.12	8.94	0.1
P	4.08	0.28	4.22	-3.3
	NPBS-Cr1			
Si	17.3	0.2	17.09	1.2
Na	12.9	0.1	13.39	-3.7
B	9.58	0.14	9.62	-0.4
P	4.33	0.30	4.52	-4.2
	NPBS-Cr2			
Si	16.5	0.2	16.88	-2.3
Na	13.2	0.1	13.20	0.0
B	9.54	0.12	9.45	1.0
P	4.28	0.26	4.44	-3.6
	NPBS-Cr4			
Si	16.8	0.2	16.40	2.4
Na	12.41	0.1	12.81	-3.1
B	9.35	0.12	9.17	2.0
P	4.19	0.28	4.35	-3.7

The mean concentration (wt%) results of four elements (Si, Na, B and P) utilizing in situ current normalized Particle Induced Gamma-ray Emission (Ext-PIGE) method using fluorine as in situ current normalizer and its comparison with the expected amount taken in the mixture of raw material are compared and given in Table 4.7. It has been observed that the concentration results of all the elements (Si, Na, B and P) are in good agreement as of raw material taken but in case of the phosphorous, the obtained results are found to be lesser than the expected amount. The % deviation, in case of phosphorous vary from 2.5%- 4.2% i.e. we are getting lower amount of P in the final product glass samples. Although phosphorus is known to exhibit evaporation losses during fabrication of glass samples, to confirm the values of P obtained in PIGE, XRF studies were performed.

4.3.4. XRF investigations

XRF analysis of three samples (NaPBS-Mo-1, NaPBS-Mo-2 and NaPBS-Cr-4) were carried out. As the concentration of phosphorous in final product glass was lower than the amount added, an alternate analytical technique i.e. XRF analysis was carried out to confirm the values of P obtained using PIGE technique.

The method was validated using two standards. They are the synthetic standard used in PIGE analysis. Determined concentration (wt%) of P in two standard and three glass samples are given in Table 4.8. The micro-XRF results showed 2.5 to 5.9% lower phosphorous concentration than the expected values. From the concentration results obtained by PIGE and XRF methods, it is confirmed that there is a loss of phosphorous during fabrication of glass samples.

Table 4.8. Comparison of determined phosphorous concentration (wt%) in three representative glass samples using PIGE and micro-XRF with amount of P added

Method		Ext-PIGE (Mean ± EU)		Micro-XRF (Mean ± EU)	
Sample ID	Expected P (wt%)	P (wt%)	% dev	P(wt%)	% dev
NaPBS-Mo-1	4.48	4.36 ± 0.30	-2.7	4.37 ±0.22	-2.5
NaPBS-Mo-2	4.39	4.28 ± 0.30	-2.5	4.13 ± 0.20	-5.9
NaPBS-Cr-2	4.45	4.28 ± 0.26	-3.6	4.21 ± 0.22	-5.4

4.3.5. LIBS investigations

The presence of emission rich Mo and Cr lines along with interference from other elements make the LIBS spectrum highly complex and a challenging task to identify a spectrally pure Mo/Cr emission lines for univariative study. In contrast, multi-variate analytical methods like Partial Least Squares Regression (PLSR) is known to be better suited for complex and unresolved spectra and hence was used for determination of Mo and Cr [112]. Two spectrometer were used for this study, Echelle Spectrometer (EH) covers 200–950nm wavelength regions and Czerny-Turner spectrometer (CT) covers 14nm wavelength. Details of instrumentation are provided in chapter 2.

Due to superiority of CT over EH, lines from CT spectrometer were used when univariate calibration methodology was applied for quantification [113]. Mo and Cr emission lines were selected by spectral comparison and database matching.

Among the identified Mo emission lines seven Mo emission lines, viz., 277.54nm, 280.77nm, 281.61nm, 284.82nm, 287.15nm, 289.09nm and 289.44nm were the most spectrally pure and hence used for univariate calibration method. Similarly, for Cr, 275.77nm, 276.25nm, 281.14nm, 283.04nm, 283.56nm, 284.32nm, 285.56nm, 285.73nm, 286.09nm, 286.19nm, 287.59nm and 288.86nm were selected for univariative analysis. For construction of calibration curves, the emission lines were normalized with respect to total light or whole spectrum area intensity prior to calibration. Fig. 4.6 shows the calibration curve obtained for Mo (277.54 nm) emission line and Cr (283.04 nm) against their concentration. The precision and accuracy were of 10.1% and 8.4%, respectively, for Mo and 12 % and 11 % for Cr quantification. These analytical values are not acceptable in analytical quality assurance of nuclear materials. To improve the results analytical spectral dependent partial least squares regression (ASD-PLSR) were performed.

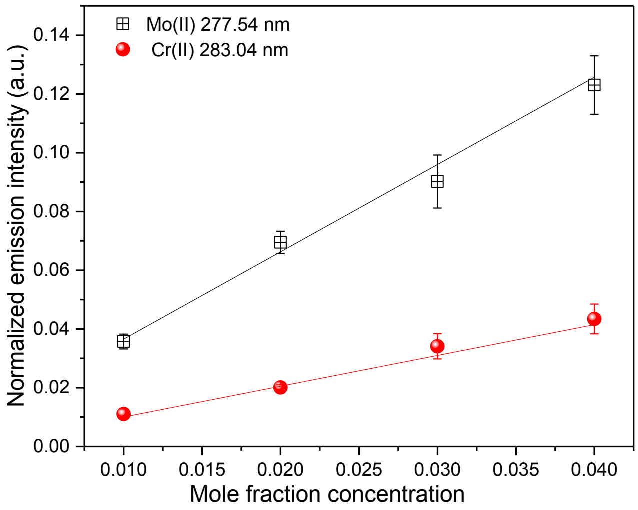

Figure 4.6. Calibration curve obtained for Mo 277.54 nm and Cr 283.04 nm emission

For analysis of Mo and Cr, wide spectral region is available for use. Such a large data analysis also means introduction of more noise component, which has to be avoided. In ASD-PLSR, to remove the noise contribution, spectra were altered by removing the noise portion. Fig. 4.7 shows a comparison of CT spectrum with the corresponding PLSR coefficient spectra for NaBS-Mo-3 sample. The high value of PLSR coefficient (indicated in green color) are more influential and important for Mo quantification. Remaining lines are considered noise for the particular elemental analysis. Using such lines, the Mo and Cr intensity against concentration was plotted. The accuracy and precision of the Mo and Cr values were found to be 3-4% in CT spectrograph.

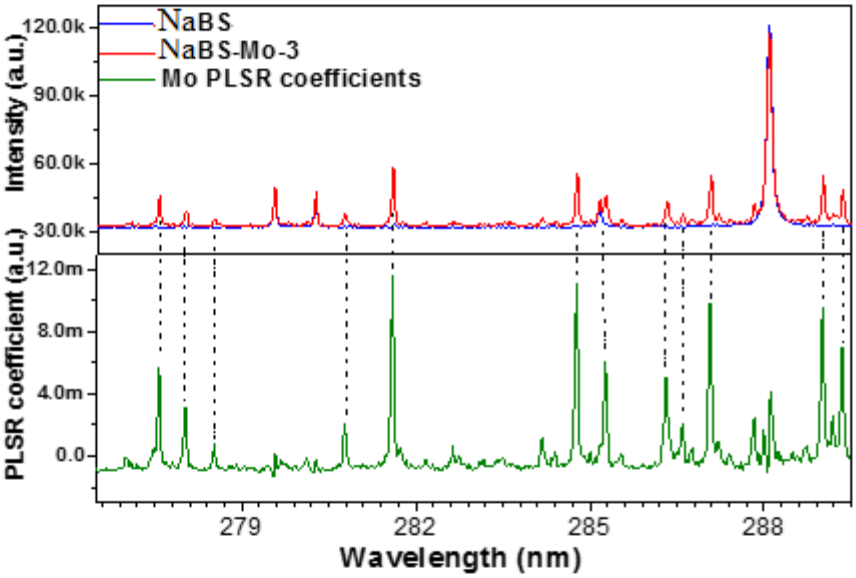

Figure 4.7. Comparison of CT spectra and PLSR coefficient values for Mo

For PBS-MoCr-x (x=1-4) glass samples, PBS-Mo-x and PBS-Cr-x glass samples were used for building the calibration curve. However the obtained accuracy and precision were be >15% irrespective of CT or EH spectra used in the analysis. These poor analytical results were due to matrix effect which is a common disadvantage of the analytical methods with direct sample analysis mode, like LIBS. For LIBS quantification, matrix matched calibration samples are required.

Hence the PBS-MoCr-x (x=1-4) samples itself were used for calibration. The accuracy and precision was found to be ~3-5% for Cr and Mo quantification. There is no significant difference in the analytical results obtained with CT or EH spectra.

4.4 Conclusions

PIGE and LIBS were found to be a viable real time elemental characterization methodology for these samples, without any type of dissolution of samples. PIGE values reported no significant thermal losses with respect to Si, Na, B at 1100^0C but for P mean concentration was found to be lower by 2.5- 4.2% for almost all samples. From obtained concentration results of glass samples, it is advisable to take ~2-4% higher amount of P in raw material for fabrication. However, the results largely depend on the experimental conditions in our laboratory facility. Using LIBS analysis, the accuracy and precision for both Mo and Cr was found to be 3-5% in all the glass samples. A part of this chapter is published in Journal of Non-Crystalline Solids (510 (2019) 172-178) where XRD results and LIBS results are presented. Two more papers consisting of PIGE and LIBS results are submitted to international journals. Treatment of HLW is based on two important factors one being able to formulate a glass matrix that would accommodate all the radionuclides and second being able to satisfy the final product acceptance criteria. Hence, evaluation of properties of final product glass is also important. Therefore, the properties of the product glass like chemical durability and glass transition temperature were also determined. The glass transition temperature and chemical durability of all the glass samples are presented in the next chapter.

CHAPTER 5

Study of thermal and chemical durability of MoO_3 and CrO_3 containing glasses

5.1. Introduction

The management of HLW is approached differently from that of other waste forms. The radioactivity is concentrated into a smaller volume and confined or immobilized in a suitable matrix [114]. This philosophy in short is called “Concentrate and Confine”. The radionuclides are immobilised in a durable matrix that can remain stable in environment for millions of years. Numerous studies are carried out to check the integrity of base matrix and the final product material. Thermal characteristics like coefficient of thermal expansion, glass transition temperature, thermal conductivity, chemical characteristics like leaching of elements, physical characteristics like mechanical strength, viscosity etc. are monitored thoroughly for quality assurance of the final product matrix [115]. Borosilicate glass is the most suitable candidate that shows all the properties in optimum range. Natural glasses like the Obsidians with age of more than 10 million years prove that glasses are good choice for immobilization of HLW [116]. The durability of these product glasses is of prime importance because they have to stay stable under earth surface at harsh condition like elevated pressure and temperature. Not only this, glasses have to remain resistant to self-irradiation for a long period. However, all these properties of glass depends on the structural characteristics of glass. Whenever there is any change in glass composition that would find an applicability in vitrification of HLW, the properties of the product glass should also be investigated. In the previous chapter an attempt was made to enhance the solubility of Mo and Cr in modified borosilicate glass. This modification was brought about by addition of 5 mol% of P_2O_5 in borosilicate glass. XRD patterns and SEM-EDS studies revealed that all the glass samples were completely amorphous and there were no phase separation in the glass samples. PIGE and LIBS data were useful in quantification of the glass samples. In this chapter the effect of P_2O_5, MoO_3 and CrO_3 on glass transition temperature (Tg) and leaching behavior of all elements are discussed.

5.2. Experimental details

With introduction of Mo, Cr and P, the change in glass transition temperature (Tg) and leaching behavior of all the elements were studied. In our investigation, the DTA measurement was carried out to determine the glass transition temperature of the glass samples. Leaching pattern of all the elements were observed for a period of 90 days. The experimental part is provided in chapter 2. The leachate obtained during the experiment was analysed using ICP-AES for concentration of different elements.

5.3. Results and Discussion

5.3.1. DTA investigations

To understand the thermal stability of glass samples with introduction of P_2O_5 and with increase in concentration of MoO_3 and CrO_3, DTA investigations were carried out. The DTA patterns of the glass samples containing MoO_3 and CrO_3 are shown in Fig. 5.1 and Fig. 5.2, respectively. Table 5.1 provides the three Tg readings for each sample and associated standard deviation (SD). DTA analysis of all the glass samples shows an endothermic hump in 450-550°C region. This hump is known as glass transition temperature (Tg), which appears due to glass transition process (i.e., onset of structural relaxation process) [131] and can be clearly seen in all the samples.

Table 5.1. Glass transition temperature (Tg) of each sample (in triplicate), average (Avg) and standard deviation (sd)

	Sample	Tg (°C)			Avg +_ sd(°C)
1	NaBS	519	517	519	518.33 ±0.54
2	NaBS-Mo-2	527	526	528	527.00±0.47
3	BaBS	531	530	533	531.33±0.72
4	BaBS-Mo-1	535	536	535	535.33±0.27
5	NaPBS	487	487	489	487.67±0.54
6	NaPBS-Mo-1	476	475	476	475.67±0.27
7	NaPBS-Mo-2	471	469	472	470.66±0.72
8	NaPBS-Mo-3	468	468	467	467.66±0.27
9	NaPBS-Mo-4	464	464	463	464.33±0.72
10	NaBS-Cr-2.5	516	516	518	527.00±0.47
11	BaBS- Cr-2	538	536	539	535.33±0.27
12	NaPBS-Cr-1	473	475	472	475.67±0.27
13	NaPBS-Cr-2	468	468	467	470.66±0.72
14	NaPBS-Cr-3	463	464	463	467.66±0.27
15	NaPBS-Cr-4	457	456	458	464.3±0.7

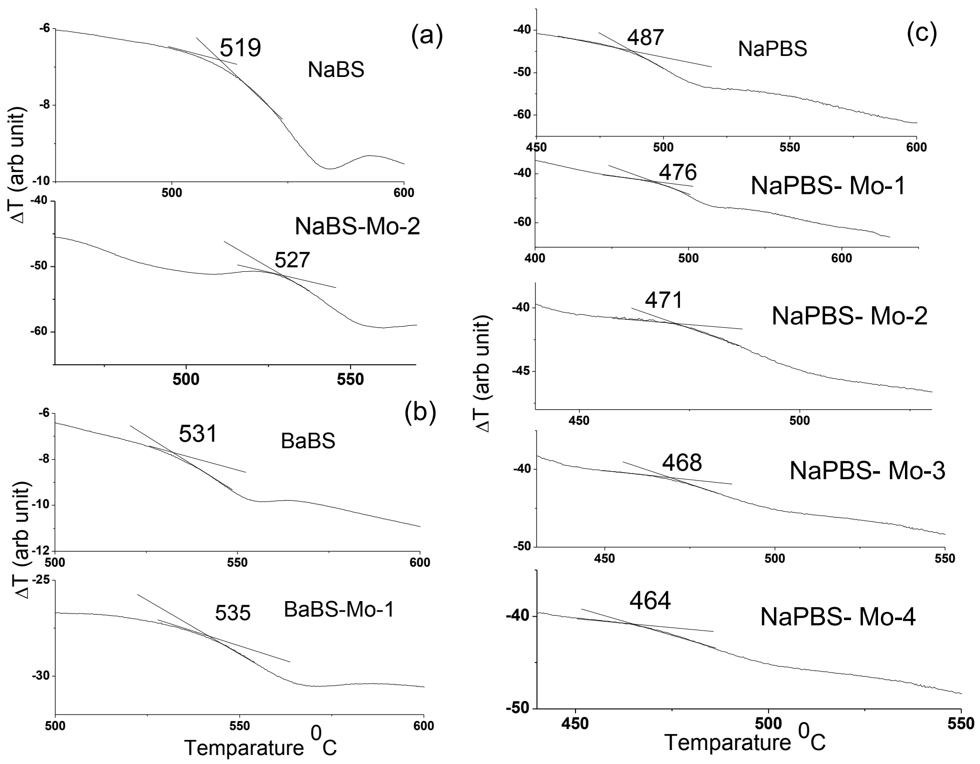

Figure 5.1. DTA patterns of (a) NaBS-Mo-x (x=0 and 2 mol%), (b) BaBS-Mo-x (x=0 and 1 mol%) and (c) NaPBS-Mo-x (x= 1 to 4 mol%) glasses

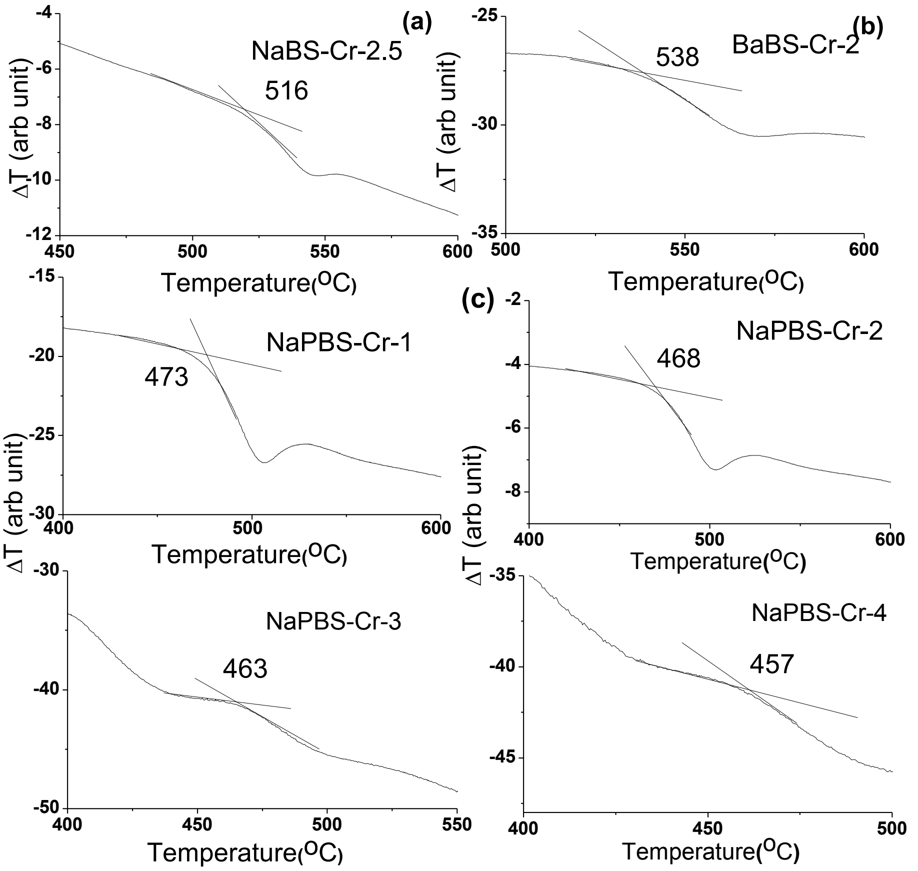

Figure 5.2. DTA patterns of (a) NaBS-Cr-2.5, (b) BaBS-Cr-2 and (c) NaPBS-Cr-x (x= 1 to 4 mol%) glasses

5.3.1.1. Effect of P_2O_5 on Tg of glass samples

The Tg of NaPBS glass sample is at 487°C which is 32°C lower than the base glass sample with no phosphorus (Fig. 5.1 (c)). Phosphate is a glass former and in these samples the introduction of phosphate results in phosphate units taking part in network formation by replacing borate and silicate units. As the bond dissociation energy of P-O bond (596 kJ/mol) is lower compared to Si-O (798 kJ/mol) and B-O bond (806 kJ/mol), this results in lower energy requirement for glass transition to occur attributing to lower Tg [118, 119].

5.3.1.2. Effect of MoO_3 and CrO_3 on Tg of glass samples

In the NaBS glass batch, on addition of 2 mol% of MoO_3 the Tg value increased from 519°C to 527 °C (Fig. 5.1 (a)). The increase in Tg value is due to formation of more polymerised silica polyhedral frame as presented in Fig. 5.3. In NaBS-Mo-2 sample, Mo^{6+} isolates from the glass network along with alkali or alkali earth metals forming Na_2MoO_4, this in turn leaves the glass network deficient of alkali atoms. A similar scheme is proposed by Caurant et al. where with introduction of MoO_3, conversion of non-bridging oxygen (NBO) into bridging oxygen (BO) occurs [117].

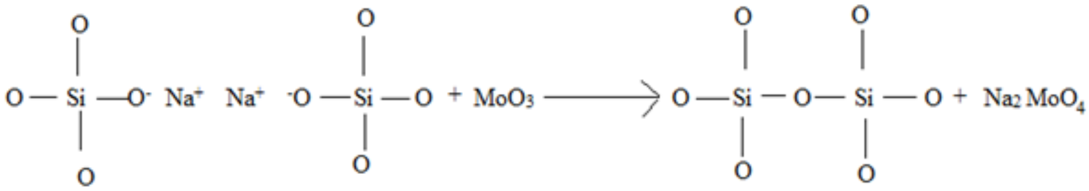

Figure 5.3. Conversion of non-bridging oxygen (NBO) into bridging oxygen (BO) in borosilicate glass matrix

Similarly, BaBS-Mo-1 and BaBS-Cr-2 glass samples show higher Tg at 535°C and 538°C respectively in comparison to BaBS base glass (531°C) (Fig. 5.1 (b) and Fig. 5.2 (b)). In XRD analyses also presence of $NaMoO_4$, $BaMoO_4$ and $BaCrO_4$ phases were observed. All these crystalline phases leave the rest of the glass network with lower number of modifier ions resulting in more polymerised silica polyhedra. However, Tg decreases with addition of Cr from 519°C to 516°C (Fig. 5.2 (a)) for NaBS-Cr-2.5. The decrease in Tg value is marginal which can be due to formation of Cr_2O_3 crystalline phase in this sample because of which the modifiers in the glass samples remain unaffected. Mirhadi et al. also observed a decrease in Tg with increasing CrO_3 content. However, there is a non-linear behaviour associated with their study [120, 133].

Fig. 5.1 (c) show that Tg of NaPBS-Mo-1, NaPBS-Mo-2, NaPBS-Mo-3 and NaPBS-Mo-4 are at 476°C, 471°C, 468°C and 464°C, respectively. Tg of NaPBS-Cr-1, NaPBS-Cr-2, NaPBS-Cr-3 and NaPBS-Cr-4 are at 478°C, 468°C, 463°C and 457°C, respectively as shown in Fig. 5.2 (c). There is a decreasing trend of Tg with increasing MoO_3 and CrO_3 content. As bond dissociation energy of Mo-O bond is low (607 kJ/mol), deformation of Mo-O bond requires less energy promoting glass transition at lower temperature [121]. Similarly, bond dissociation energy of Cr-O bond is also lower (461 kJ/mol) causing decrease in Tg.

5.3.2. Leaching studies

The leaching behavior of various elements were noted over a period, to obtain valuable information on effect of P_2O_5, MoO_3 and CrO_3on leaching trends. Fig. 5.4 and Fig. 5.5 show the leach rate of all the elements individually and how they vary in different glass samples. For all the elements the leach rate usually decreases exponentially. The general mechanism is given in chapter 2.

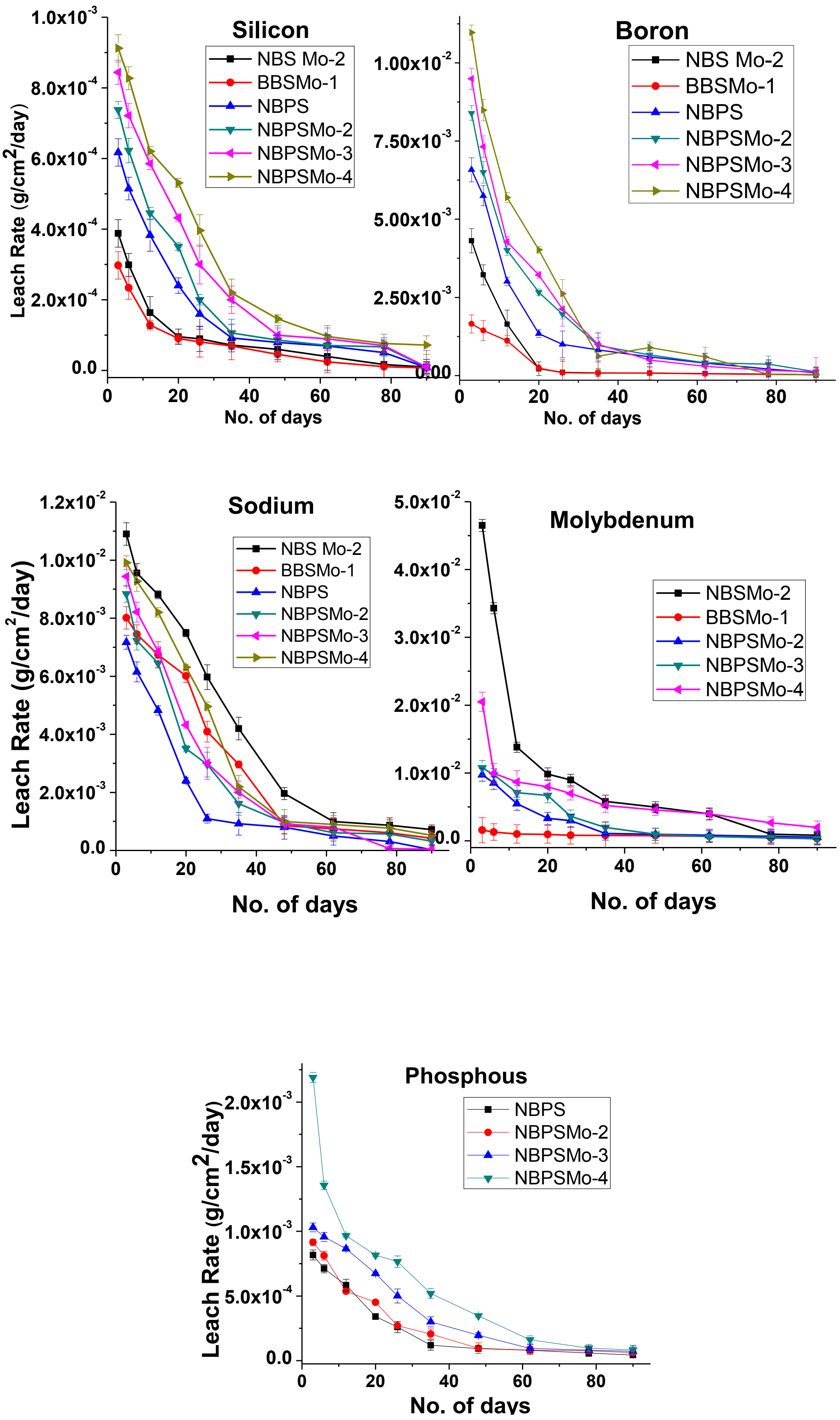

Figure 5.4. Leach rate of all elements for Mo containing glass samples

5.3.2.1. Effect of P_2O_5 on leaching characteristics

The effect of P on leaching behaviour of Si and B can be observed from comparing NaBPSMo-2 and NaBSMo-2 glass samples. In presence of P, the leach rate of both Si and B increases by 2 folds, smoothing out with time. The reason can be due to easy hydrolysis of P-O bond [122]. With release of P, there are higher number of glass- water interface within the glass sample. The hydrolysis of Si and B in these interfaces results in higher leach rate of Si and B. On comparing leach rate of Na, Mo and Cr in NaBPSMo-2, BaBSMo-2, NaBSCr2 and BaBSCr-2 glass samples, its observed that the leach rate of Na, Mo and Cr are higher in absence of P compared to samples NBPSMo-2 and NBPSCr-2 where P is present. This is clearly due to formation of water soluble molybdate and chromate salts [123].

5.3.2.2. Effect of MoO_3 and CrO_3 on leaching characteristics

Silicon, boron and phosphorous show a similar trend, where the leach rate is higher for glass samples with higher amount of Mo and Cr. The leach rate follows a trend that is NaPBS-Mo/Cr-1 < NaPBS-Mo/Cr -2 < NaPBS-Mo/Cr -3 < NaPBS-Mo/Cr -4. Higher leach rates of silicon, boron and phosphorous is correlated to higher leach rate of Mo. Mo in these glass samples is mainly present as P-O-Mo bond and some as B-O-Mo and Si-O-Mo bonds. P-O bonds are easily hydrolysed leaving Mo vulnerable to leaching. Not only this, whether Mo is present as B-O-Mo or Si-O-Mo, it is highly susceptible to leaching because of high ionic potential of Mo^{6+} species and are highly reactive [124].

In NaPBS glass samples with increasing content of CrO_3, the leach rate of silicon, boron, sodium and phosphorous also increased. Cr itself has shown a high leach rate. The explanation is very similar to one observed in Mo containing glass samples. When in contact with water, P-O bonds are easily hydrolysed leaving Cr-O-P bond broken to form Cr-O$^-$ species and P-OH species. The vulnerable Cr ions thus gradually leach out of the sample. However, the leach rate of Mo is higher than that of Cr. This can be because Cr tends to form a protective layer of Cr_2O_3 in the glass water interface. Due to formation of this layer, there is a hindrance to leaching of all the elements.

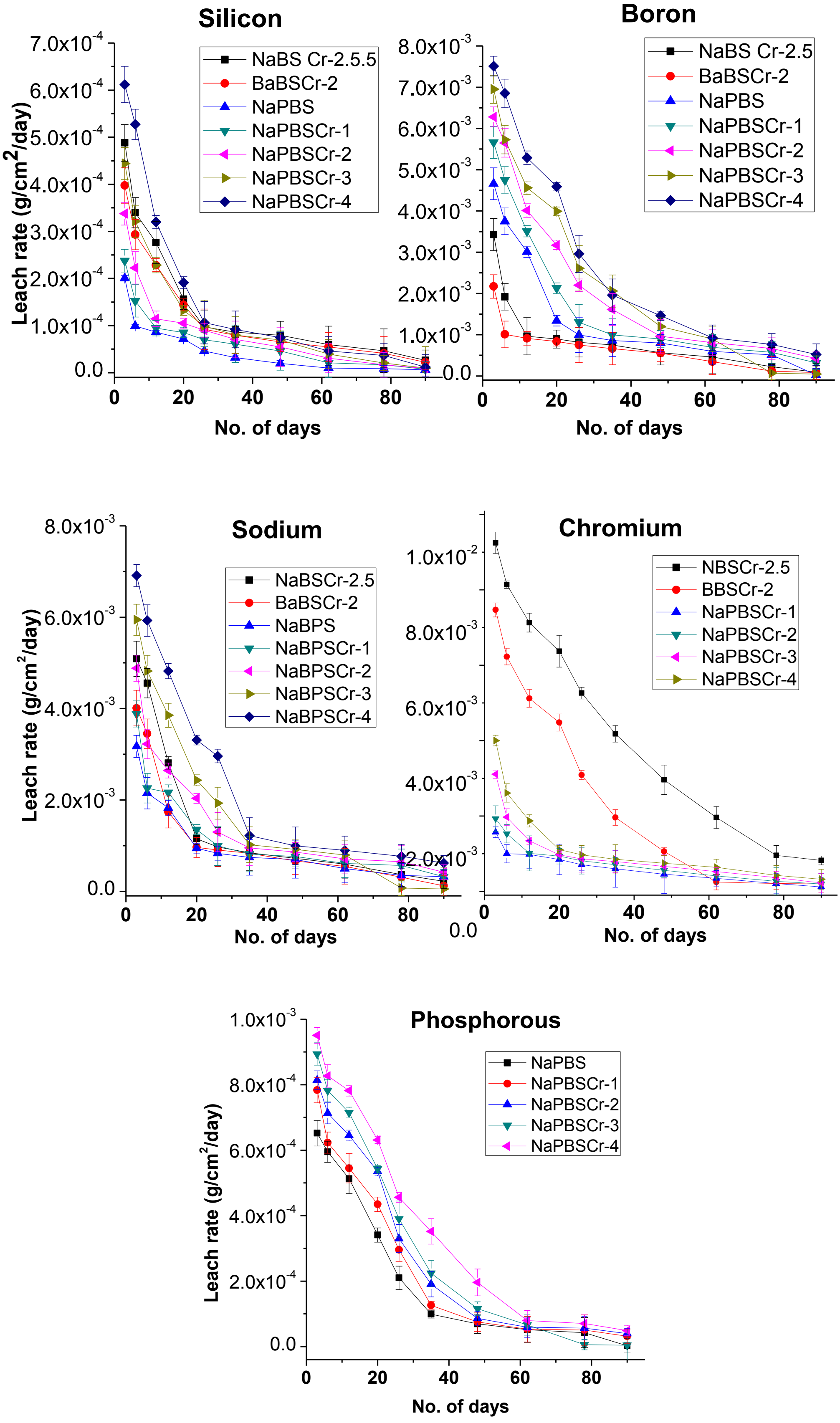
Silicon

Boron

Sodium

Chromium

Phosphorous

Figure 5.5. Leach rate of all elements for Cr containing glass samples

5.4. Conclusions

DTA studies revealed lowering of the Tg with increasing P_2O_5, MoO_3 and CrO_3 content. However, this drop in Tg is acceptable from vitrification point of view. Similarly, addition of P_2O_5, MoO_3 and CrO_3 is increasing the leach rate of glass samples. However, within 90 days the leach rate of all elements are reducing to nearly 10^{-5}(g/cm^2/day) and to address the problems associated with leaching the concentration of modifier ions like Na_2O, Fe_2O_3, ZnO etc. can be decreased in base glass during plant scale vitrification. The data in chapter 3, 4 and 5 served as input for immobilization of simulated HLW in modified borosilicate glass. Therefore, the next chapter deals with a HLW composition containing increased amount of Cr and Mo and its solubility in newly formulated base glass was compared with conventional base glass.

CHAPTER 6

Study of solubility of simulated HLW in modified borosilicate glass

6.1. Introduction

In the previous chapters we could establish that addition of 5mol% of P_2O_5 has increased the solubility of two elements Cr and Mo. However, HLW that is required to be immobilized in glass matrix would contain a large number of elements [125]. Table 6.1 show a general nature of HLW. [90, 126].

Table 6.1. HLW nature

Property	
Molarity (free acid, M), HNO_3	4.1
Density (g/mL)	1.18
Gross β activity (Ci/L)	30.05
Gross α activity (mCi/L)	83.11
Total Solids (g/L)	Solubility in borosilicate glass (%)
Fe_2O_3	15-25
Na_2O	
UO_2	
K_2O	
NiO	3-5
CrO_3	
MnO	
MoO_3	

SrO	15-25
BaO	
Cs_2O	
Al_2O_3	>25
ZrO_2	5-15
La_2O_3	
CeO_2	
Pr_2O_3	
Nd_2O_3	
Sm_2O_3	
Y_2O_3	
RuO	<1
PdO	
TeO_2	1-3
SeO_2	

Among all the elements different elements show different degree of solubility limit in borosilicate glass. For example, elements displaying multiple oxidation states like transition metals form various crystalline phases like spinel in glass matrix. Noble group metals like, Pd, Rh, Ru show solubility of <1wt%, beyond this concentration the noble metals and spinel crystals settle at the bottom of the melter due to high density [127-132]. They remain separated from the glass matrix and pose numerous problems like channeling of electrical conductivity in Joule Heated Ceramic Melter (JHCM) and cause problem during glass pouring.

Thermal properties of these crystals (like thermal conductivity) differ from that of glass and during an increase in temperature caused by decay of radionuclides there can be stress in the glass matrix which can lead to cracking. Besides this, presence of crystalline phases in glass matrix results in numerous other problems. For example, the crystalline phases can trap radionuclide within them and, if they are aqueous soluble, leaching of that particular radionuclide occurs or if volatile, the radionuclide might evaporate [97]. Luckscheiter and Nesovic reported that during idling of melter, the melter stays at a temperature of 800-900°C for a long time, during this period devitrification tendency increases. In borosilicate glass, SiO_2 phases crystallises and becomes rich in SiO_2 and the remaining section of glass is deficient in SiO_2 or rich in B_2O_3 [134, 135]. Thereby hampering the strength of the glass matrix. Increasing the waste loading within glass increases the efficiency of the vitrification process, but could also increase the tendency for devitrification, which could have a negative effect on properties of final product glass. Apart from all these considerations there are certain important ratios that were reported in chapter 1 that needs to be satisfied in order to yield a product glass with desired thermal, chemical and physical properties. Jiawei Sheng et al. reported that borosilicate glass matrix with greater than 30wt% of waste oxide compromises the chemical durability of the glass [136]. However, depending on the composition of HLW this percentage varies. For example, in the case of a particular HLW with higher amount of MoO_3, the waste oxide loading was limited to 15wt% to avoid formation of alkali molybdate crystalline phase [137]. Based on the composition of HLW, often the base glass matrix composition is also altered. Stefanovsky et al. employed aluminophosphate base glass to incorporate high content of iron oxides within the glass matrix. They observed that substitution of B_2O_3 for Al_2O_3 in the materials increases resistance to devitrification and glasses with Al_2O_3:Fe_2O_3 ratio close to 1 were found to be the highest chemically durable [138]. Valsala et al. reported modification in base glass composition in order to incorporate higher amount of HLW. In that particular glass, a five component (SiO_2-B_2O_3-Na_2O-Fe_2O_3-TiO_2) base glass, sodium concentration of the base glass was lowered and this has increased the waste loading into the product glass by 25% (by volume) [137].

In view of the above factors, a HLW composition containing higher concentration of Mo, Cr and Fe was taken up for this part of the study. Presently, HLW loading in base glass is limited due to high salt concentration. Therefore, for this study a different HLW was chosen. HLW obtained in WIP, Trombay is used for extraction of Cs-137 for making Cs pencil for medical application. This is accomplished by solvent extraction process involving 1,3-Di-n-OctyloxyCalix[4]arene-Crown-6 (CC6). In view of this the HLW is subjected to 3 solvent extraction steps. They are: (a) removal of U using 30% TBP in dodecane (b) removal of Cs using Calix Crown Ether solution (c) removal of actinides and Sr using N,N,N',N' Tetra-(2-ethylhexyl) diglycolamide (TEHDGA) in dodecane solution. The Actinides and Sr rich organic solution is stripped using 0.01M HNO_3, this HLW composition that has high radioactivity and low salt content was taken up for the present study [144]. The composition in provided in Table 6.2.

Two different borosilicate base glass one with phosphate and one without phosphate were taken up. Vitrification of simulated HLW in two different base glasses were studied. Product glass i.e. a mixture of base glass and waste oxide in a different ratios were prepared and their properties were evaluated.

6.2. Experimental details

6.2.1 Synthesis of glass samples

Different product glass formulations having different ratios of waste oxide to base glass were prepared. The composition of HLW is provided in Table 6.2, composition of base glasses are provided in Table 6.3. Six product glass samples were prepared and investigated thoroughly. The base glass matrix were of two types a) borosilicate glass without phosphate (NBS) and b) borosilicate glass with 5mol% of P_2O_5 (PBS). Out of those six samples, two product glass samples were prepared with NBS base glass matrix. Four glass samples were prepared with PBS base glass matrix. The ratio in which the waste oxide and base glass oxide were taken are- 20:80, 27:73, 30:70 and 33:67 as given in Table 6.4.

Table 6.2: HLW composition

Element	Concentration (g/L)	oxide	Concentration (g/L)
Al	0.069	Al_2O_3	0.132
Ba	0.0213	BaO	0.024
Ca	2.6	CaO	3.6
Ce	0.663	CeO_2	0.814
Cr	1.016	CrO_3	1.95
Fe	4.725	Fe_2O_3	6.71
La	0.299	La_2O_3	0.35
Mg	0.0013	MgO	0.002
Mn	0.173	MnO_2	0.223

Mo	0.863	MoO_3	1.295
Na	0.528	Na_2O	0.71
Ni	0.547	NiO	0.69
Sr	0.259	SrO	0.31

Table 6.3. Composition of base glasses

	PBS wt% (mol%)	NBS wt% (mol%)
SiO_2	37.24 (42)	41.60 (44.5)
B_2O_3	33.95(33)	37.93 (34.5)
Na_2O	18.32 (20)	20.47 (21)
P_2O_5	10.49 (5)	

Table 6.4. Ratio of waste oxide to base glass for preparation of product glass

	Waste oxide	base glass with P_2O_5	base glass without P_2O_5
PBS-1	20	80	
NBS-1	20		80
PBS-2	27	73	
NBS-2	27		73
PBS-3	30	70	
PBS-4	33	67	

6.2.2. Structural characterization

To determine the presence of crystalline phases in glass samples XRD patterns were recorded. Introduction of waste oxide produces a negative impact on glass transition temperature (Tg). Therefore, Tg has been evaluated for all the glass samples. The results are discussed in the following section.

6.3. Results and discussion

6.3.1. XRD investigations

Fig. 6.1 show XRD patterns of all the product glass samples. The glass samples PBS-1 and NBS-1 are completely amorphous in nature and there are no sharp peaks present in them indicating that 20% waste oxide can be easily accommodated in both these base glasses. Addition of 27% waste oxide in PBS base glass did not show formation of any crystalline phase. This is evident from Fig. 6.1. However, on addition of 27% waste oxide in NBS base glass, $BaCrO_4$ and Cr_2O_3 crystalline phases appear within the glass. In NBS-2 glass sample, the wt% (mol%) of CrO_3 are 3.13 (2.37). All peaks correspond to $BaCrO_4$ (JCPDS-15-0376) and Cr_2O_3 (JCPDS-74-0326) phases. PBS-3 glass sample containing 30% waste oxide is still completely amorphous. However, PBS-4 glass sample containing 33% waste oxide reveals formation of Pyroxene, Powellite and spinel crystalline phases. Here in PBS-4 glass sample wt% (mol%) of MoO_3 and CrO_3 are 2.53(1.3) and 3.8(2.9) respectively. Szumera et al. and Brinkman et al. reported formation of $(Ba,Ca)MoO_4$ powelite phase in SiO_2–P_2O_5–K_2O–CaO–MgO–MoO_3 glass system [139, 140]. Luckscheiter et at. also reported minimizing waste oxide loading to 15wt% in order to limit MoO_3 content to 1.8wt% in final product glass to avoid formation of molybdate rich phase [135]. Samples with high content of Fe, Cr and Mn, often results in formation of spinel crystals [141]. In this particular HLW the amount of Fe_2O_3 was high and in PBS-4 glass sample the concentration of Fe_2O_3 was 13.15 wt% (6.2 mol%). Such high content of Fe resulted in spinel formation in PBS-4 glass sample. Sam A. Walling et al. has also reported Olivine or Pyroxene phases in magnesium, iron rich silicates [142].

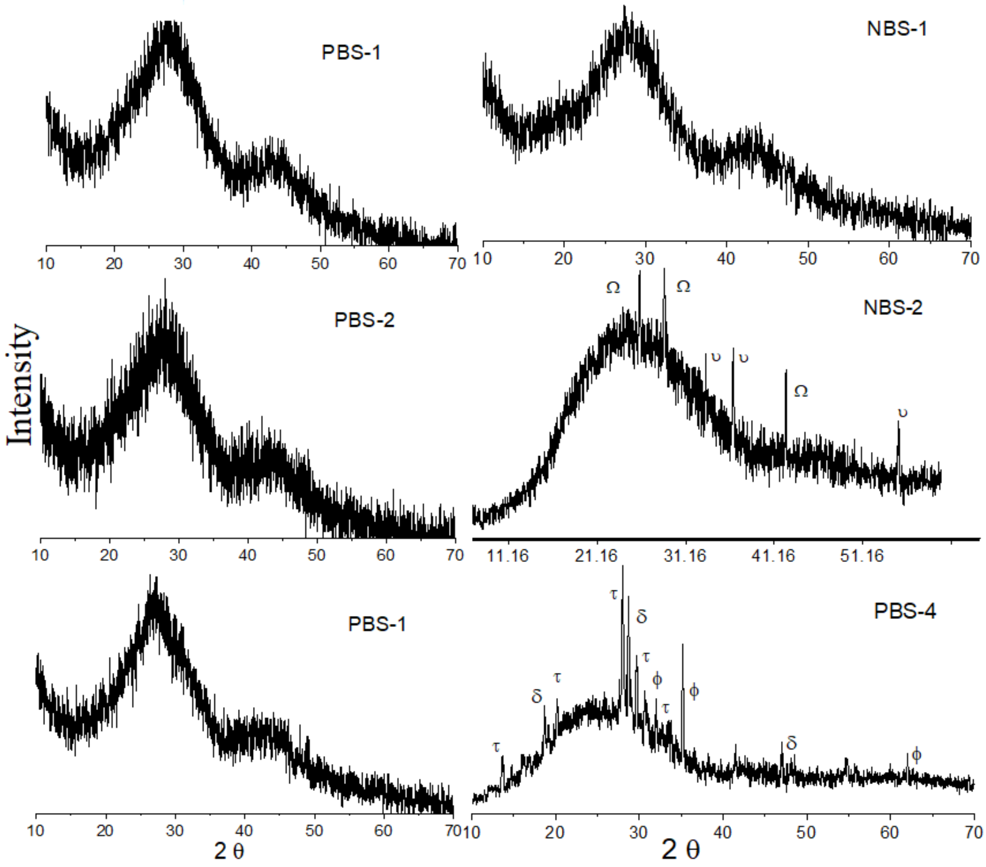

Figure 6.1. XRD patterns of product glass samples (Ω-$BaCrO_4$, υ-Cr_2O_3, τ-Pyroxene, δ-Powellite, ϕ- spinel)

6.3.2. DTA investigations

Most of the elements present in HLW act as network modifier [131]. Therefore, an increase in percentage of waste oxide result in decrease in Tg value. This is evident from DTA patterns shown in Fig. 6.2. The Tg value of PBS-1, PBS-2, PBS-3 and PBS-4 are 524^{o}C, 514^{o}C, 510^{o}C and 502^{o}C, respectively. Similarly, Tg value of NBS-1, NBS-2 are 533^{o}C and 526^{o}C, respectively. Tg of PBS-1 is lowered by 7^{o}C compared to NBS-1 due to presence of 5mol% P_2O_5. However, addition of 33wt% of waste oxide to P_2O_5 decreased the Tg of product glass to 502°C. This reduction in temperature is acceptable from devitrification point of view. Kaushik et al. have reported that during long term storage of canister in repository, the centreline temperature is not expected to rise such high temperature [143]. However, this finding depends largely on radioactivity of HLW.

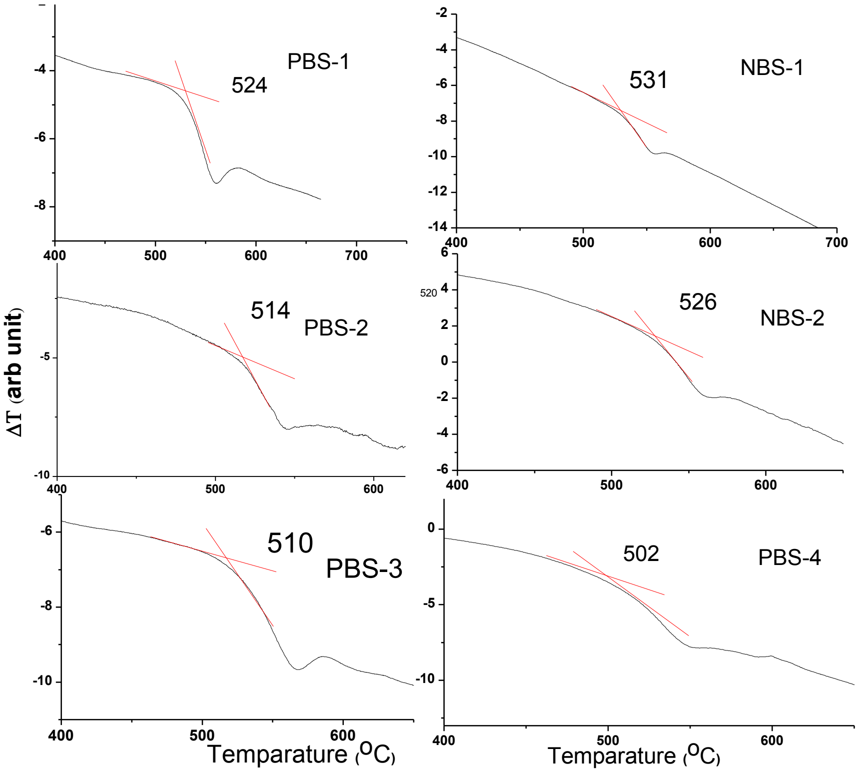

Figure 6.2. DTA patterns of product glass samples

6.4. Conclusions

The simulated HLW showed a greater degree of solubility limit in phosphate modified borosilicate glass. However, Tg shows a gradual decrease with increasing HLW content but this decrease was within the acceptable limit. With increasing HLW content in glass, various crystalline phases appeared in the glass samples. This database will be beneficial for improving immobilization efficiency.

CHAPTER 7

Conclusions and future scope

In the present work, an attempt was made to investigate the solubility of various HLW constituents in borosilicate glass and its physico-chemical properties, which can be further improved by formulating a modified glass matrix. Numerous glass samples were formulated using melt-quench technique and were characterized using various instrumental techniques like X-ray Diffraction (XRD) and scanning electron microscope (SEM) was used to detect the presence of crystalline phase in glass samples. Magic Angle Spinning Nuclear Magnetic Resonance (MAS-NMR) was used to observe changes in nature of bonding with respect to additives. Laser Induced Breakdown Spectroscopy (LIBS) and Proton Induced Gamma Emission (PIGE) were employed to quantify the samples. Differential Thermal Analysis (DTA) and Inductively Coupled Plasma – Atomic Emission Spectroscopy (ICP-AES) were used to observe durability of the samples. The experimental findings are discussed in chapters 3, 4, 5 and 6 of this thesis work.

Although borosilicate glass is well-known for immobilization of HLW, choice of base glass matrix involves thorough analysis of its structural and phsysico-chemical properties of product glass before applying it to plant level. Therefore, incorporation of HLW constituents, originating from futuristic reactors, in glass matrix needs to be explored in detail.

7.1. Summary

Al may be required in reprocessing of thoria based fuel for its dissolution. To demonstrate the effect of Al in borosilicate glass, various Al containing glass samples were prepared and structural, thermal and chemical properties of the samples were investigated in detail. The results can be summarized as follows:

I. It was found that 15 mol% of Al_2O_3 to borosilicate glass could be incorporated without any phase separation.

II. The structural studies were carried out using MAS-NMR technology. Based on ^{29}Si, ^{11}B and ^{27}Al MAS-NMR the following findings were established:

a. At least till 15mol% Al exists as glass former in tetrahedral arrangement.

b. Si-O- Si/B linkages are replaced by Si-O-Al linkages.

c. With increasing Al_2O_3, more and more BO_4 are getting converted to BO_3.

III. Addition of Al_2O_3 to borosilicate glass decreases the glass transition temperature but the glass transition temperature was above 500°C for all samples which is acceptable for HLW vitrification purpose.

IV. The durability of glass improves in presence of Al due to formation of protective layer on them.

In the second stage reactors Mo is one of the many elements showing high fission yield and the increased radiation level of second stage reactor is known to increase release of corrosion products in HLW. Cr is one such element, which needs to be investigated. The solubility of these two elements in borosilicate glass is very low.

I. XRD patterns revealed formation of $NaMoO_4$ and $BaMoO_4$ in Mo based glass and Cr_2O_3 and $BaCrO_4$ in Cr based glass.

II. Tg increases in presence of Mo and Cr, because of formation of the alkali/alkaline earth salts which in turn polymerizes the glass network.

III. Due to formation and phase separation of salts. The leach rate of Na, Mo and Cr increased but that of Si and B decreased.

Phosphate based glasses is an emerging field with respect to immobilization of HLW. However, poor thermal properties and chemical durability pose a disadvantage. Therefore, 5 mol% P_2O_5 was added to borosilicate glass to improve the solubility of these two elements. Various glass samples were formulated and characterized. Based on the results the following conclusions can be made:

I. XRD results revealed that 4 mol% of MoO_3 and CrO_3 could be added without any crystalline phase formation.

II. LIBS, XRF and PIGE data validated the composition of glass samples. The deviation in final product glass composition and raw materials composition were within 5%.

III. Addition of P_2O_5, MoO_3 and CrO_3 to borosilicate glass decreased the glass transition temperature. However, the decrease is within the acceptable limits.

IV. Leach rate increased in presence of P_2O_5, MoO_3 and CrO_3.

These findings served as an input for immobilization of HLW having increased content of MoO_3 and CrO_3. Therefore, as a conclusion to the previous findings an HLW solubility was studied in phosphate modified borosilicate glass. The findings revealed that additional 6wt% waste oxide could be loaded to borosilicate glass with 5 mol% P_2O_5 compared to base glass without P_2O_5.

All these findings will serve immense application in immobilization of HLW originating from 2nd and 3rd stage reactors. The work carried out so far will be beneficial during choice of base glass during plant scale vitrification.

7.2. Future scope and extension of the work

- Study of mechanism of Mo and Cr incorporation in modified glass.
- There are numerous elements in HLW having low solubility in borosilicate glass that needs to be investigated.
- Radiation stability of the developed product glass is to be established.
- Compatibility of the process vessel with respect to introduction of phosphate needs attention.

References

[1] P.S.R. Murty Chapter 24 - Renewable Energy Sources, Electrical Power Systems (2017) 783-800.

[2] Data from EIA, Electric Power Monthly, Table 1.1, http://www.eia.gov/beta/epm/.

[3] M. L. Mittal, C. Sharma and R. Singh. Estimates of emissions from coal fired thermal power plants in India. Radio and Atmospheric Sciences Div., Nat. Phy. Lab., Council of Sci. and Ind. Res., 39 (2011) 1-22.

[4] University of texas, Nuclear and wind power estimated to have lowest levelized CO_2 emissions, https://energy.utexas.edu/news/nuclear-and-wind-power-estimated-have-lowest-levelized-co2-emissions.

[5] V. Venugopal, Societal Applications of Nuclear Technology in Health Care, Industry and Water Resource Management in India, Energy Procedia, 7 (2011) 553-559.

[6] https://pris.iaea.org/pris/CountryStatistics/CountryDetails.aspx?current=IN.

[7] https://www.renewable-ei.org/en/activities/column/20180302.html.

[8] J. Stephen Herring, Uranium and thorium resource assessment, Encyclopedia of Energy (2004) 279-298.

[9] Ronald A. Knief, Nuclear Fuel Cycles, Encyclopedia of Physical Science and Technology (Third Edition) (2003) 655-670.

[10] Turan Ünak, What is the potential use of thorium in the future energy production technology? Progress in Nuclear Energy, 37 (2000) 137-144.

[11] Gianni Petrangeli, Chapter 23 - Radioactive waste, Nuclear Safety (2006) 221-223.

[12] Charles W. Forsberg, Encyclopedia of Physical Science and Technology (Third Edition) (2003) 643-659.

[13] R. W. Baker, Encyclopedia of Separation Science, Membrane separation (2000) 189-210.

[14] D. Banerjee, M. A. Rao, J. Gabriel, S. K. Samanta, Recovery of purified radio cesium from acidic solution using ammonium molybdophosphate and resorcinol formaldehyde polycondensate resin, Desalination Volume 232 (2008) 172-180.

[15] W. J. Weber, A. Navrotsky, S. Stefanovsky, E. R. Vance, E. Vernaz, Materials science of high-level nuclear waste immobilization, MRS Bull. 34 (2009) 46–53.

[16] D. D. Sood & S. K. Patil, Chemistry of nuclear fuel reprocessing: Current status, Journal of Radioanalytical and Nuclear Chemistry, 2031996 547–573.

[17] J. Malvyn mckibben, Chemistty of the Purex Process, Radiochimica Acta 36 (1-2)

[18] M. I. Ojovan, W. E. Lee, An introduction to nuclear waste immobilisation (2005) 215.

[19] Neil C. Hyatt, Michael I. Ojovan, Special Issue: Materials for Nuclear Waste Immobilization, Materials (Basel). 12 (2019) 3611.

[20] A. E. Ringwood, V. M. Oversby, S. E. Kesson, W. Sinclair, N. Ware, W. Hibberson, A. Major, Immobilization of high-level nuclear reactor wastes in SYNROC: A current appraisal Nuclear and Chemical Waste Management, 2 (1981) 287-305.

[21] Michael I. Ojovan, William E. Lee, Stepan N. Kalmykov,An Introduction to Nuclear Waste Immobilisation (Third Edition) Chapter 20 - Ceramics and Novel Technologies (2019) 369-395.

[22] C. M. Jantzen, Handbook of Advanced Radioactive Waste Conditioning Technologies Woodhead Publishing Series in Energy (2011) 230-292.

[23] IAEA-TECDOC-239, Evaluation of solidified high-level waste forms (1979) 17-19.

[24] Rodney C. Ewing, Werner Lutze, High-level nuclear waste immobilization with ceramics Ceramics International 17 (1991) 287-293.

[25] J. D. Mackenzie, Applications of zachariasen's rules to different types of non-crystalline solids, Journal of Non-Crystalline Solids 95 (1987) 441-448.

[26] M. I. Ojovan, W.E. Lee, An Introduction to Nuclear Waste Immobilisation, (2005) 222.

[27] T.Ogata, Yeon Soo Kim, A. M. Yacout, Metal Fuel Performance Modeling and Simulation, Comprehensive Nuclear Materials 3 (2012) 713-753.

[28] J. G. Cuninghame, The mass-yield curve for fission of natural uranium by 14-MeV neutrons, Journal of Inorganic and Nuclear Chemistry, 5 (1957) 1-5.

[29] R. H. Iyer, C. K. Mathews, N. Ravindran, K. Rengan, V. Singh, M. V. Ramaniah, H. D. Sharma, Fission of ^{232}Th by reactor neutrons: Mass-yield curve, Journal of Inorganic and Nuclear Chemistry, 25 (1963) 465-472.

[30] D. Banerjee, V. Sudarsan, A. Joseph, R.K. Mishra, I.J. Singh, P. K. Wattal, D. Das, Role of TiO_2 on the physicochemical properties of cesium borosilicate glasses, J. Am. Ceram. Soc. 93 (2010) 3252–3258.

[31] M. Szumera, Molybdenum modified phosphate glasses studied by ^{31}P MAS-NMR and Raman spectroscopy, Spectrochim. Acta A Mol. Biomol. Spectrosc. 137 (2015) 111–115.

[32] R. K. Mishra, V. Sudarsan, C. P. Kaushik, K. Raj, S. K. Kulshreshtha, A. K. Tyagi, Effect of BaO addition on the structural aspects and thermophysical

properties of sodium borosilicate glasses, J. Non-Cryst. Solids 353 (2007) 1612–1617.

[33] R. K. Mishra, V. Sudarsan, P. Sengupta, R. K. Vatsa, A. K. Tyagi, C. P. Kaushik, D. Das, K. Raj, Role of sulfate in structural modifications of sodium barium borosilicate glasses developed for nuclear waste immobilization, J. Am. Ceram. Soc. 91 (2008) 3903–3907.

[34] R. Agarwal, V. Venugopal, Chemical states of fission products in irradiated (U0.3Pu0.7)C1+x fuel at high burn-ups, J. Nucl. Mater. 359 (2006) 122–131.

[35] Pavel Hrma, John D Vienna, Benjamin K. Wilson, Trevor J. Plaisted, Steve M. Heald, Chromium phase behavior in a multi-component borosilicate glass melt Journal of Non-Crystalline Solids, 352 (2006) 2114-2122.

[36] Robert B. Minogue, Abraham L. Eiss, Nuclear regulatory commission regulations and licensing. Nuclear Power Safety (1976) 57-86.

[37] Reinhard Conradt, II.24 - The industrial glass-melting process, The SGTE Casebook (Second edition) (2008) 282-303.

[38] B.D. Cullity, Elements of X-ray diffraction, Addison-Wilson Publishing Comp. Inc., USA, (1959).

[39] H.P. Klug, L.E. Alexander, X-ray diffraction procedures, Wiley-Interscience Publication, New York, USA (1974).

[40] Photis Dais, Apostolos Spyros, Chapter 4 - Nuclear Magnetic Resonance, Chemical analysis of food: techniques and applications (2012) 91-115.

[41] P. K. Madhu, High-resolution solid-state NMR spectroscopy of protons with homonuclear dipolar decoupling schemes under magic-angle spinning, Solid State Nuclear Magnetic Resonance 35 (2009) 2-11.

[42] Qian Wang, Ulla Gro Nielsen, Applications of solid-state NMR spectroscopy in environmental science, Solid state nuclear magnetic resonance, 110 (2020) 101698.

[43] M. Abd Mutalib, M. A. Rahman, M. H. D. Othman, A. F. Ismail, J. Jaafar, Chapter 9 - Scanning Electron Microscopy (SEM) and Energy-Dispersive X-Ray (EDX) Spectroscopy, Membrane Characterization (2017) 161-179.

[44] Jörgen Bergström, 2 - Experimental characterization techniques, Mechanics of solid polymers theory and computational modeling (2015) 19-114.

[45] Ankur Baliyan, Hideto mai, Vinit Kumar, Chapter 7 – Microscopy, Data processing handbook for complex biological data sources (2019) 97-117.

[46] Alessandro Zucchiattia, Piero Corvisiero, PIGE: A useful technique for the study of innovative energy related materials. Technical Note on the Measurement of Gamma-ray Production Cross Sections, Energy Procedia 41 (2013) 110-118.

[47] S.K. Samanta, S.W. Raja, V. Sharma, P.S. Girkar, R. Acharya, P.K. Pujari Development of an external (in air) in situ current normalized particle induced gamma-ray emission method utilizing 3.5 MeV proton beam from FOTIA for rapid quantification of low Z elements in glass and ceramic samples. J Radioanal Nucl Chem 325 (2020) 923–931.

[48] M. Singh, V. Karki, R.K. Mishra, A. Kumar, C.P. Kaushik, X. Mao, R.E. Russo, A. Sarkar, Analytical spectral dependent partial least squares regression: A study of nuclear waste glass from thorium based fuel using LIBS, J. Anal. At. Spectrom. 30 (2015) 2507-2515.

[49] C. P. Asquini, 19 - Laser induced breakdown spectroscopy (LIBS), Handbook of Solid-State Lasers, (2013) 551-571.

[50] Maria Cristina Tanzi, Silvia Farè Gabriele Candiani, Chapter 7 - Techniques of Analysis, Foundations of Biomaterials Engineering, (2019) 393-469.

[51] A. D. Micheals, Materials Analysis and Failure Analysis, Encyclopedia of Forensic Sciences (2013) 483-493.

[52] Chapter 3 - Solidification, Vitrification, Crystallization and Formation of Quasicrystalline and Nanocrystalline Structures, Pergamon Materials Series, 12 (2007) 125-255.

[53] A. Ledieu, F. Devreux, P. Barboux, L. Sicard, O. Spalla, Leaching of borosilicate glasses. I. Experiments, Journal of Non-Crystalline Solids 343 (2004) 3-12.

[54] Joseph M. Perez Jr, Joseph H. Westsik Jr., Effects of cracks on glass leaching, Nuclear and Chemical Waste Management, 2 (1981) 165-168.

[55] M.I. Ojovan, W.E. Lee, An Introduction to Nuclear Waste Immobilisation, (2005) 216.

[56] S. Cherevko, K. J. J. Mayrhofer, On-Line Inductively Coupled Plasma Spectrometry in Electrochemistry: Basic Principles and Applications, Encyclopedia of Interfacial Chemistry, Surface Science and Electrochemistry, (2018) 326-335.

[57] R. K. Sinha, A. Kakodkar, Design and development of the AHWR—the Indian thorium fuelled innovative nuclear reactor, Nuclear Engineering and Design 236 (2006) 683-700.

[58] P. K. Dey, N. K. Bansal, Spent fuel reprocessing: A vital link in Indian nuclear power program, Nuclear Engineering and Design 236 (2006) 723-729.

[59] Emtethal Hashem, Alice Seibert, Jean François Vigier, Mohamed Naji, Sara Mastromarino, Andrea Ciccioli, Dario Manara, Solid-liquid equilibria in the ThO_2–

ZrO_2 system: An experimental study, Journal of Nuclear Materials 521 (2019) 99-108.

[60] D. Das, S. R. Bhardwaj, Thoria-based Nuclear Fuels, Thermophysical properties, fabrication, reprocessing and waste management, A Springer-Verlag Publication, London (2013) 335.

[61] D. P. Le, Y. H. Yoo, J. G. Kim, S. M. Cho, Y. K. Son, Corrosion characteristics of polyaniline-coated 316L stainless steel in sulphuric acid containing fluoride, Corrosion Science 51 (2009) 330-338.

[62] N. K Pandey, N. Desigan, A. Ramanujam, PUREX and THOREX Processes (Aqueous Reprocessing), Reference Module in Materials Science and Materials Engineering (2016).

[63] C. P. Kaushik, Indian Program for Vitrification of High Level Radioactive Liquid Waste, Procedia Materials Science 7 (2014) 16 – 22.

[34] A. Quintas, D. Caurant, O. Majérus, T. Charpentier, J. L. Dussossoy, Effect of compositional variations on charge compensation of AlO_4 and BO_4 entities and on crystallization tendency of a rare-earth-rich alumino borosilicate glass, Materials Research Bulletin 44 (2009) 1895-1898.

[65] L. J. Criscenti, S. L. Brantley, K. T. Mueller, N. Tsomaia, J.D. Kubicki, Theoretical and ^{27}Al

CPMAS-NMR investigation of aluminum coordination changes during alumino-silicate dissolution, Geochim. Cosmochim. Acta 69 (2005) 2205–2220.

[66] J. McCloy, N. Washton, P. Gassman, J. Marcial, J. Weaver, R. Kukkadapu, Nepheline crystallization in boron-rich alumino-silicate glasses as investigated by multinuclear NMR, Raman, & Mössbauer spectroscopies, J. Non-Cryst. Solids 409 (2015) 149-165.

[67] Sung Keun Lee, George D. Cody, Yingwei Fei, Bjorn O. Mysen, The effect of Na/Si on the structure of sodium silicate and alumino-silicate glasses, Chemical Geology 229 (2006) 162-172.

[68] R. K. Mishra, V. Sudarsan, A. K. Tyagi, C. P. Kaushik, Kanwar Raj, S. K. Kulshreshtha, Structural aspects of barium borosilicate glasses containing thorium and uranium oxides, J. Nucl. Mater. 359 (2006) 132–138.

[69] R. K. Mishra, V. Sudarsan, C. P. Kaushik, K. Raj, S. K. Kulshreshtha, A. K. Tyagi, Effect of BaO addition on the structural aspects and thermo-physical properties of sodium borosilicate glasses, J. Non-Cryst. Solids 353 (2007) 1612–1617.

[70] R.K. Mishra, V. Sudarsan, A.K. Tyagi, C.P. Kaushik, Kanwar Raj, S.K. Kulshreshtha, Structural studies of ThO_2 containing barium borosilicate glasses, J. Non-Cryst. Solids 352 (2006) 2952–2957.

[71] R. K. Mishra, V. Sudarsan, C. P. Kaushik, Kanwar Raj, R. K. Vatsa, M. Body, A. K. Tyagi, Effect of fluoride ion incorporation on the structural aspects of barium–sodium borosilicate glasses, J. Non-Cryst. Solids 355 (2009) 414–419.

[72] M. Goswami, G. P. Kothiyal, V. Sudarsan, S. K. Kulshreshtha, The effects of alumina content on the thermomechanical and structural properties of machineable magnesiumalumino-silicate glasses and their glass ceramics, Glass Technol. 469 (2005) 341–346.

[73] Q. Caurant, O. Maje'rus, T. Charpentier, J. L. Dussossoy, Effect of compositional variations

on charge compensation of AlO_4^- and BO_4^- entities and on crystallization tendency of a rare-earth-rich alumino borosilicate glass, Mater. Res. Bull. 44 (2009) 1895–1898.

[74] W. J. Dell, P. J. Bray, S. Z. Xiao, ^{11}B NMR studies and structural modeling of Na_2O-B_2O_3-SiO_2 glasses of high soda content, Journal of Non-Crystalline Solids 58 (1983) 1–16.

[75] D. Manara, A. Granjean, D.R. Neuville, Structure of borosilicate glasses and melts: a revision of the Yun, Bray and Dell model, Journal of Non-Crystalline Solids 355 (2009) 2528–2531.

[76] Arpad W. Imre, Sergiy V. Divinski, Stephan Voss, Frank Berkemeier, Helmut Mehrer, A revised view on the mixed-alkali effect in alkali borate glasses, Journal of Non-Crystalline Solids 352 (2006) 783–788.

[77] Yitian Xiao and Antonio C. Lasaga, Ab i&i0 quantum mechanical studies of the kinetics and mechanisms of silicate dissolution: H^+(H_30^+) catalysis, Geochimica et Cosmochlmica Acta. 58 (1994) 5379-5400.

[78] Louise J. Criscenti, James D. Kubicki, and Susan L. Brantley, Silicate Glass and Mineral Dissolution: Calculated Reaction Paths and Activation Energies for Hydrolysis of a Q_3 Si by H_3O^+ Using Ab Initio Methods, J. Phys. Chem. 110 (2006) 198–206.

[79] Frédéric Bouyer, Grégory Geneste, Simona Ispas, Walter Kob, Water solubility in calcium aluminosilicate glasses investigated by first principles techniques, Journal of Solid State Chemistry 183 (2010) 786-2796.

[80] Barry R. Bickmore, Kathryn L. Nagy, Amy K. Gray, A. Riley Brinkerhoff, The effect of $Al(OH)_4^-$ on the dissolution rate of quartz, Geochimica et Cosmochimica Acta 70 (2006) 290-305.

[81] G. Geneste, F. Bouyer, and S. Gin, Hydrogen–sodium interdiffusion in borosilicate glasses investigated from first principles, J. Non-Cryst. Solids 352 (2006) 3147.

[82] Céline Cailleteau, Coralie Weigel, Aurélien Ledieu, Philippe Barboux, François Devreux, On the effect of glass composition in the dissolution of glasses by water, Journal of Non-Crystalline Solids 354 (2008) 117-123.

[83] R. K. Mishra, Sumit Kumar, B. S. Tomar, A. Tyagi, C. P. Kaushik, Kanwar Raj, V. K. Manchanda, Effect of barium on diffusion of sodium in borosilicate glass, Journal of Hazardous Materials 156 (2008) 129–134.

[84] Konstantinos Konstantinou, Peter V. Sushko 1, Dorothy M. Duffy, Structure and ionic diffusion of alkaline-earth ions in mixed cation glasses A_2O–$2MO$–$4SiO_2$ with molecular dynamics simulations, Journal of Non-Crystalline Solids 422 (2015) 57–63.

[85] Sumit Kumar, R. K. Mishra, B. S. Tomar, A. K. Tyagi, C. P. Kaushik, Kanwar Raj, V. K. Manchanda, Heavy ion Rutherford backscattering spectrometry (HIRBS) study of barium diffusion in borosilicate glass, Nuclear Instruments and Methods in Physics Research B 266 (2008) 649–652.

[86] R. D. Kale, India's fast reactor programme – A review and critical assessment, Progress in Nuclear Energy, 122 (2020) 103265.

[87] R. Agarwal, V. Venugopal, Chemical states of fission products in irradiated $(U_{0.3}Pu_{0.7})C_{1+x}$ fuel at high burn-ups, J. Nucl. Mater. 359 (2006) 122–131.

[88] M. B. Chadwick, M. Herman, P. Obložinský, M. E. Dunn, Y. Danon, A. C. Kahler, D. L. Smith, B. Pritychenko, G. Arbanas, R. Arcilla, R. Brewer, D. A. Brownb, R. Capote, A. D. Carlson, Y. S. Cho, H. Derrien, K. Guber, G. M. Hale, G. Young. ENDF/B-VII.1 Nuclear Data for Science and Technology: Cross Sections, Co-variances, Fission Product Yields and Decay Data, Nuclear Data Sheets 112 (2011) 2887-2996.

[89] D. Caurant, O. Majérus, E. Fadel, A. Quintas, C. Gervais, T. Charpentier, D. Neuville, Structural investigations of borosilicate glasses containing MoO_3 by MAS NMR and Raman spectroscopies, J. Nucl. Mater. 396 (2010) 94–101.

[90] M.I. Ojovan, W.E. Lee, An Introduction to Nuclear Waste Immobilisation, (2005) 226.

[91] Pavel Hrma, John D Vienna, Benjamin K. Wilson, Trevor J. Plaisted, Steve M. Heald, Chromium phase behavior in a multi-component borosilicate glass melt. Journal of Non-Crystalline Solids, 352 (2006) 2114-2122.

[92] R. Baldev, U. Kamachi Mudali, M. Vijayalakshmi, M. D. Mathew, A. K. Bhaduri, P. Chellapandi, S. Venugopal, C. S. Sundar, B. P. C. Rao, B. Venkatraman, Development of Stainless Steels in Nuclear Industry: With Emphasis on Sodium Cooled Fast Spectrum Reactors History, Technology and Foresight, Advanced Materials Research, 794 (2013) 3-25.

[93] Inger Odnevall Wallinder, Jianshu Lu, Sofia Bertling, Christofer Leygra, Release rates of chromium and nickel from 304 and 316 stainless steel during urban atmospheric exposure—a combined field and laboratory study, Corrosion Science. 44 (2002) 2303-2319.

[94] G. P. Marsh, K. J. Taylor, G. Bryan, S. E. Worthington. 1986. The influence of radiation on the corrosion of stainless steel. Corrosion Science. 26 (1986) 971-982

[95] Tina M. Hayward, Igor M. Svishchev Ramesh C. Makhija, S Stainless steel flow reactor for supercritical water oxidation: corrosion tests, The Journal of Supercritical Fluids. 27 (2003) 275-281.

[96] G. Calas, M. Le Grand, L. Galoisy, D. Ghaleb, Structural role of molybdenum in nuclear glasses: an EXAFS study, J. Nucl. Mater. 322 (2003) 15–20.

[97] P.B. Rose, D.I. Woodward, M.I. Ojovan, N.C. Hyatt, W.E. Lee, Crystallisation of a simulated borosilicate high-level waste glass produced on a full-scale vitrification line, Journal of Non-Crystalline Solids 357 (2011) 2989–3001.

[98] Ashutosh Goel, John S. McCloy, Richard Pokorny, Albert A. Kruger, Challenges with vitrification of Hanford High-Level Waste (HLW) to borosilicate glass – An overview. Journal of Non-Crystalline Solids, 4 (2019) 100033.

[99] M. V. Sambasiva Rao, Ch. Rajyasree, T. Narendrudu, S. Suresh, A. Suneel Kumar, N. Veeraiah, D. Krishna Rao. Physical and spectroscopic properties of multi-component Na2O–PbO–Bi_2O_3–SiO_2 glass ceramics with Cr_2O_3 as nucleating agent, Optical Materials. 47 (2015) 315-322.

[100] Jesse Alton, T J Plaisted, P Hrma. Kinetics of growth of spinel crystals in a borosilicate glass, Chemical Engineering Science 57 (2002) 2503-2509.

[101] M. Szumera, Molybdenum modified phosphate glasses studied by ^{31}P MAS NMR and Raman spectroscopy, Spectrochimica Acta Part A: Molecular and Biomolecular Spectroscopy, 137 (2015) 111-115.

[102] A. Šantić, Ž. Skoko, A. Gajović, S.T. Reis, D.E. Day, A. Moguš-Milanković, Physical properties of lead iron phosphate glasses containing Cr_2O_3, Journal of Non-Crystalline Solids, 357 (2011) 3578-3584.

[103] G. Tricot, B. Revel, S. Wegner, Thermal stability of a low Tg phosphate glass investigated by DSC, XRD and solid state NMR, Journal of Non-Crystalline Solids 357 (2011) 2708–2712.

[104] F. Farges, R. Siewert, G.E. Brown Jr., A. Guesdon, G. Morin, Structural environments around molybdenum in silicate glasses and melts. I. Influence of composition and oxygen fugacity on the local structure of molybdenum, Can. Mineral. 44 (2006) 731–753.

[105] Zhenguo Yang, Jeff W. Stevenson, Kerry D. Meinhardt, Chemical interactions of barium–calcium–aluminosilicate-based sealing glasses with oxidation resistant alloys, Solid State Ionics 160 (2003) 213 – 225.

[106] G. D. Khattak, M. A. Salim, A. S. A1-Harthi, David J. Thompson, L.E. Wenger, Structure of molybdenum-phosphate glasses by X-ray photoelectron spectroscopy (XPS), Journal of Non-Crystalline Solids 212 (1997) 180–191.

[107] Youssef Makhkhas, Said Aqdim, El Hassan Sayouty, Study of Sodium-Chromium-Iron- Phosphate Glass by XRD, IR, Chemical Durability and SEM, Journal of Materials Science and Chemical Engineering, 1 (2013) 1-6.

[108] John S. McCloy and Ashutosh Goel, Glass-ceramics for nuclear-waste immobilization MRS bulletein, 42 (2017) 233-240.

[109] Brandon J. Greer and Scott Kroeker, Characterisation of heterogeneous molybdate andchromate phase assemblages in model nuclear waste glasses by multinuclear magnetic resonance spectroscopy, Phys. Chem. Chem. Phys., 14 (2012) 7375–7383.

[110] Cheng, G. Yang, Y. Zhao, M. Peng, J. Skibsted, Y. Yue, Quantification of the boron speciation in alkali borosilicate glasses by electron energy loss spectroscopy, Scientific Reports. 5 (2015) 1-7.

[111] P. Stoch, W. Szczerba, W. Bodnar, M. Ciecinska, A. Stoch, E. Burkel Structural properties of iron-phosphate glasses: spectroscopic studies and ab initio simulations, Phys. Chem. Chem. Phys. 16 (2014) 19917–19927.

[112] M. Singh, V. Karki, R.K. Mishra, A. Kumar, C.P. Kaushik, X. Mao, R.E. Russo, A. Sarkar, Analytical spectral dependent partial least squares regression: a study of nuclear waste glass from thorium based fuel using LIBS, J. Anal. At. Spectrom. 30 (2015) 2507-2515.

[113] M. Singh, R. K. Mishra, A. Kumar, C. P. Kaushik, P. G. Jaison, A. Sarkar, Comparison of univariate and multivariate data analysis models for uranium quantification in Trombay historical nuclear waste glass, Radiochimica Acta, 106 (2018) 453.

[114] C.P. Kaushik, Indian Program for Vitrification of High Level Radioactive Liquid Waste, Procedia Materials Science 7 (2014) 16-22.

[115] M.I. Ojovan, W.E. Lee, An Introduction to Nuclear Waste Immobilisation, (2005) 247.

[116] P. K. Wattal, Indian programme on radioactive waste management, Sadhana 38 (2013) 849–857.

[117] Daniel Caurant, Odile Majérus, Edward Fadel, Marion Lenoir, Christel Gervais, Olivier Pinet. Effect of Molybdenum on the Structure and on the Crystallization of SiO_2–Na_2O–CaO–B_2O_3 glasses, Journal of the American Ceramic Society 90 (2007) 774-783.

[118] R. K Brow, C. A Click, T. M Alam, Modifier coordination and phosphate glass networks, Journal of Non-Crystalline Solids 274 (2000) 9-16.

[119] A. E. Marino S. R. Arrasmith, L. L. Gregg, S. D. Jacobs, Guorong Chen, Yongjuan Duc, Durable phosphate glasses with lower transition temperatures, Journal of Non-Crystalline Solids 289 (2001) 37-41.

[120] B. Mirhadi, B. Mehdikhani, Crystallization behavior and microstructure of ($CaO\cdot ZrO_2\cdot SiO_2$)–Cr2O3 based glasses, Journal of Non-Crystalline Solids 357 (2011) 3711–3716.

[121] Omar A. Lafi, What are the parameters that glass transition temperature of chalcogenide glasses depend on? An overview, Journal of Non-Oxide Glasses 8 (2016) 11–15.

[122] Hirohide Kofuji, Tetsuji Yano, Munetaka Myochin, Kanae Matsuyama, Takeshi Okita, Shinya Miyamoto Chemical Durability of Iron-phosphate Glass as the High Level Waste from Pyrochemical Reprocessing, Procedia Chemistry 7 (2012) 764-771.

[123] K. Brinkman, Kevin Fox, James Marra, Jason Reppert, Jarrod Crum, Ming Tang, Single phase melt processed powellite (Ba,Ca)MoO_4 for the immobilization of Mo-rich nuclear waste, Journal of Alloys and Compounds 551 (2013) 136–142.

[124] Ram Pyare, Lai Ji Lai, V C. Joshi, V K. Singh, Leachability of Molybdenum from Ternary Phosphate Glasses, Journal of the American Ceramic Society 79 (2005) 1329-1334.

[125] V. S. Yalmali, D. S. Deshingkar, P. K. Wattal, S. R. Bharadwaj, Preparation and characterization of vitrified glass matrix for high level waste from MOX fuel processing, Journal of Non-Crystalline Solids 353 (2007) 4647–4653.

[126] C. P. Kaushik, Indian Program for Vitrification of High Level Radioactive Liquid Waste, Procedia Materials Science 7 (2014) 16-22.

[127] M. J. Larkin Development of highly active waste conditioning at Sellafield, Nucl. Energy 25 (1986) 343–354.

[128] J.A.C. Marples, The preparation, properties, and disposal of vitrified high level waste from nuclear fuel reprocessing, Glass Technol. 29 (1988) 230–247.

[129] W. Lutze, R.C. Ewing (Eds.), Radioactive Waste Forms for the Future, North-Holland, Amsterdam, (1988) 1–159.

[130] I. W. Donald, B.L. Metcalfe, R.N.J. Taylor, The immobilization of high level radioactive wastes using ceramics and glasses, J. Mater. Sci. 32 (1997) 5851–5887.

[131] Michael I. Ojovan, Viscosity and Glass Transition in Amorphous Oxides, Advances in Condensed Matter Physics, (2008) Article ID 817829.

[132] W. E. Lee, M. I. Ojovan, M. C. Stennett, N. C. Hyatt, Adv. Appl. Ceram. 105 (2006) 3–12.

[133] P. Srinivasa Rao, P. Ramesh Babu, R. Vijay, T. Narendrudu, N. Veeraiah, D. Krishna Rao, Spectroscopic and dielectric response of zinc bismuth phosphate glasses as a function of chromium content, Materials Research Bulletin 57 (2014) 58–66.

[134] B. Luckscheiter and M. Nesovic, Short-term corrosion of HLW glass in aqueous solutions enriched with various metal cations, J. of Nucl. Mater. 327 (2004) 182-187.

[135] B. Luckscheiter and M. Nesovic, Development of glasses for the vitrification of high level liquid waste (HLLW) in a joule heated ceramic melter, Waste Management.16 (1996) 571-578.

[136] S. V. Stefanovsky, O. I. Stefanovsky, M. B. Remizov, P. V. Kozlov, E. A. Belanova, R. A. Makarovsky, B. F. Myasoedov, Sodium aluminum iron phosphate glasses as legacy high level waste Forms, Progress in Nuclear Energy 94 (2017) 229-234.

[137] Jiawei Sheng, Kwansik Choi, Myung-Jae Song, Vitrification of liquid waste from nuclear power plants, Journal of Nuclear Materials, 297 (2001) 7-13.

[138] T. P. Valsala, S. Chattopadhyay, R. V. Jayan, N. L. Sonar, P. K. Mishra, Vinit Kumar Mittal, Vaishali De, D. A. Thakur, R. K. Sah, Amrita Dhara, Soumya Sen, R. K. Dubey, I. Vishwaraj and Y. Kulkarni, Development and adoption of Low Sodium Glass frit for Vitrification of High Level Radioactive Liquid Waste at Tarapur, BARC Newsletter. 339 (2014) 1-4.

[139] Magdalena Szumera, Irena Wacławska, Effect of molybdenum addition on the thermal properties of silicate–phosphate glasses, Therm. Anal. Cal. 109 (2012) 649.

[140] K. Brinkman, K. Fox, J. Marra, J. Reppert, J. Crum, M. Tang, Single Phase Melt Processed Powellite (Ba,Ca)MoO4 for the Immobilization of Mo-rich Nuclear Waste, J. Alloys Compd. 551 (2013) 136–142.

[141] Jacob G. Reynolds, Spinel structure and liquidus temperature relationships in nuclear waste glass, J. Mater. Sci. 40 (2005) 3987-3991.

[142] Sam A. Walling, Marcus N. Kauffmann, Laura J. Gardner, Daniel J. Bailey, Martin C. Stennett, Claire L. Corkhill, Neil C. Hyatt, Characterisation and disposability assessment of multi-waste stream in-container vitrified products for higher activity radioactive waste, Journal of Hazardous Materials 401 (2021) 123764.

[143] C. P. Kaushik, R. K. Mishra, P. Sengupta, Amar Kumar, D. Das, G. B. Kale, Kanwar Raj, Barium borosilicate glass – a potential matrix for immobilization of sulfate bearing high-level radioactive liquid waste, Journal of Nuclear Materials 358 (2006) 129–138.

[144] Satish B. Patil, Jyoti Jha, Puneet Srivastava, Shakti Mishra, Rituparna Datta and Siddhartha S. Khan, Design & Development of Facility for Production of Active Cs-137 Source Pencils for Blood Irradiator, BARC newsletter (2013) 1-8.